DISSERTATION

THE INFLUENCE OF CLOUD RADIATIVE EFFECTS ON HYDROLOGIC SENSITVITY AND VARIABILITY

Submitted by

Alexandra Claire Naegele

Department of Atmospheric Science

In partial fulfillment of the requirements

For the Degree of Doctor of Philosophy

Colorado State University

Fort Collins, Colorado

Spring 2021

Doctoral Committee:

Advisor: David A. Randall

Michele M. Betsill
Kristen L. Rasmussen
Susan C. van den Heever

ABSTRACT

THE INFLUENCE OF CLOUD RADIATIVE EFFECTS ON HYDROLOGIC SENSITIVITY AND VARIABILITY

The global-mean precipitation change in response to CO_2-forced warming, normalized by global-mean surface warming, is referred to as the hydrologic sensitivity. It is estimated at 1-3% K^{-1}, much lower than the rate of increasing atmospheric moisture availability. Here, we study the role of cloud radiative effects (CREs) in constraining the hydrologic sensitivity. Often, the change in clear-sky atmospheric radiative cooling (ARC) is used to constrain the change in precipitation, but this constraint is incomplete. CMIP5 model data are analyzed to show that although the all-sky ARC increases at a lower rate than the clear-sky ARC, the smaller change in ARC due to CREs is balanced by the change in the surface sensible heat flux. Together, the change in the all-sky ARC with the change in the surface sensible heat flux provide a more accurate and complete energetic constraint on hydrologic sensitivity than by using the clear-sky radiative cooling alone.

Idealized aquaplanet simulations using SP-CAM are analyzed to assess the temperature dependence of the hydrologic cycle and the large-scale circulation responses to CREs. We examine the response of the hydrologic cycle and the large-scale circulation to CREs at a range of sea surface temperatures (SSTs), including a cool (280 K) SST that is representative of the mid-latitudes; typically, the extratropics have been less studied than the tropics in similar idealized simulations. We use simulations with uniform SSTs to test the hypothesis that CREs enhance precipitation variability at cool temperatures, and reduce

precipitation variability at warm temperatures. In these simulations, our hypothesis is confirmed. In less idealized simulations with a more realistic SST pattern, the influence of CREs on precipitation variability is obscured by other circulation changes.

Can the hydrologic response to CREs be explained by the large-scale circulation response to CREs? Using the same idealized simulations, the vertical velocity —used here as an indicator of the circulation response to CREs—is compared to precipitation. We find that the influence of CREs on vertical velocity variability is very similar to the influence of CREs on precipitation variability.

ACKNOWLEDGEMENTS

First and foremost, I would like to thank my advisor, Dave Randall, for bringing me into this program. Without a background in atmospheric science, it is safe to say that I had no idea what I was getting myself into when I started this journey. The PhD process can be a challenging one, and in moments of doubt I was buoyed by the reflection that everything I know about atmospheric science, I learned while I was here.

Dave, over the years, your scientific intuition and endless curiosity has never ceased to inspire me. Thank you for walking me through this journey, fostering my independence, and perhaps most of all, for giving me the freedom to pursue non-traditional paths. The coursework for my certificate in international development studies exposed me to new ideas and opened the door for countless conversations that I continue to think about and that have shaped me as a scientist.

I thank my committee for their time and for their insights. Sue, you've always been supportive of not only my research, but also of my interest in applying climate science to societally relevant issues. Kristen, participating in the RELAMPAGO field campaign through ASI was a highlight of my PhD, and I learned so much in those few short weeks. Michele, I appreciate your outside perspective and that you continually push me to consider to the bigger picture.

To all the faculty, I owe you all for building my foundation of atmospheric science knowledge. Thank you for your passion, the formal lessons inside the classroom, and the informal discussions outside. And to the ever-helpful staff, thank you for all that you do to keep this department running.

A special thank you to everyone I worked with on the Diversity, Equity, and Inclusion Committee. I look forward to seeing where you take this work, and I truly believe the impact will reach well beyond our department in making this field more inclusive for all people.

Over the years I have received so much help from the Randall group, especially Mark and Kelley Branson, Don Dazlich, and Mostafa Elkady—I hope you've always known how appreciative I've been. Melissa Burt, your mentorship has been beyond helpful in navigating this process; I cannot thank you enough for all the times you have been there for me. And to the Randall group students of past and present, especially Leah Lindsey, Casey Patrizio, Andrea Jenney, Michael Needham, and Ann Casey Hughes, thank you for your thoughtful conversations, your feedback, and most importantly for the laughter. And thank you to ESMEI intern Charlotte Connolly for your contribution to Chapter 2.

Above all, I am most grateful for the Atmos community as a whole. This is an impressive group of students, and an inviting and fun group of friends. I consider myself incredibly lucky to have been part of this community, and I'm thankful for all of the meaningful relationships that have grown out of my time here, many of which I have grown from as well. It is no exaggeration to say that I could not have done this without the support of the friends I have made in this program. These friendships are close to my heart, and I look forward to carrying them with me as I move on and in the many years to come.

And finally, to my friends and family near and far, thank you. Especially to my parents, your support is unwavering, and it means the world to me.

TABLE OF CONTENTS

CHAPTER 1

INTRODUCTION

1.1 CHANGES IN PRECIPITATION

The hydrologic cycle is arguably one of the most important and relevant processes in the climate system to life on earth. The hydrologic cycle is constantly exchanging water between the earth's atmosphere, surface, and sub-surface. Evaporation from the oceans and surface freshwater sources in combination with plant transpiration from land surfaces are the processes primarily responsible for transferring water from the earth's surface to the atmosphere, whereas precipitation from clouds in the atmosphere falls as, for example, rain or snow to earth's surface. Broadly, this dissertation aims to understand changes in the hydrologic cycle by focusing on changes in precipitation.

Precipitation is often characterized by the mean precipitation, which can be used as a climate indicator (U.S. E.P.A., 2016). Average precipitation rates partially define terrestrial ecosystems and determine vegetation. This applies not only to natural systems, but to human systems as well. Consider agriculture, for example. Along with temperature and solar radiation, average precipitation rates determine the types of agricultural crops that will grow, when they will grow, and how well (Hollinger and Angel, 2009). In response to warming surface temperatures, the globally averaged precipitation rate is expected to increase by approximately 1-3% K^{-1} (Allen and Ingram, 2002). Not only will changes in average precipitation rates affect ecosystems and agriculture, but also fresh water resources that provide water for drinking and irrigation. Furthermore, the impacts of precipitation

changes can be exacerbated by water and land management practices as well as by changes in land use (Lin et al., 2008; Field et al., 2014).

Over a given period of time, however, the precipitation will not fall as the average amount. Rather, the amount of precipitation that falls varies around the average, and therefore variability is an important statistic to consider as well. In a future, warmer climate, precipitation variability is expected to increase (Pendergrass et al., 2017). As with changes in the mean precipitation, changes in precipitation variability will also have major consequences for agriculture (Shortridge, 2019).

Variability is inherently connected to extreme values as it relates them to the mean. Changes in precipitation variability enhance both wet and dry extremes, which can lengthen and intensify drought, and increase the frequency and intensity of heavy rain events. Extreme drought can have devastating impacts on agriculture and livestock, can threaten fresh water supplies, and can lead to conditions conducive to wildfires. On the other end of the spectrum, extreme rain events can result in erosion, landslides, and flash flooding. Taken together, these changes can increase the vulnerability of certain populations to climate change while they simultaneously face other stressors (Thornton et al., 2014; Dilling et al., 2015).

Whereas a change in the variability alone will increase both the frequency and intensity of extreme values on both ends of a distribution, a change in the mean alone will shift the entire distribution, so that if extreme events increase (in either frequency or intensity) on one end of the distribution, they are reduced on the other end (Meehl et al., 2000). The combination of these changes can dramatically affect wet and dry precipitation extremes (Figure 1.1.), both of which have severe impacts on society.

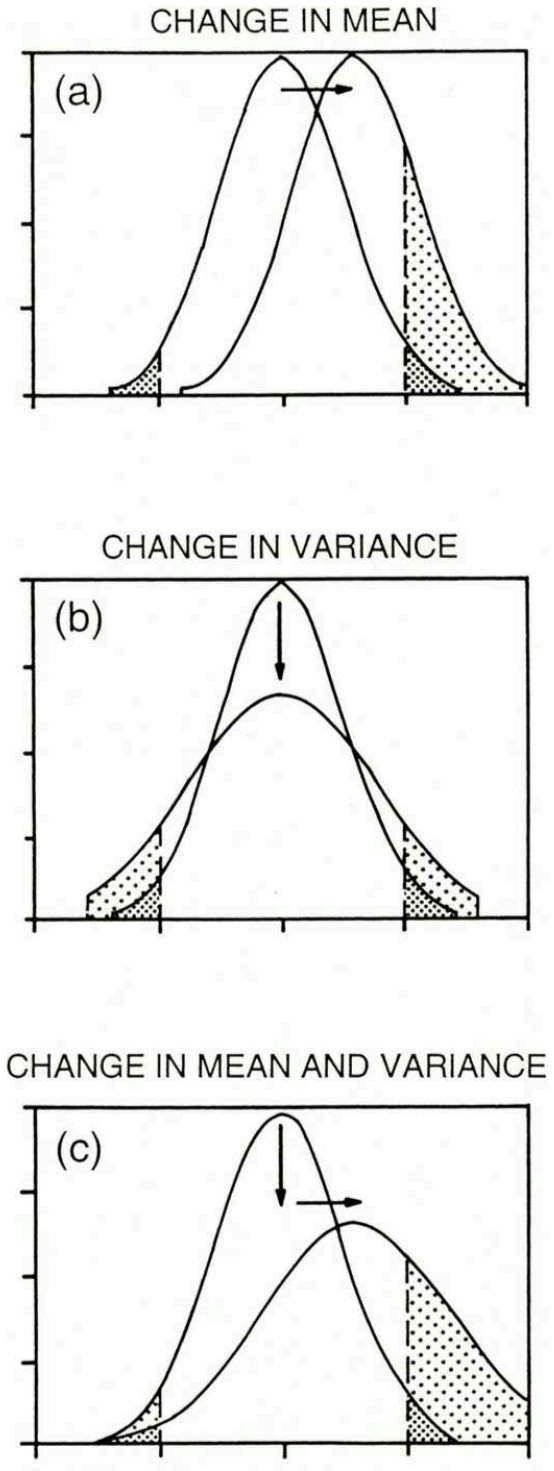

Figure 1.1. Schematic diagram depicting how changes in the (a) mean and (b) variance of a distribution can affect extreme weather and climate events by changing the frequency of extreme events and making them even more (or less) extreme. Changes in (c) both the mean and variance can have even stronger impacts on extreme events. Figure from Meehl et al. (2000).

1.2 CLOUD RADIATIVE EFFECTS

Much like the hydrologic cycle, clouds are an integral piece of the climate system puzzle. They produce precipitation, redistribute moisture in the atmosphere through convection, release latent heat, and affect the Earth's atmospheric energy budget. Radiatively, clouds reflect incoming solar energy, and absorb and re-emit longwave energy; these cloud radiative effects (CREs) can influence the atmospheric circulation and the hydrologic cycle.

The overarching goal of this dissertation is to examine the influence of CREs on the hydrologic cycle. In Chapter 2, we investigate the role of CREs in constraining the global-mean precipitation change in response to CO_2-forced warming. In Chapter 3, we shift our focus from changes in the mean to changes in the variability. In Chapters 4 and 5, we explore the temperature dependence of precipitation variability in response to CREs within the context of the hydrologic cycle, atmospheric radiative cooling (ARC), and the large-scale circulation.

1.3 OUTLINE

The focus of Chapter 2 is on hydrologic sensitivity: the change in global-mean precipitation normalized by the change in global-mean surface warming. Hydrologic sensitivity is energetically constrained, such that any change in precipitation must be balanced by changes in the net cooling in the atmosphere, which includes changes in the radiative cooling of the atmosphere and in the surface sensible heat flux. Attempts to simplify this balance frequently ignore the changes in CREs on the ARC as well as changes in the surface sensible heat flux. Perhaps out of convenience, numerous studies have focused on

the clear-sky radiative cooling as the primary constraint on hydrologic sensitivity; however, there is no physical basis for this constraint. In this study, we use 18 models from the 5th Coupled Model Intercomparison Project to examine the validity of this simplified constraint, and examine the role of CREs in constraining the change in global-mean precipitation in response to warming.

In Chapter 3, we introduce the subject of precipitation variability. Whereas average precipitation changes have been widely studied, changes in precipitation variability have received relatively little attention. Unlike changes in the global mean, however, variability can be used to better understand the changes that are felt. Furthermore, variability is useful because it connects extreme dry events on one end of the precipitation spectrum (e.g. drought) to extreme wet events on the other (e.g. flooding from heavy precipitation).

Chapters 4 and 5 examine the temperature dependence of precipitation variability in response to CREs. Motivated by observational results of precipitation, the ARC, and CREs, Naegele and Randall (2019) hypothesized that CREs reduce precipitation variability in the tropics and that CREs enhance precipitation variability in the extratropics; they further suggested that these different responses were tied to differences in the surface temperatures of those regions. To test this hypothesis, we analyze several sets of highly idealized aquaplanet simulations. Aquaplanet simulations with globally uniform sea surface temperatures (SSTs) of 280, 290, and 300 K are used to represent a range of environments from the midlatitudes to the tropics. The vast majority of research examining the influence of CREs using similar idealized model experiments has focused solely on the tropics.

In Chapter 4, the temperature dependence of the response of precipitation variability and extreme precipitation to CREs is considered within the context of the hydrologic cycle.

Specifically, comparisons are made with changes in precipitable water. Additionally, we consider the influence of CREs on the ARC and its shortwave and longwave components, and how those relate to changes in precipitation.

Cloud radiative effects have also been shown to influence the large-scale circulation, and in Chapter 5 we examine the temperature dependence of that response. We also consider the large-scale circulation as it relates to the hydrologic cycle. In particular, we focus on the vertical velocity because of its importance to extreme precipitation.

CHAPTER 2

THE ROLE OF CLOUD RADIATIVE EFFECTS IN CONSTRAINING HYDROLOGIC SENSITVITY

2.1 THE ENERGETIC CONSTRAINT ON THE HYDROLOGIC CYCLE

Precipitation is an important climate process, and is of course necessary to sustain life on earth. The ways in which precipitation might change with warming have received considerable attention and study. For example, it is now generally well known that global-mean precipitation rates are constrained by the atmospheric energy budget, rather than by moisture availability alone.

In an analysis of model projections from the second Coupled Model Intercomparison Project (CMIP) under the transient climate response scenario, Allen and Ingram (2002) were among the first to thoroughly examine the energetic constraint on the future hydrologic cycle beyond the more conceptual musings of Mitchell et al. (1987) and the surface-budget approach of Boer (1993). Allen and Ingram (2002) noted the discrepancy between the change in global-mean tropospheric humidity and the change in the global-mean precipitation rate in response to warming surface temperatures, in which water vapor increases at a rate of approximately 7% K^{-1} in accordance with the Clausius-Clapeyron relation, but precipitation increases at a much lower rate between 1-3% K^{-1}. From this discrepancy, they concluded that precipitation changes are not constrained by changes in moisture availability alone; rather, precipitation is energetically limited by the radiative cooling of the atmosphere which predominantly balances the latent heat of condensation

that gives rise to precipitation. This balance can be understood by considering the energy budget of the Earth's atmosphere:

$$\frac{dE_a}{dt} = LP + SHF - ARC, \qquad \text{(eq. 2.1)}$$

where E_a is the Earth's atmospheric energy, LP is the latent heat of precipitation, SHF is the sensible heat flux, and ARC is atmospheric radiative cooling. As in Naegele and Randall (2019), the ARC is used for convenience so that cooling is positive, rather than the conventional diabatic heating rate, Q. The hydrologic cycle equilibrates on the order of a month, so we can expect precipitation, ARC, and sensible heating to balance globally, and on sufficiently long timescales:

$$LP = ARC - SHF. \qquad \text{(eq. 2.2)}$$

Considering the ways in ways these quantities change with warming, equation 2.2 can be rewritten in terms of perturbations, as:

$$L\delta P = \delta ARC - \delta SHF. \qquad \text{(eq. 2.3)}$$

2.1.1 AN ENERGETIC OR RADIATIVE CONSTRAINT?

Following Allan and Ingram (2002), a number of modeling studies have since examined the energetic constraint on future precipitation changes. For example, in their analysis of CMIP3 projections, Held and Soden (2006) found a similarly stark difference in the trends of global-mean column-integrated water vapor (7.5% K^{-1}) and precipitation (2.2% K^{-1}) with warming (Figure 2.1). What has differed among these numerous studies, however, is an emphasis on either a more inclusive *energetic* or a purely *radiative* constraint on precipitation changes—the issue boils down to the relative importance of the sensible heat flux in this balance.

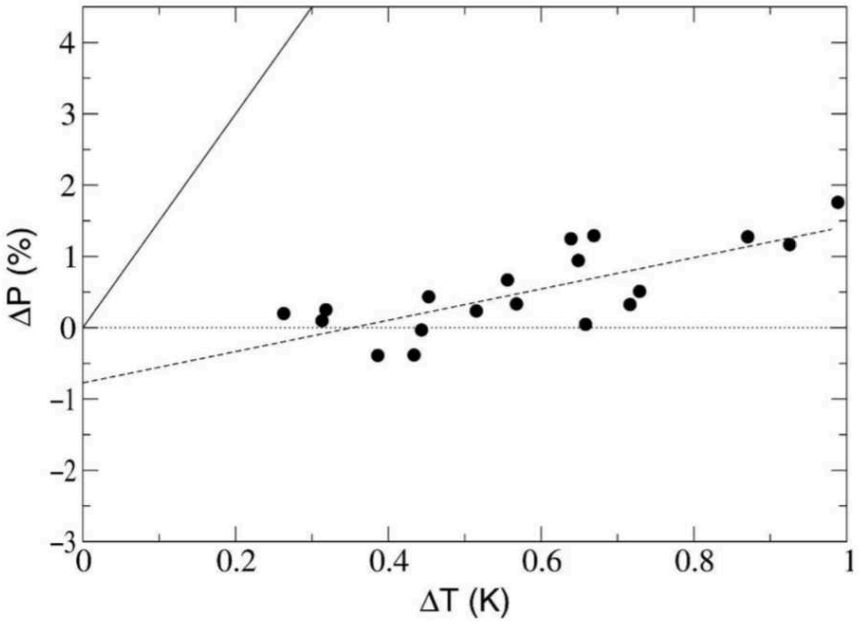

FIGURE 2.1. Scatterplot of the percentage change in globally averaged preciptation against the globally averaged change in surface air temperature. The dashed line shows the linear fit of ΔP to ΔT (2.2% K^{-1}) and the solid line shows the rate of change of column-integrated water vapor (7.5% K^{-1}). Figure from Held and Soden (2006).

In current estimates of the atmospheric energy budget, the surface latent heat flux is greater than the sensible heat flux by roughly three- (L'Ecuyer et al., 2015) to four-fold (Trenberth et al., 2009). Presumably it is because of this dominance of latent heating over sensible heating that some studies assume that the sensible heat flux will remain unchanged or that any changes are negligible (Wild and Liepert, 2010; Watanabe et al., 2018). Others acknowledge that the change in the surface sensible heat flux may not be trivial, but still focus on only the radiative portion of the constraint (e.g. Pendergrass and Hartmann, 2014).

Although the role of the SHF has been dismissed by some authors, others have acknowledged that it is non-negligible (e.g. O'Gorman and Schneider, 2008; O'Gorman et al., 2012) in the constraint on changes in the global-mean precipitation rate. Stephens and Ellis

(2008) for example, explicitly state that any reduction in SHF must be balanced by an increase in precipitation if the ARC remains constant. Although it is neither given nor expected that the ARC will remain unchanged, it is clear that any change in global-mean precipitation does not depend on changes in the ARC alone, but also on changes in the SHF (O'Gorman et al., 2012).

More recently, however, in an analysis of multiple scenarios from the Precipitation Drivers and Response Model Intercomparison Project (PDRMIP), Myhre et al. (2018) showed a near one-to-one relationship between the change in latent heating due to precipitation and the change in ARC – SHF—a much better fit than the more typically examined relationship between the change in precipitation and the change in ARC alone. Notably, but perhaps unsurprisingly, the difference between the two is much stronger in the fast (atmospheric energy budget-driven) response to warming than in the slow (surface temperature-driven) response.

2.1.2 ALL-SKY OR CLEAR-SKY?

In addition to the focus on the relative importance of the sensible heat flux in this balance, another subject of debate is the significance of the cloud contribution to the total ARC in the radiative constraint on precipitation. In one camp, a number of studies have focused on the change in clear-sky (rather than all-sky) radiative cooling in constraining the global-mean change in the hydrologic cycle. For example, although Allan (2006) acknowledges the necessity of accounting for cloud radiative effects (CREs) in future studies, they specifically emphasize the importance of clear-sky longwave cooling in the global hydrologic cycle. Pointing out that the cloud contribution to the total longwave cooling is

typically only 20% (Sohn, 1999), and the considerable uncertainties of global cloud datasets from observations (which therefore increases uncertainty in determining the CRE on radiative cooling), they focus solely on the clear-sky radiative cooling. Similarly, Stephens and Ellis (2008) point out that the clear-sky contribution to the ARC dominates the total ARC and that changes in the clear-sky contribution are far more predictable than changes in the all-sky contribution. In an analysis of an ensemble of GCMs with a doubling of CO_2 concentrations, Lambert and Webb (2008) find that changes in clear-sky longwave and shortwave cooling are the principal drivers of changes to the tropospheric energy budget that in turn drive changes in the latent heat of precipitation.

In their analysis of transient CO_2 simulations from CMIP5, Pendergrass and Hartmann (2014) investigate how well the radiative constraint holds in a warming climate. In their study, they find that the clear-sky ARC is more strongly correlated with precipitation changes than the all-sky ARC (Figure 2.2). Furthermore, in the multimodel mean, they find that changes in all-sky radiative changes would act to *reduce* global precipitation in a future climate, rather than increase it as is generally predicted. They thus conclude that the clear-sky ARC—rather than the all-sky ARC—is a better constraint on global precipitation changes.

A theme of the studies that focus primarily on clear-sky rather than all-sky ARC is that (a) the cloud contribution is relatively much smaller than the clear-sky contribution and (b) there is considerable uncertainty around observational estimates of cloudiness. Although both of these points are true, neither justifies the disregard of the role of CREs on changes in the mean hydrologic cycle. In that vein, it has been suggested that GCM projections may actually underestimate the slow precipitation response to increased CO_2 concentrations as a

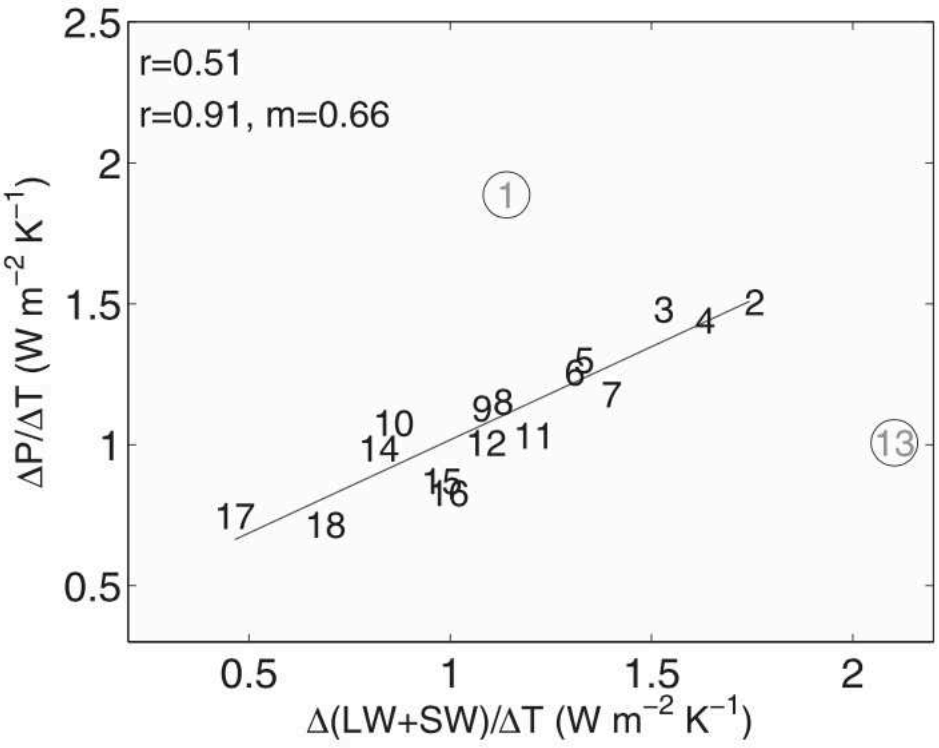

FIGURE 2.2. Normalized change in clear-sky radiative cooling against the change in the latent heat of precipitation, normalized by the global-mean surface temperature change from CMIP5 simulations. Figure from Pendergrass and Hartmann (2014).

result of incomplete representations of low-level cloud feedbacks (Siler et al., 2018, Allan et al., 2020).

In this study we aim to examine the following questions:

1) Is it true that the clear-sky ARC—rather than the all-sky ARC—is the best constraint on global-mean precipitation changes?
2) If so, why?

In order to answer these questions, we focus not only on radiative changes—including those due to clouds—but also on changes in the SHF.

2.2 METHODS

Eighteen models from CMIP5 were used to study the hydrologic sensitivity to CO_2-forced warming (Table 2.1). Simulations from the transient scenario were used, in which CO_2 concentrations increase at a rate of 1% $year^{-1}$ until doubling. All models that fit the criteria were used, and those criteria included the availability of monthly output and complete radiative fluxes to calculate all-sky and clear-sky ARC, as well as the SHF and surface air temperature. Only the first realization from each model was used.

TABLE 2.1. List of CMIP5 models used, their institution, and country.

Model	**Institution (Country)**
ACCESS1.0	Commonwealth Scientific and Industrial Research (Austrailia)
CANESM2	Canadian Centre for Climate Modeling and Analysis (Canada)
CCSM4	National Center for Atmospheric Research (USA)
CNRM-CM5	Centre National de Recherches Météorologiques, Centre Européen de Recherche et de Formation Avancée en Calcul Scientifique (France)
GFDL-CM3	NOAA Geophysical Fluid Dynamics Laboratory (USA)
GFDL-ESM2G	NOAA Geophysical Fluid Dynamics Laboratory (USA)
GFDL-ESM2M	NOAA Geophysical Fluid Dynamics Laboratory (USA)
GISS-E2-R	NASA GISS (USA)
HADGEM2	Met Office Hadley Centre (UK)
INMCM4	Institute for Numerical Mathematics (Russia)
IPSL-CM5A_LR	Institut Pierre-Simon Laplace (France)
IPSL-CM5A_MR	Institut Pierre-Simon Laplace (France)
IPSL-CM5B	Institut Pierre-Simon Laplace (France)
MIROC5	Institute for Environmental Studies (Japan)
MIROC-ESM	Institute for Environmental Studies (Japan)
MPI-EMS-MR	Max Planck Institute for Meteorology (Germany)
MPI-EMS-P	Max Planck Institute for Meteorology (Germany)
MRI-CGCM3	Meteorological Research Institute (Japan)

The normalized change is calculated first as the difference between the global mean of the last 10 years before the doubling of CO_2 and the first 10 years of the simulation. The difference is then divided by the global-mean change in surface temperature between the last 10 years and the first 10 years.

Outliers are identified using the 1.5-Interquartile range method and are not included in calculations of the correlation coefficient or linear regression.

2.3 RESULTS

Many studies have focused on the clear-sky radiative constraint on hydrologic sensitivity, but here we also consider the role of clouds in this constraint. Figure 2.3 shows the normalized change in precipitation (shown as the latent heat of precipitation, LδP) against the normalized change in all-sky (δARC_{all}) and clear-sky (δARC_{all}) ARC. The inter-model spread of the precipitation change is not small, and (excluding outliers) ranges from 0.62 W m^{-2} to 1.30 W m^{-2}, with a multimodel mean of 0.99 W m^{-2}. These values correspond to hydrologic sensitivities of 0.84% K^{-1} (minimum), 1.76% K^{-1} (maximum), and 1.34% K^{-1} (mean). The wide inter-model spread of hydrologic sensitivity has been previously observed (e.g. Allen and Ingram, 2002; Pendergrass and Hartmann, 2014; Thackeray et al., 2018). The inter-model spread of δARC_{all} (0.90 W m^{-2}) and δARC_{clr} (1.28 W m^{-2}) both exceed the inter-model spread of LδP. For a given value of LδP, the corresponding δARC_{all} is generally smaller, and the corresponding δARC_{clr} is larger. Because of δARC_{clr} is the larger of the two, and has a slightly higher correlation with LδP, it does appear to better constrain LδP—why?

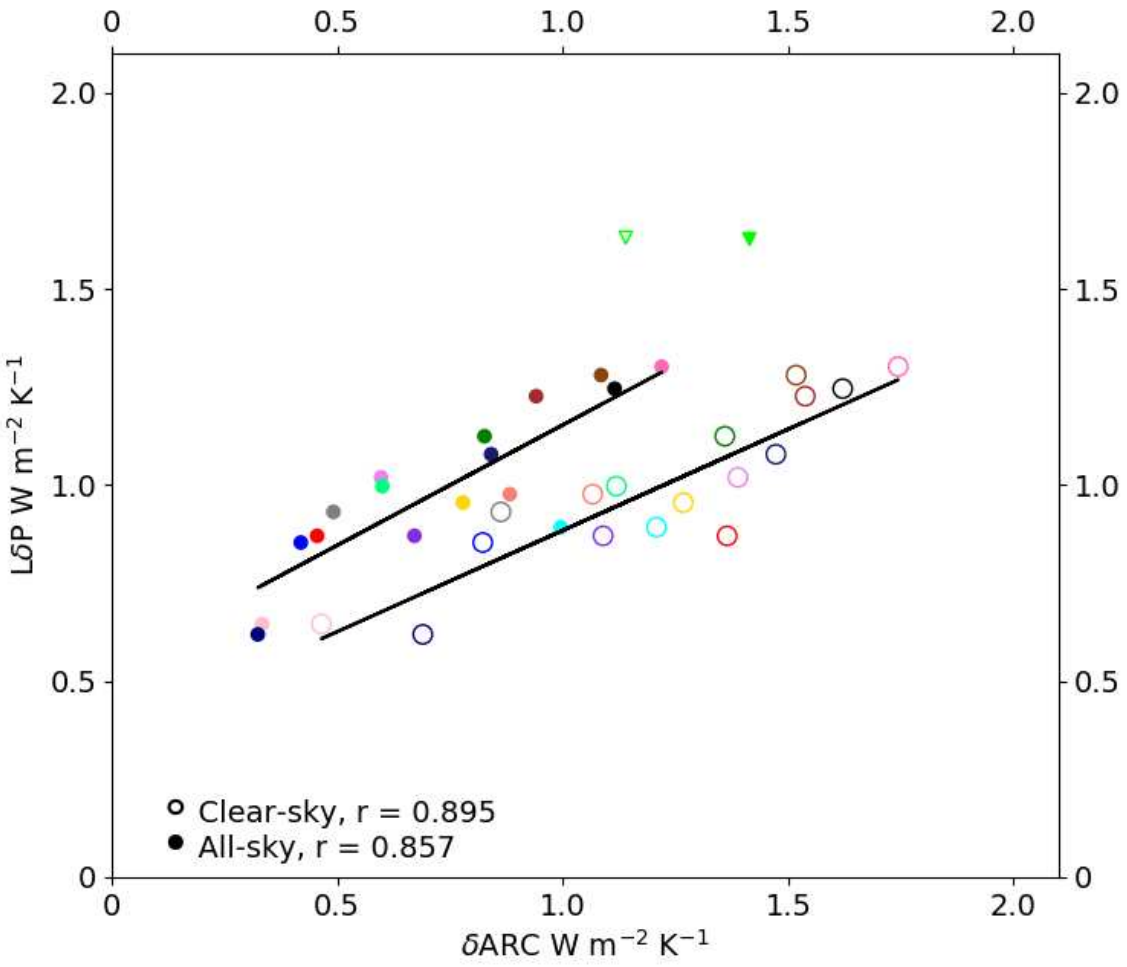

FIGURE 2.3. The normalized change in the latent heat of precipitation ($L\delta P$) plotted against the normalized change in the clear-sky ARC (open circles) and all-sky ARC (filled circles) for 18 CMIP5 models. Outliers are shown as triangles.

To better understand the differences between the global-mean all-sky and clear-sky δARC shown in Figure 2.3, Figure 2.4 shows the multimodel mean of the zonally averaged change in all-sky ARC and clear-sky ARC between the last 10 years before the doubling of CO_2 and the first 10 years of the simulation. The largest difference between the changes in the all-sky ARC and clear-sky ARC occurs in the Intertropical Convergence Zone (ITCZ) near

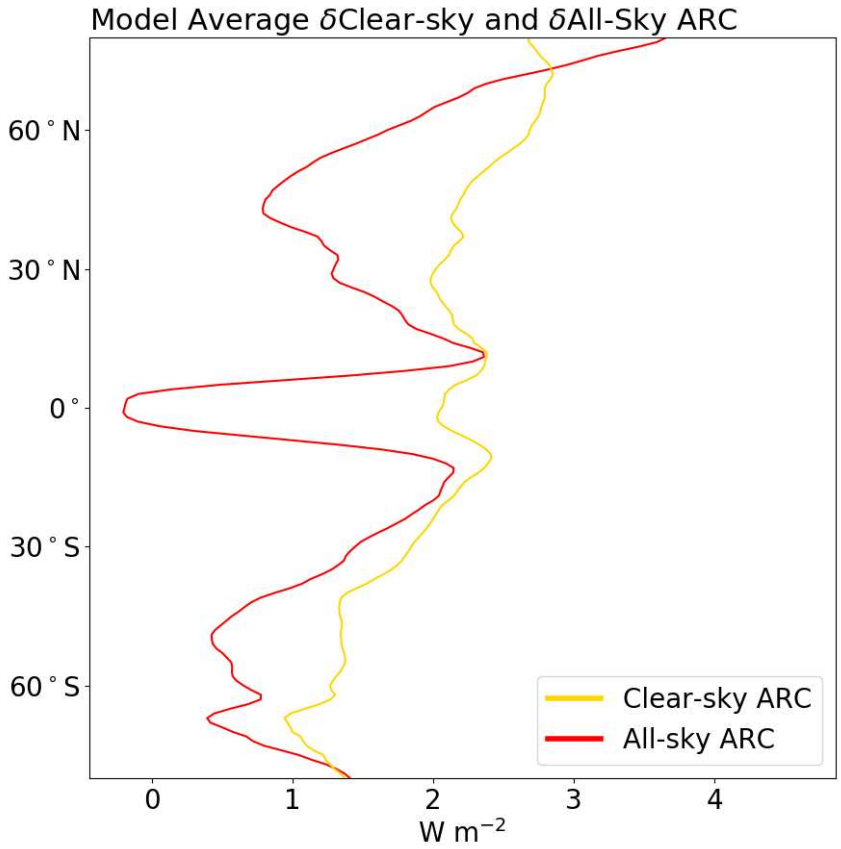

FIGURE 2.4. The zonally averaged multimodel means of the change in clear-sky ARC (yellow) and all-sky ARC (red) between the last 10 years before the doubling of CO_2 concentrations and the first 10 years of the simulation. Note that these changes are not normalized.

the equator, and it makes sense that this would occur in a very cloudy region. Here, the zonally averaged ARC_{clr} increases with warming due to increases in water vapor, but in ARC_{all}, this change is masked by clouds that block outgoing longwave radiation (OLR). The near-zero change in the ITCZ is consistent with the Fixed Anvil Temperature Hypothesis (Hartmann and Larson, 2002) and subsequent Proportionally Higher Anvil Temperature Hypothesis (Zelinka and Hartmann, 2010). According to these hypotheses, the cloud top temperature of anvil clouds changes much less than surface temperatures in a warming

climate. Therefore, high anvil clouds reduce the OLR and cool the atmosphere less efficiently in a warmer climate.

In the characteristically clear subtropics where CREs are expected to be small, the difference between δARC_{clr} and δARC_{all} is also small. In the extratropics, ARC_{clr} changes more than ARC_{all}, primarily due to increased downwelling longwave radiation (Vargas Zeppetello et al., 2019). Here, the change in downwelling longwave radiation from increased water vapor is masked by the downwelling longwave radiation from clouds. In total, the longwave contribution increases the ARC with warming, whereas the shortwave contribution reduces the ARC with warming. In both cases, clouds reduce the magnitude of shortwave warming and longwave cooling (not shown). A map of δARC_{all} from one of the 18 models used in the analysis is shown as an example, and highlights the reduction of ARC in cloudy regions, predominantly in the ITCZ, and to a lesser extent, in the Southern Ocean (Figure 2.5).

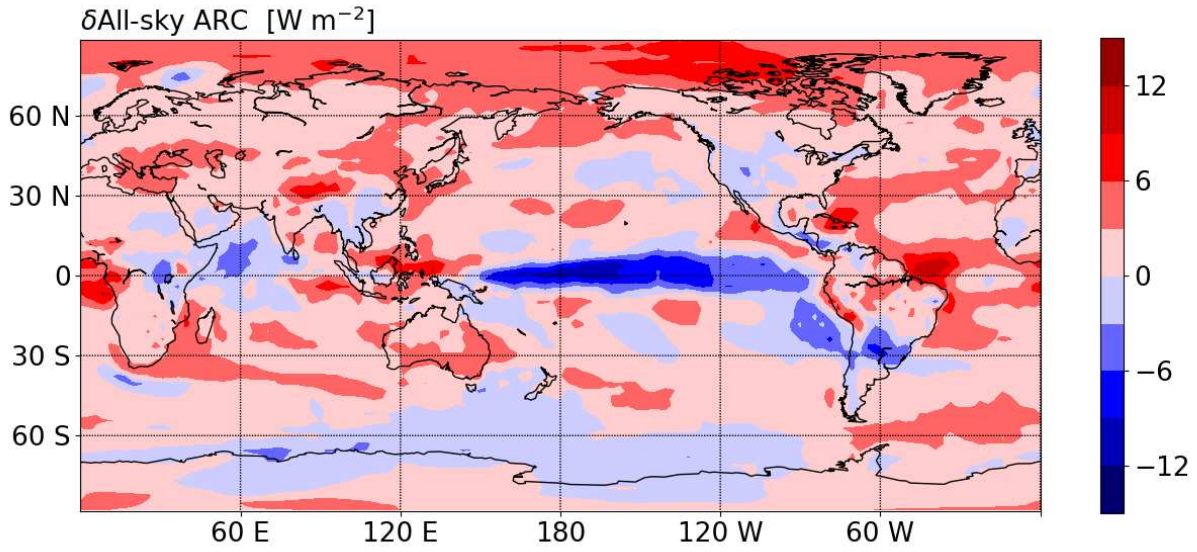

FIGURE 2.5. A map of the difference in the all-sky ARC from the last 10 years before the doubling of CO_2 and the first 10 years of the simulation in the CanESM2 model.

2.3.1 ROLE OF THE SENSIBLE HEAT FLUX

As shown in equation 2.1, the ARC itself does not fully balance precipitation. The multimodel global means of precipitation (as LP), all-sky ARC, clear-sky ARC, the CRE, and SHF for the first ten years of the simulation are shown in Table 2.2, and shows that the role of the SHF in the energy budget is small relative to the ARC and precipitation. The normalized change in each quantity due to a doubling of CO_2 (Table 2.3), however, does not reflect the relative contributions shown in Table 2.2. In particular, the magnitude of the normalized SHF perturbation (δSHF) is over half that of δARC_{all}, and is no longer so small that its exclusion from the energy balance can be justified. Furthermore, whereas the CRE is an order of magnitude smaller than the ARC at present, this is no longer the case in the perturbation.

Instead of remaining constant with warming, as some have assumed, the (upward) surface SHF is projected to decrease with warming (Stephens and Ellis, 2008; O'Gorman et al., 2012) due to a reduction of the air-sea temperature difference at the surface (Goody, 1964). In historical simulations, the SHF is shown to decrease over the oceans, with regional patterns of increased and decreased SHF found over land (Myhre et al., 2018).

TABLE 2.2 Global means over the first 10 years. Values are shown in W m^{-2} for the latent heat of precipitation, the clear-sky ARC, the all-sky ARC, the CRE, and the SHF.

LP	**ARC_{clr}**	**ARC_{all}**	**CRE**	**SHF**
73.9	108	106	2	23.3

TABLE 2.3. Global means of the normalized change between the first 10 years and the last 10 years before a doubling of CO_2 concentrations. Values are shown in W m^{-2} for the latent heat of precipitation, the clear-sky ARC, the all-sky ARC, the CRE, and SHF.

LδP	**δARC_{clr}**	**δARC_{all}**	**δCRE**	**δSHF**
0.99	1.21	0.73	.48	-0.41

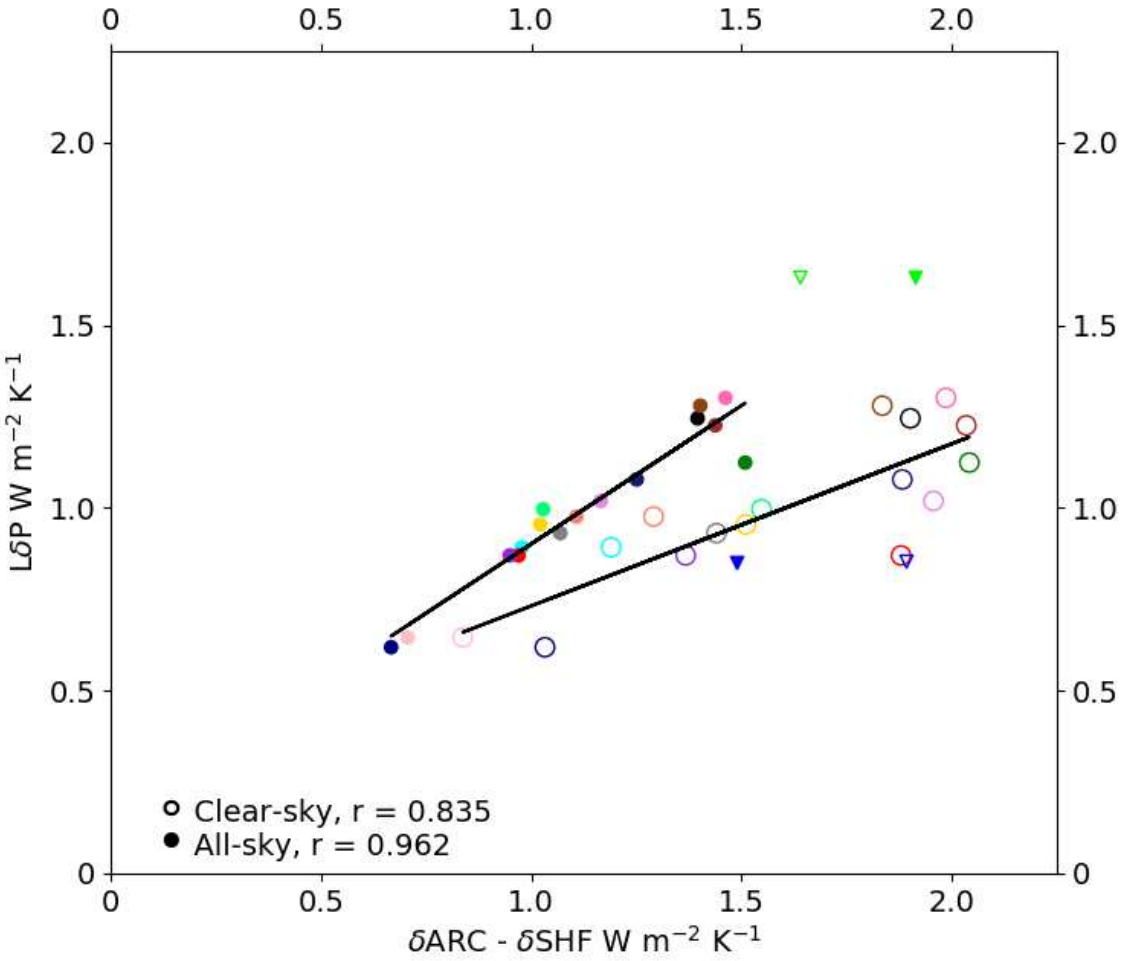

FIGURE 2.6. The normalized global-mean change in the latent heat of precipitation ($L\delta P$) plotted against the normalized change in the clear-sky (open circles) and all-sky (filled circles) net atmospheric cooling, which includes the SHF, for 18 CMIP5 models. Outliers are shown as triangles.

As expected, when δSHF is accounted for in the net change in atmospheric cooling (δARC – δSHF), δSHF acts to increase the atmospheric cooling, and the normalized change in all-sky atmospheric cooling better constrains LδP (Figure 2.6). In fact, the combined δARC_{all} – δSHF shows a strongly correlated (r = 0.96), near one-to-one relationship with LδP. The combined δARC_{all} – δSHF ranges from a minimum of 0.67 W m^{-2} to a maximum of 1.51 W m^{-2} (excluding outliers), closely matching the range in LδP. These results agree with similar findings from Myhre et al. (2018), who find that in the RCP8.5 scenario, the inclusion of δSHF in the normalized change of atmospheric cooling also produces a near one-to-one relationship with LδP. They show that this holds for a range of scenarios, including those with increased aerosol concentrations which lead to global cooling, and particularly for the fast precipitation response. Whereas the change in the all-sky atmospheric cooling more closely matches the change in precipitation, the change in clear-sky atmospheric cooling (δARC_{clr} – δSHF) far exceeds the change in precipitation. The contribution of δSHF to the clear-sky atmospheric cooling and all-sky atmospheric cooling for each model is shown in Figure 2.7.

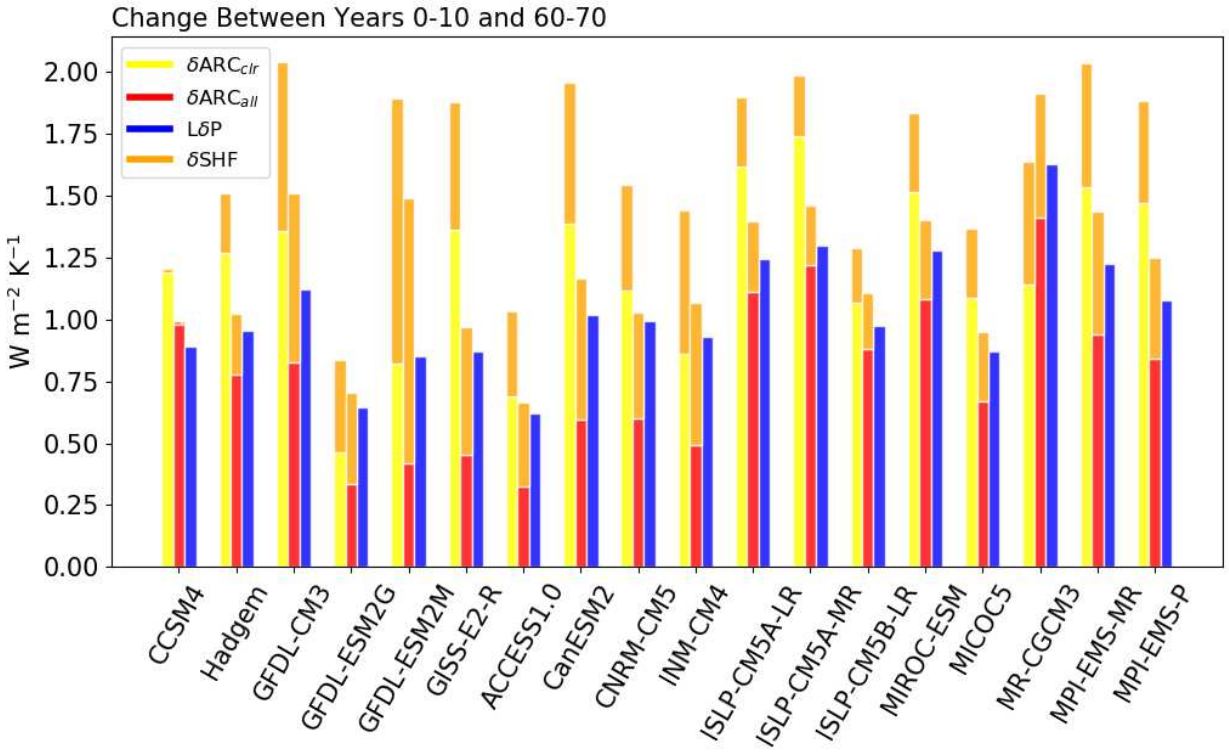

FIGURE 2.7. Bar chart showing the relative contributions of the clear-sky (yellow) and all-sky (red) δARC and the δSHF (orange) to the normalized change in the net clear-sky and all-sky atmospheric cooling for each of the 18 CMIP5 models used. These changes are compared to the change in the latent heat of precipitation (LδP) (blue).

Do the changes in CREs on the ARC balance the changes in the SHF? In Figure 2.8, δSHF is plotted against δCRE (calculated as $\delta ARC_{all} - \delta ARC_{clr}$). Although δSHF and δCRE do not correlate strongly, the magnitude of a given δCRE is noticeably larger than its associated δSHF. A strong correlation is not be expected, however, given (a) the imperfect constraint of δARC_{clr} alone on hydrologic sensitivity, and (b) the lack of an apparent physical basis for why δCRE would balance with δSHF. Because δARC_{all} overestimates LδP to a greater extent than the combined δARC_{clr} – δSHF, we do not expect δCRE and δSHF to balance each other

completely, although they are shown to partially compensate one another. Instead, this suggests that the "better" constraint of δARC_{clr} (as opposed to δARC_{all}) on LδP is coincidental.

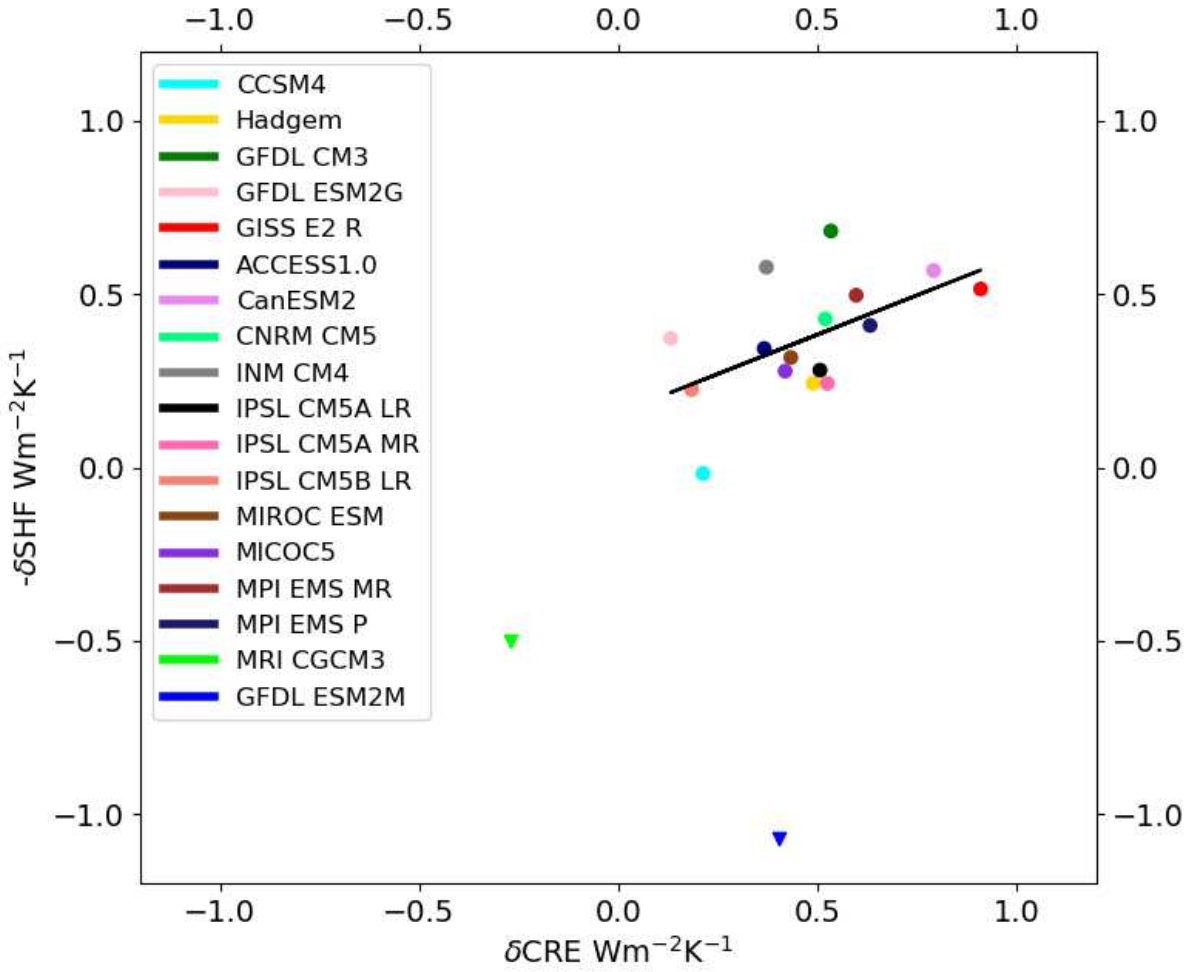

FIGURE 2.8. The normalized change of the sensible heat flux plotted against the normalized change of the cloud radiative effect on the ARC for 18 CMIP5 models. Outliers are shown as triangles.

2.4 DISCUSSION

The energetic constraint on hydrologic sensitivity is well established, however, the extent to which the balance between LδP, δARC, and δSHF can be reduced to its dominant components has been debated. Often, these simplified balances between precipitation and atmospheric radiative cooling disregard δSHF, the contribution of the CRE to δARC, or both.

For example, several studies (Lambert and Webb, 2008; Pendergrass and Hartmann, 2014) have emphasized the strong correlation between clear-sky δARC and LδP with warming. The uncertainties associated with cloud observations, combined with the notorious inter-model variability of cloud feedbacks in simulations (Soden and Held, 2006), certainly motivate a desire to exclude the influence of CREs on the energy balance. Furthermore, when radiative cooling alone is used to constrain hydrologic sensitivity, the clear-sky δARC appears to match the change in precipitation better than the all-sky δARC (Figure 2.3). Although the changes in the global-mean clear-sky ARC *appear* to fit the changes in global-mean precipitation, this constraint is incomplete and does not share the full picture.

By focusing not only on radiative changes, but also on the contribution of δSHF to the energetic constraint on hydrologic sensitivity, we find that contrary to previous studies, changes in the all-sky ARC are the most useful constraint on changes in the global hydrologic cycle, *when the change in the sensible heat flux is accounted for.* Although CREs reduce the change in the ARC, those reductions are compensated by reductions in the upward surface SHF which act to increase atmospheric cooling.

The extent to which the SHF is accounted for in this balance has typically left much to be desired, with SHF contributions often glossed over and left unquantified. The assumption that in response to warming, δSHF is negligible, persists, despite that this has repeatedly

shown not to be true. By including δSHF, as well as the CRE on δARC, we are able to obtain a more accurate and thorough representation of the energetic constraint on changes in the global hydrologic cycle. That the full expression of atmospheric cooling—including the CRE and the SHF—is a better constraint on hydrologic sensitivity (Figure 2.6) is not surprising, and indeed, it would be worrisome if the energy budgets of the models were shown not to balance. Rather, these results emphasize that the neither the CRE on δARC, nor the δSHF are negligible quantities in the energetic constraint on hydrologic sensitivity.

Although δSHF and the CRE on δARC do partially compensate for one another, the comparison of δSHF and the CRE on δARC (Figure 2.8) shows that δCRE and -δSHF are not well correlated, and this is not surprising. A stronger correlation likely exists between δSHF and LδP, which are connected through the surface energy balance, although an exploration of that relationship is beyond the scope of this study.

In a study using a simple radiative-convective equilibrium model, the surface latent heat flux is shown to increase with warming at the expense of the surface SHF (Takahashi, 2009). Similar results are found when the surface energy budget is used instead of the more commonly used atmospheric energy budget (Lorenz et al., 2010). More recently, the surface energy budget approach has been used by Siler et al. (2018) to illuminate the partitioning of the surface latent heat flux (LHF) and the SHF. They find that the LHF and the SHF respond to a combination of changes in the ARC, the near-surface air temperature, and the rate in oceanic heat storage.

The inter-model spread of the change in the SHF is large, and even includes some disagreement over the sign of the change due to warming, with one outlier model projecting a slight increase in the surface SHF when all others project a reduction. Therefore, the surface

budget approach could be useful in reducing the uncertainty between models around the change in the surface SHF with warming. Of course, the change in the SHF is only one of several factors that remain uncertain, and the change of the CRE on the ARC has plenty of potential to be further constrained. However, the surface energy budget approach can be used to complement the traditional atmospheric energy budget approach, and taken together, can be useful in further constraining hydrologic sensitivity.

CHAPTER 3

BRIDGE: PRECIPITATION VARIABILITY

Chapter 2 examined the role of cloud radiative effects (CREs) on the global mean precipitation change in response to warming. Although it is both important and necessary to understand changes in the global mean, this measure fails to provide a meaningful representation of how the impacts of precipitation on the environment and society will change in the future, given that such changes are felt locally, not globally. To that end, broad regional projections of precipitation changes—for example, the wet-get-wetter paradigm (Held and Soden, 2006)—are somewhat more useful. Changes in spatial and temporal precipitation variability, on the other hand, are highly relevant to society, but research on the subject is lacking. Precipitation variability provides a means of connecting (extreme) wet and dry events, which, for example, are relevant to flooding and agricultural drought. Therefore, an examination of the changes in extreme precipitation with warming—a topic that has received ample attention—can facilitate an understanding of the response of precipitation variability to warming.

Trenberth (1999) proposed that extreme precipitation will increase with increasing greenhouse gas (GHG) concentrations. The reasoning is straightforward: increasing GHG concentrations increase downwelling longwave radiation at the surface. This raises surface temperatures, which increase evaporation rates and results in an exponential increase in specific humidity by approximately 6.5% K^{-1}, as dictated by the Clausius-Clapeyron relation. This ultimately leads to an increase in atmospheric moisture availability and can result in more intense local precipitation events and higher local precipitation rates. Early projections

using general circulation models (GCMs) supported this hypothesis and showed increases in extreme precipitation rates with warming surface temperatures (Meehl et al., 2000; Allen and Ingram, 2002). Since then, increases in extreme precipitation have consistently been found in more recent projections from the Fifth Coupled Model Intercomparison Project (CMIP), and furthermore, some regional observations show an amplified response in extreme precipitation changes compared to models (Myhre et al., 2019).

Of course, changes in extreme precipitation are not driven by changes in moisture availability alone, as evidenced by the sub-Clausius-Clapeyron scaling of extreme precipitation in the extratropics (e.g. O'Gorman and Schneider, 2009) and super-Clausius-Clapeyron scaling of extreme precipitation in the tropics (e.g. Allen and Ingram, 2002). Although the thermodynamic contribution to extreme precipitation is useful for understanding the general response to warming, the dynamic contribution is necessary to capture the spatial variability of extreme precipitation (Pfahl et al., 2017). The dynamic contribution to precipitation extremes and variability within the context of the large-scale circulation is explored further in Chapter 5.

Precipitation variability, however, reflects more than just changes related to extreme precipitation; it also reflects changes related to the extreme *lack* of precipitation. In CMIP3 and CMIP5 projections, an increase in the fraction of precipitation above the 95th percentile in tandem with increasing wet spell lengths were balanced by an increase in the number of dry days (defined as precipitation less than 1 mm day^{-1}) and the length of dry spells (Giorgi et al., 2011; Giorgi et al., 2014). This pattern is consistent with other CMIP5 analyses showing an increase in the number of both consecutive (Lau et al., 2013; Sillman et al., 2013) and total dry days (Pendergrass and Hartmann, 2014b).

Given the significant societal impacts of both drought and extreme rainfall events, and the role of precipitation variability in linking these two ends of the spectrum, research on precipitation variability has been surprisingly limited in its scope. The majority of studies have focused on interannual variability, particularly in relation to the El Niño Southern Oscillation (e.g. Trenberth et al., 2005). For example, in response to warming, the change in mean precipitation correlates strongly with the change in interannual precipitation variability in the Niño 3.4 and Niño 4 regions (Watanabe et al., 2014). Another emphasis has been on the Madden-Julian Oscillation (e.g. Zhang, 2005), a major source of tropical intraseasonal precipitation variability.

Beyond the tropics, using CMIP3 projections, Seager et al. (2012) found that the interannual variability of *precipitation – evaporation* increases with warming over most of the globe. More recent analyses, however, have shown that the changes in interannual variability with warming are not the same everywhere. He and Li (2019) compared the change of interannual precipitation variability in ascending and descending regions, and found that ascending regions increase by 3.2% K^{-1}, whereas variability decreases slightly by 0.3% K^{-1} in descending regions. A similar spatial pattern of increasing and decreasing variability was shown in Pendergrass et al. (2017), who also found that global precipitation variability increases at about 5% K^{-1} on daily timescales, but only increases at approximately 3% K^{-1} on decadal timescales. As in Myhre et al. (2019), the regional observational changes were found to be much larger than those in CMIP5 projections.

From these studies, several gaps in the understanding of precipitation variability remain. As shown in Pendergrass et al. (2017), the change in precipitation variability is timescale-dependent and increases on shorter timescales. Therefore, the more thoroughly

researched understanding of precipitation variability on interannual and decadal timescales does not necessarily translate to an understanding of intraseasonal or daily precipitation variability. Additionally, the bulk of the research on precipitation variability has a tropical focus, leaving the extratropics largely ignored. Finally, the relationships between atmospheric energy budget components, precipitation extremes, and precipitation variability have thus far been overlooked (Thackeray et al., 2018).

Motivated by prior observational work, we aim to address some of these gaps. Using observations, Naegele and Randall (2019) noticed that clouds tend to reduce atmospheric radiative cooling (ARC) in tropical regions where precipitation and ARC are negatively correlated, and that clouds tend to increase the ARC in extratropical regions where precipitation and ARC are positively correlated. Based on this observation, the following question is raised: Do CREs on the ARC reduce precipitation variability in the tropics and enhance precipitation variability at middle and high latitudes (Figure 3.1)?

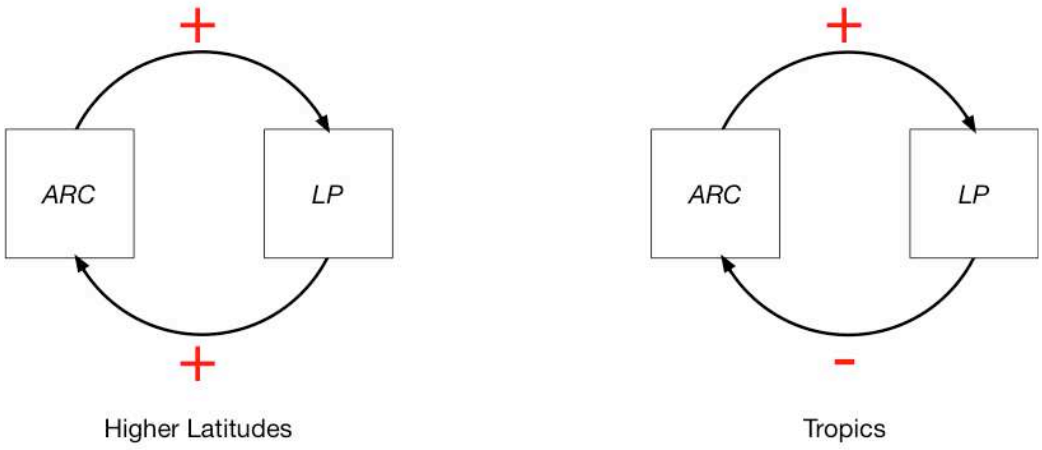

FIGURE 3.1. The positive feedback between atmospheric radiative cooling (ARC) and the latent heat of precipitation (LP) at higher latitudes (left), and the negative feedback in the tropics (right). Figure from Naegele and Randall (2019).

The negative feedback in the tropics stems from the reduction of outgoing longwave radiation—and thus ARC—by precipitating cloud systems, which reduces the energetic demand for precipitation and thus dampens precipitation fluctuations there (Fowler and Randall, 1994). At higher latitudes, the positive feedback is driven by enhanced ARC from precipitating cloud systems which increase downwelling longwave radiation, and can in turn amplify fluctuations in the precipitation there.

To test the temperature sensitivity of these feedbacks, we run a series of idealized global simulations at a range of temperatures, with CREs both turned on and off. An overview of these simulations, the results, and a summary of previous research using idealized simulations to examine the influence of CREs are described in Chapter 4.

CHAPTER 4

THE TEMPERATURE DEPENDENCE OF THE HYDROLOGIC CYCLE RESPONSE TO CLOUD RADIATIVE EFFECTS

4.1 THE USE OF IDEALIZED SIMULATIONS TO STUDY CLOUD RADIATIVE EFFECTS

Numerical simulations have long shown that cloud radiative effects (CREs) impact the climate system, from large-scale atmospheric circulation patterns (e.g. Slingo and Slingo, 1988; Randall et al., 1989; Sherwood et al., 1994) to the hydrologic cycle (Fowler and Randall, 1994). In particular, the influence of the CRE on the overturning tropical circulation has received widespread attention. For example, Harrop and Hartmann (2016) suggest that the radiative effects of clouds acts to enhance the Hadley Circulation in the current climate. Not only do high clouds affect the Hadley Circulation, but the low cloud CRE has been found to increase the overturning circulation as well as tropical precipitation (Fermepin and Bony, 2014).

In the future, however, the Hadley Circulation is expected to weaken with warming (Vecchi and Soden, 2007). This weakening is often attributed to the discrepancy between precipitation increasing at a slower rate than atmospheric moisture with warming (Held and Soden, 2006). Clouds, however, play an important role in the changing Hadley Circulation as well. By "masking" warming in the deep convective region but not in the clear, descending regions, the CRE contributes to a slowing of the circulation (Merlis, 2015).

In a warming climate, CREs influence not only the strength of the Hadley Circulation, but its meridional extent as well (Voigt and Shaw, 2015). Furthermore, the precipitation response to CREs is inconsistent between models, implying that CREs are an important

source of model uncertainty for predictions of precipitation and circulation changes with warming (Voigt and Shaw, 2015). Focusing on the ascending branch of the Hadley Cell, the CRE has been shown to strongly contribute to the meridional shift (Kang et al., 2008; Voigt et al., 2014), strengthening (Popp and Silvers, 2017), and narrowing (Byrne and Schneider, 2016) of the Intertropical Convergence Zone (ITCZ) with warming, all of which have implications for tropical precipitation. Observations of the contraction of the ITCZ (Su et al., 2017) have been suggested as evidence of convective aggregation, and simulations show that both longwave and shortwave CREs are necessary for the evolution and maintenance of convective aggregation (Muller and Held, 2012; Wing and Emanuel, 2014).

The majority of studies looking at the radiative effects of clouds on precipitation and circulation have focused on the tropics, but of course, CREs are not just constrained to low-latitude regions, and they should not be expected to behave similarly in different environments. For example, Li et al. (2015) found that in the extratropics, the response of precipitation to the CRE is opposite of that in the tropics. Outside of the tropics, most attention to the influence of CREs has been placed on changes in midlatitude dynamics via the poleward shift (Ceppi et al., 2012; Ceppi and Hartmann, 2015) and strengthening (Li et al., 2015) of the midlatitude jet, and on changes in the extratropical stormtracks (Albern et al., 2019; Grise et al., 2019).

Not only do CREs affect the circulation, but they affect precipitation variability as well. Cloud radiative effects have been shown to influence moist processes in the tropics (Bony and Emanuel, 2005), variability associated with the El Niño Southern Oscillation (Rädel et al., 2016; Middlemas et al., 2019), and the Madden-Julian Oscillation (Raymond, 2001;

Crueger and Stevens, 2015; Del Genio and Chen, 2015). Again, these studies all focus on tropical variability.

The differences between the tropical and extratropical circulation and precipitation responses to CREs (Li et al., 2015), combined with the relative lack of research on extratropical precipitation variability, motivate a closer look at the differences in the response of tropical and extratropical precipitation variability to CREs. Naegele and Randall (2019) hypothesized that CREs reduce precipitation variability at low latitudes and that CREs enhance precipitation variability at high latitudes. The opposite signs of the negative feedback between atmospheric radiative cooling (ARC) and precipitation in the tropics and the positive feedback in the extratropics is likely due to the different surface temperatures in those regions: warm in the tropics, and cool at higher latitudes.

In this chapter, we use a series of idealized simulations to investigate the temperature dependence of precipitation variability in response to CREs. These results focus on the response of the hydrologic cycle to CREs, and the accompanying circulation response will be examined in Chapter 5.

4.2 MODEL AND SIMULATIONS

The simulations presented in this study use SP-CAM, the super-parameterized version of the NCAR Community Atmosphere Model (CAM4). The super-parameterization is the two-dimensional cloud-resolving model in each grid cell that replaces the conventional parameterizations (Khairoutdinov and Randall, 2001).

Our focus on precipitation variability compels the use of a model that can most accurately capture the salient features of the precipitation distribution, including extreme

precipitation. The inter-model spread of extreme precipitation rates can be attributed to the inter-model spread of upward velocities, which is a result of the different moist convective parameterizations used (O'Gorman and Schneider, 2009; Wilcox and Donner, 2007). SP-CAM resolves convection instead of parameterizing it, and in theory, this should produce more accurate extreme precipitation rates. Indeed, SP-CAM has been found to simulate more realistic extreme and light precipitation rates (Kooperman et al., 2016), as well as the dominant modes of precipitation variability, including the Madden-Julian Oscillation (Benedict and Randall, 2009; Arnold and Randall, 2015).

SP-CAM was run with an approximate 1°×1° horizontal grid-spacing and 26 vertical levels. Rotation is included. The cloud-resolving model uses a single-moment microphysics scheme. There is no diurnal or seasonal cycle and the solar insolation is fixed at 650 W m^{-2} with a solar zenith angle of 50.5°, following Bretherton et al. (2005) and others. An aquaplanet configuration is used for all simulations, meaning that the globe is covered with water everywhere.

In the initial set of simulations, sea surface temperatures (SSTs) are prescribed uniformly at 280, 290, and 300 K, and we simulate a state of radiative-convective equilibrium in a rotating framework. At each temperature, simulations were run in which cloud radiative effects were both included and turned off. The cloud radiative effect is turned off by making clouds transparent in the radiation code; some studies refer to this method as the COOKIE (Cloud On-off Klimate Intercomparison Experiment) approach (e.g. Stevens et al., 2012). In the second set of simulations, the shortwave and longwave CREs were turned off individually at each temperature. In the final set of experiments, an idealized equator-pole SST gradient was imposed (Figure 4.1).

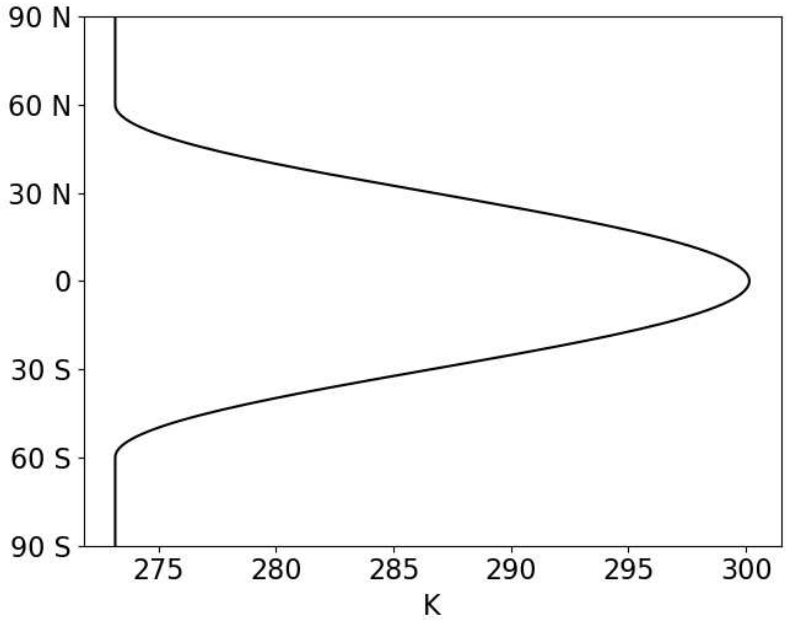

FIGURE 4.1. The zonally uniform, equatorially symmetric idealized SST profile used in the third set of simulations.

The fixed SST simulations were each run for 300 days. The simulations with a meridional SST gradient were run for 16 months. In all simulations, the model equilibrates by day 100, and in all analyses where the temporal mean is taken, only days after 100 are used.

4.3 RESULTS

4.3.1 SIMULATIONS WITH UNIFORM SSTs

PRECIPITATION. In the attempt to understand the influence of the CRE on hydrologic cycle variability, a look at the precipitation distribution is an appropriate place to start. For each SST, distributions of the daily precipitation rate are shown by the percentage of global area covered in Figure 4.2. In all simulations, the vast majority of the globe does not receive

precipitation on any given day. The maximum precipitation rates, however, increase rapidly with warming SSTs. At 280 K, the CRE reduces the area covered by low precipitation rates, but the CRE steadily increases both the occurrence of heavy precipitation, as well as the rate of extreme precipitation. This pattern reverses at 300 K, so that the CRE reduces not only the area over which high precipitation rates occur, but also the rates associated with extreme precipitation. The opposite influence of the CRE on extreme precipitation rates at cool and warm temperatures is shown more concisely in Table 4.1. At 290 K, the CRE on extreme precipitation is neither as strong, nor as consistent as at 280 and 300 K.

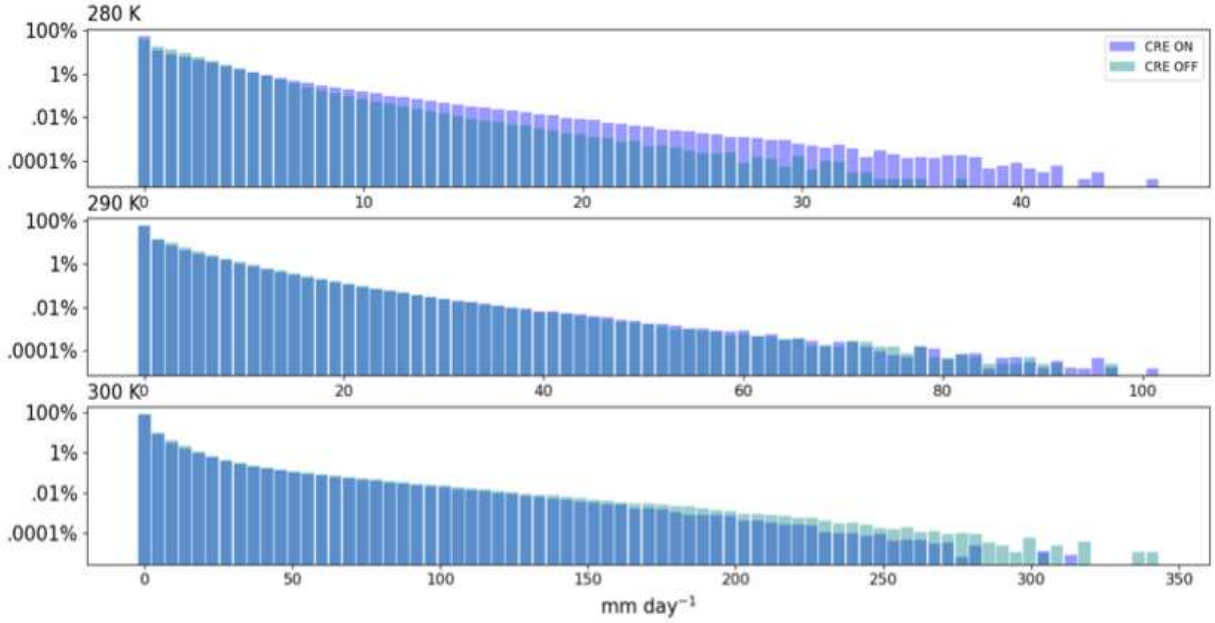

FIGURE 4.2. The daily precipitation distributions for SSTs of 280, 290, and 300 K. The distributions with CREs on (purple) and CREs off (teal) are overlaid, so that areas of overlap are shown in blue. The vertical axis shows the percentage of the globe covered (by area) for each bin. Note the different scales on the horizontal axes.

TABLE 4.1. The precipitation rate (mm day^{-1}) associated with extreme (90th, 99th, and 99.9th) percentiles for simulations at 280 and 300K, with CREs on and CREs off.

	90%	**99%**	**99.9%**
280 ON	11.84	21.35	23.69
280 OFF	9.78	15.81	17.44
300 ON	72.34	146.1	161.7
300 OFF	81.36	163.8	181.8

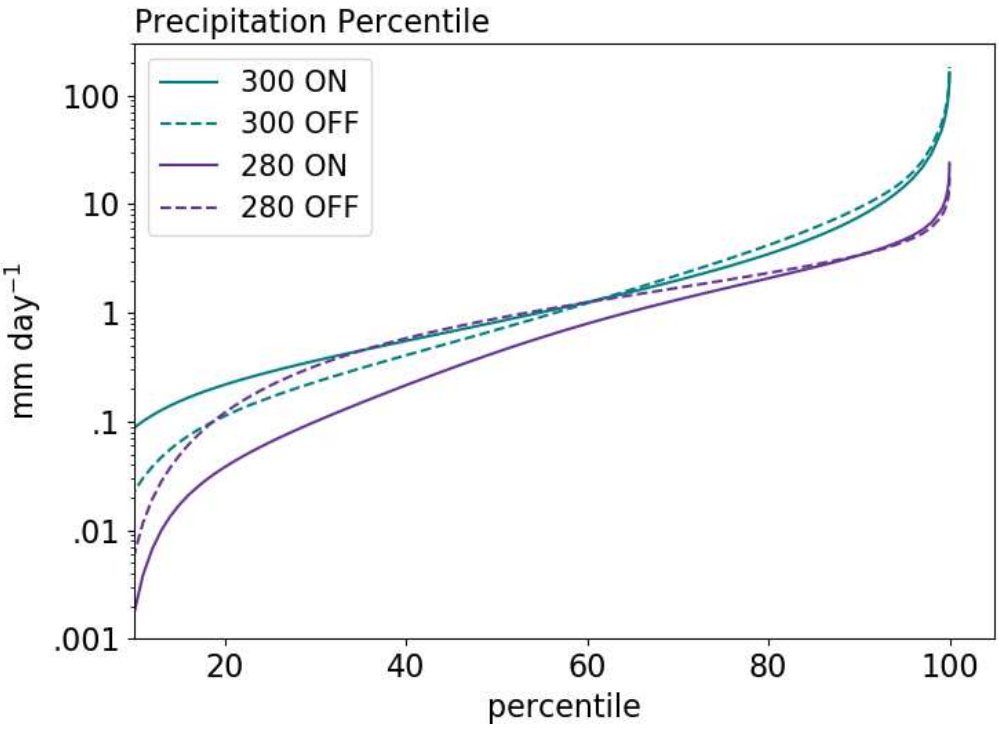

FIGURE 4.3. The daily precipitation rate associated with each percentile (above the 10th) for simulations at 280 (purple) and 300 K (teal), with CREs on (solid) and CREs off (dashed).

As shown in Figure 4.3, the influence of the CRE on extreme precipitation is not necessarily the same for low-to-mid precipitation rates. Although the CRE enhances extreme precipitation at 280 K, at most percentiles, the CRE actually reduces the precipitation rate; the opposite is true at 300 K. The influence of the CRE over the majority of the distribution is reflected in the zonal means, and the influence of the CRE on extreme precipitation is reflected in the standard deviation (Figure 4.4).

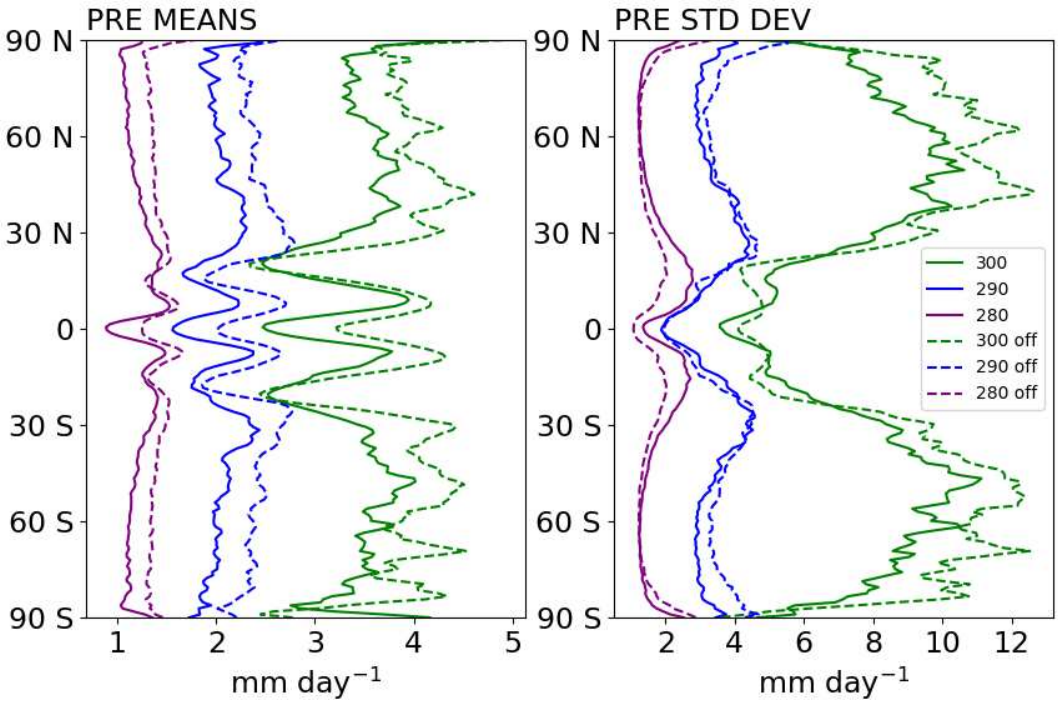

FIGURE 4.4. The zonal mean (left) and zonal standard deviation (right) of the daily precipitation rate for SSTs of 280 (purple), 290 (blue), and 300 K (green) with CREs on (solid) and CREs off (dashed).

As expected, the zonal-mean precipitation increases with warming, and the sensitivity to temperature increases with warming as well. In these simulations with uniform SSTs, it is important to note that the meridional structure is influenced by circulation changes due to rotation alone, and not by changes in SST with latitude. A notable meridional pattern is the set of three tropical minima in zonal-mean precipitation centered at the equator; warming enhances these minima and shifts them poleward. The three tropical minima are separated by maxima on either side of the equator, which are indicative of double ITCZs, although tropical rain bands might be a more appropriate term in these idealized simulations. At all SSTs, the CRE reduces the zonal-mean precipitation at nearly all latitudes, and this reduction is enhanced with warming.

The standard deviation is one measure of variability, and the standard deviation of the precipitation rate around latitude circles is shown in the right panel of Figure 4.4. Excluding the poles, the highest daily precipitation variability occurs in the tropics at 280 K, whereas at 290 K, the highest variability occurs near 30° N and S. At 300 K, high variability occurs over a large portion of the extratropics. Unlike the zonal-mean precipitation, the influence of the CRE on the precipitation variability is temperature dependent. At 280 K, the CRE primarily enhances precipitation variability. In the warmer simulations, the primary influence of the CRE is to reduce precipitation variability. This effect is small at 290 K and is seen at high latitudes, whereas at 300 K, the CRE significantly reduces the variability throughout the extratropics. To better understand why the influence CREs on precipitation variability is strongest in the tropics at 280 K but in the extratropics at 300 K, it is helpful to look at maps of the precipitable water (PW).

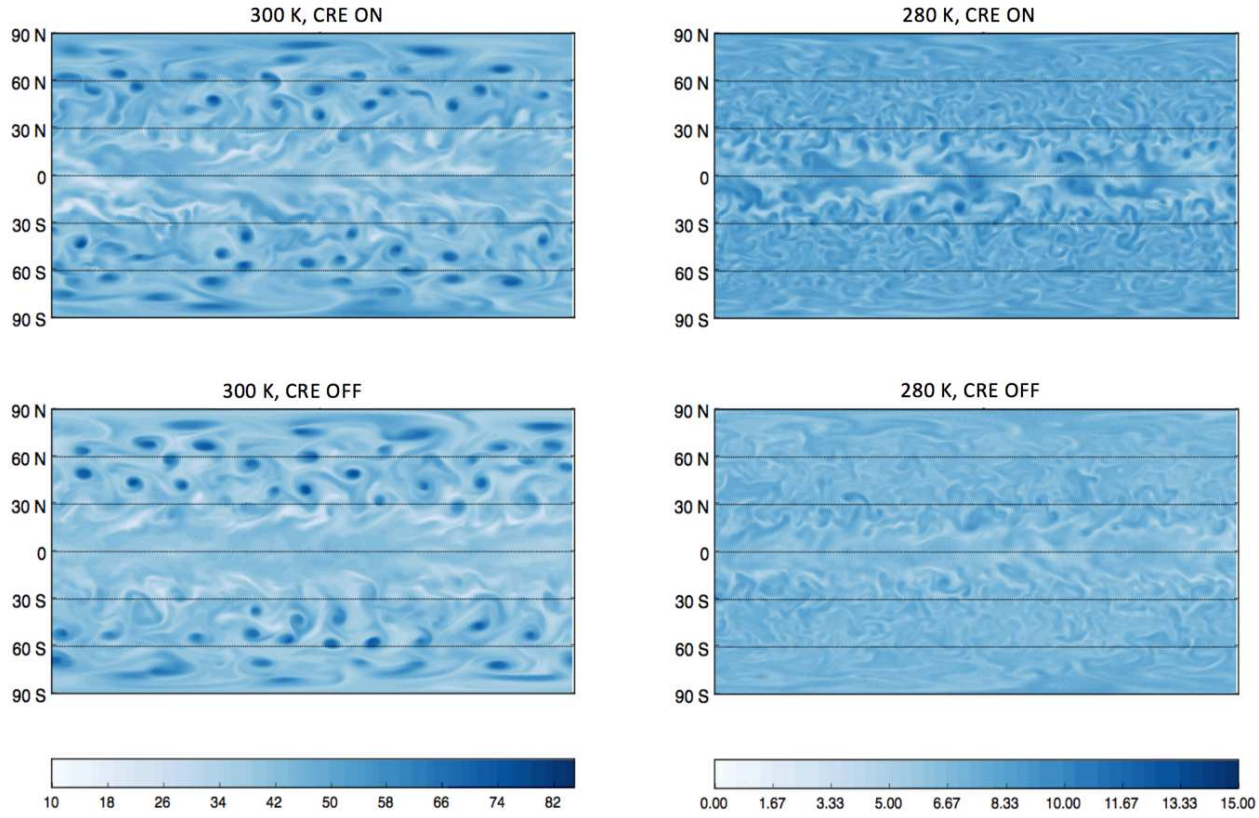

FIGURE 4.5. Maps of the precipitable water (mm day^{-1}) at day 150 for SSTs of 280 (right) and 300 K (left), with CREs on (top) and CREs off (bottom). Note the different scales for the different SSTs.

TABLE 4.2. The coefficient of variation (CoV) of the precipitable water for SSTs of 280 and 300 K, with CREs on and CREs off.

	PW CoV
280 ON	.124
280 OFF	.090
300 ON	.141
300 OFF	.146

PRECIPITABLE WATER. Comparing maps of the PW (Figure 4.5), a striking—but not surprising—difference between SSTs is that moisture becomes more organized with warming. At 300 K, "tropical" cyclones develop and move to high latitudes, where the Coriolis parameter is large. Similar global simulations of RCE in a rotating environment in previous studies have been shown to evolve into a "tropical cyclone world" (Khairoutdinov and Emanuel, 2013; Shi and Bretherton, 2014; Reed and Chavas, 2015). These "tropical" cyclones have been interpreted as manifestations of convective aggregation in a rotating environment, and convective aggregation has been shown to occur only at warm temperatures (Khairoutdinov and Emanuel, 2010; Wing and Emanuel, 2014), which may explain why cyclones don't develop in the cool simulation.

The coefficient of variation—defined as the standard deviation normalized by the mean—of the precipitable can be used to measure the degree of organization (Naegele, 2016). The coefficient of variation shows that the CRE slightly reduces organization at 300 K, but enhances organization at 280 K (Table 4.2). This effect can be seen in the map of precipitable water at 280 K, where the spatial distribution of PW—especially near 20° N and S—is noticeably more homogenous when the CRE is turned off, but is harder to see at 300 K (Figure 4.5).

Distributions of the PW (as the percentage of global area covered) are shown in Figure 4.6, and do not resemble the distributions of precipitation (Figure 4.2). Unlike precipitation, PW varies smoothly in both space and time. At all temperatures, the CRE causes the PW distribution to shift to the right, increasing both the mean and the maximum PW. This shift occurs because clouds warm the atmosphere (Figure 4.9), which increases column moisture. The (relative) effect is largest at 280 K, where clouds strongly enhance

downwelling longwave radiation in the cool, dry environment (Figure 4.14). Not only does the CRE cause the distribution to shift, but it also increases the width of the distribution, particularly at 280 K.

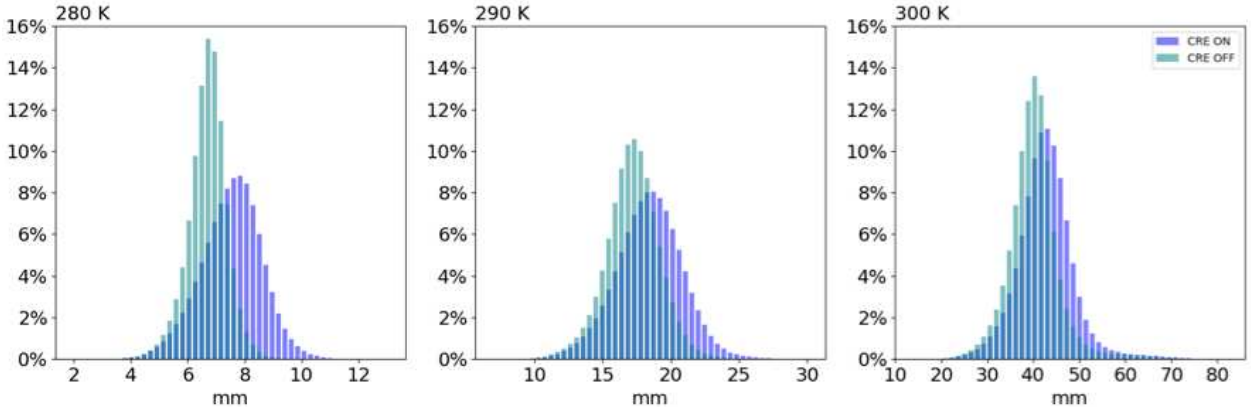

FIGURE 4.6. The daily precipitation distributions for SSTs of 280, 290, and 300 K. The distributions with CREs on (purple) and CREs off (teal) are overlaid, so that areas of overlap are shown in blue. The vertical axis shows the percentage of the globe covered (by area) for each bin. Note the different scales on the horizontal axes.

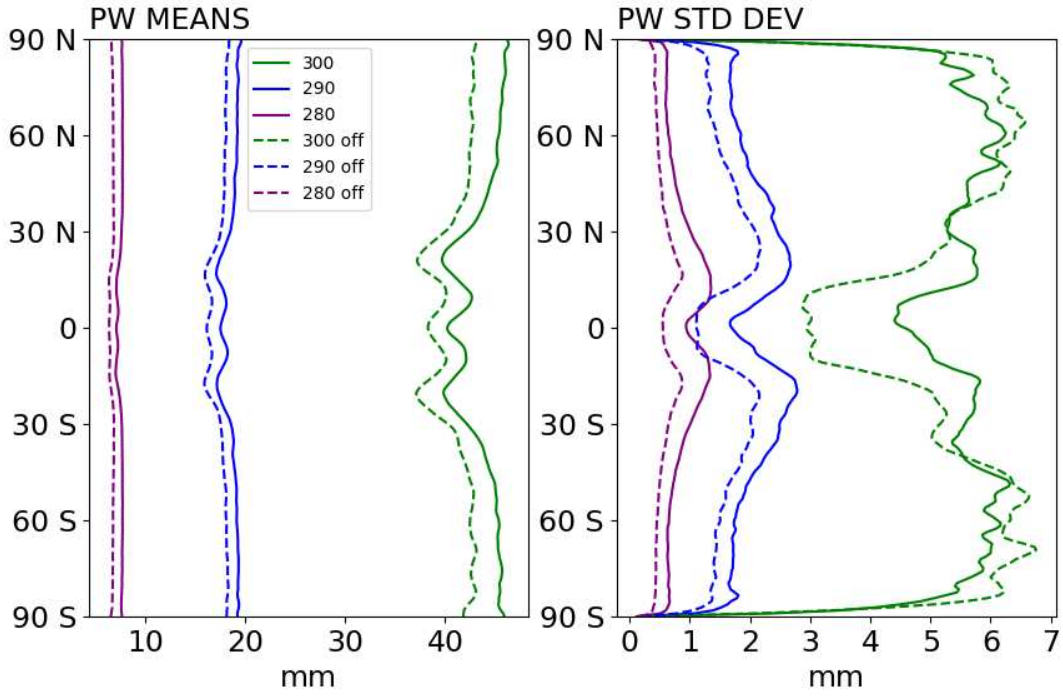

FIGURE 4.7. The zonal mean (left) and zonal standard deviation (right) of the precipitable water for SSTs 280 (purple), 290 (blue), and 300 K (green) with CREs on (solid) and CREs off (dashed).

Figure 4.7 shows the zonal mean and zonally averaged standard deviation of PW. Compared to the precipitation rate, the meridional structure of the zonal-mean PW is smoother, again due to its spatially continuous nature. As seen in the zonal means, PW is highly dependent on the surface temperature, and the exponential increase of PW with warming temperatures is expected from the Clausius-Claperyon relation. Reflecting the PW distributions in Figure 4.6, the zonal means show that the CRE increases the PW at all SSTs and at all latitudes. The influence of the CRE on zonal-mean PW is strongest at 300 K, because for a given change in the ARC due to clouds, that change will disproportionately affect the PW at higher temperatures.

Because PW is dependent on temperature, its variability generally increases with warming, and thus the CRE on variability increases with warming as well. Whereas the CRE increases variability everywhere at 280 and 290 K (as implied by Figure 4.6, but shown explicitly in Figure 4.7), the CRE increases PW variability only at lower latitudes in the 300 K simulation, and reduces variability at higher latitudes[1]. The influence of the CRE on PW variability shown here reflects the influence of the CRE on convective organization (Figure 4.5), especially at 300 K, where the enhanced tropical variability with CREs on corresponds to existence of extreme dry patches.

CLOUDS AND RADIATION. Zonal means of the cloud fraction are shown in Figure 4.8. Interestingly, unlike precipitation and PW, cloud fraction does not change monotonically with temperature, except for the mid-level cloud fraction. For example, the zonally averaged low cloud fraction is low at 290 K, with 300 K having the highest fraction at high latitudes, and 280 K having the highest fraction in the tropics. In all panels, the double ITCZs are marked by cloud fraction maxima on either side of the equator.

The influence of the CRE on the ARC is shown in Figure 4.9. Like the hydrologic variables, the ARC increases with SST, as does its sensitivity. This response to warming reflects the PW response to warming, since shortwave absorption by water vapor increases with SST and so does longwave cooling (Figure 4.12). The CRE reduces the zonal-mean ARC at all SSTs, especially just off of the equator where the double ITCZs are located. The

[1] Note that the strong change in the variability at 300 K with latitude near the poles is likely an artifact of the latitude-longitude grid used by the finite volume dynamical core. It could also be due to the fact that a latitude band of given width has much less area near the poles, compared to lower latitudes. This applies to polar extremes shown in other figures as well.

variability of the ARC is predominantly driven by clouds, as shown by the grouping of the CRE-on and CRE-off simulations. Second to the influence of the CRE, ARC variability increases with SST.

The ARC can be decomposed into shortwave and longwave (Figure 4.11) contributions, such that their sum is equal to the total ARC (Figure 4.9). The shortwave contribution warms the atmosphere and reduces the total ARC, and the magnitude of the shortwave contribution increases with SST. Clouds enhance the shortwave contribution to the total ARC, and the magnitude of the CRE on the shortwave contribution decreases with warming. Although clouds increase upper level shortwave heating more strongly at 300 K than at 280 K, clouds reduce shortwave heating throughout the lower half of the troposphere at 300 K, so that the net CRE on the shortwave contribution is smaller at the warm SST (Figure 4.10).

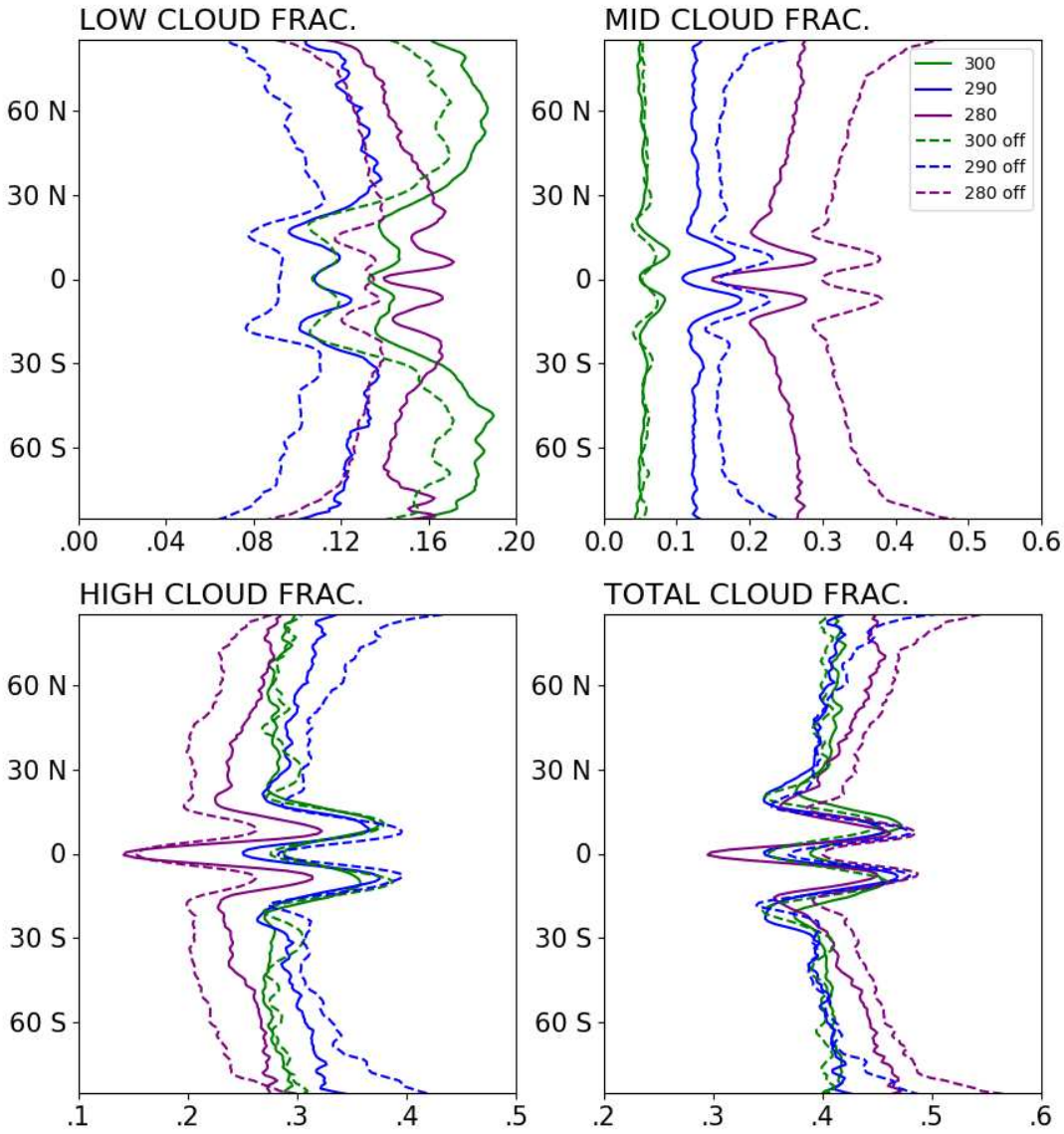

FIGURE 4.8. The zonally averaged low, mid, high, and total cloud fraction for SSTs of 280 (purple), 290 (blue), and 300 K (green) with CREs on (solid) and CREs off (dashed).

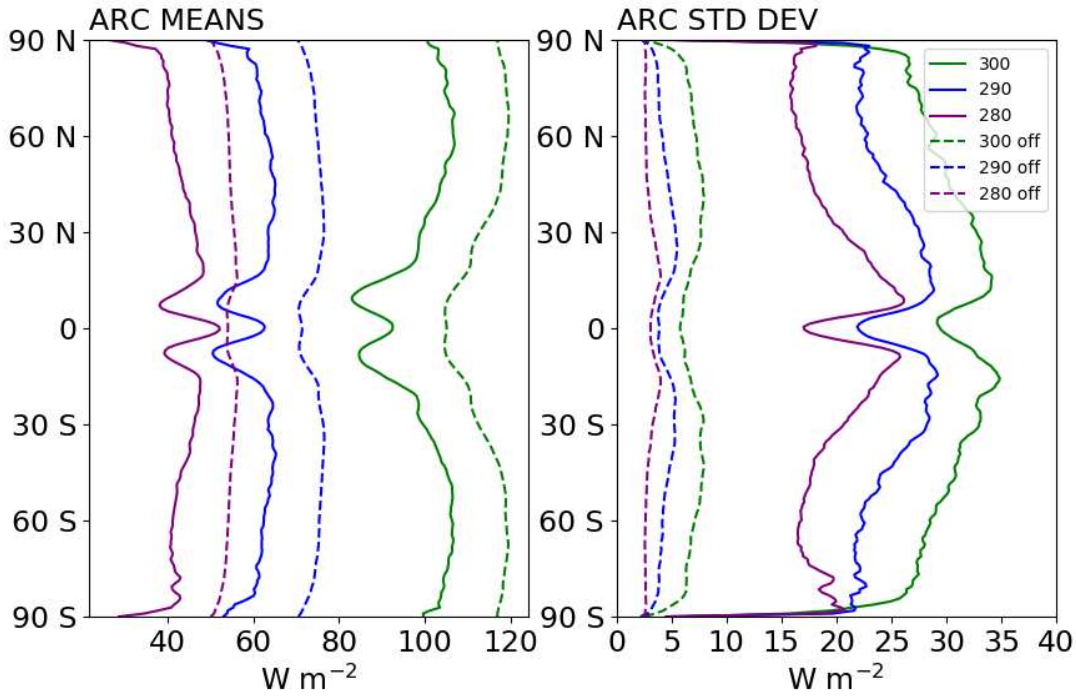

FIGURE 4.9. The zonal mean (left) and zonal standard deviation (right) of the ARC for SSTs of 280 (purple), 290 (blue), and 300 K (green) with CREs on (solid) and CREs off (dashed).

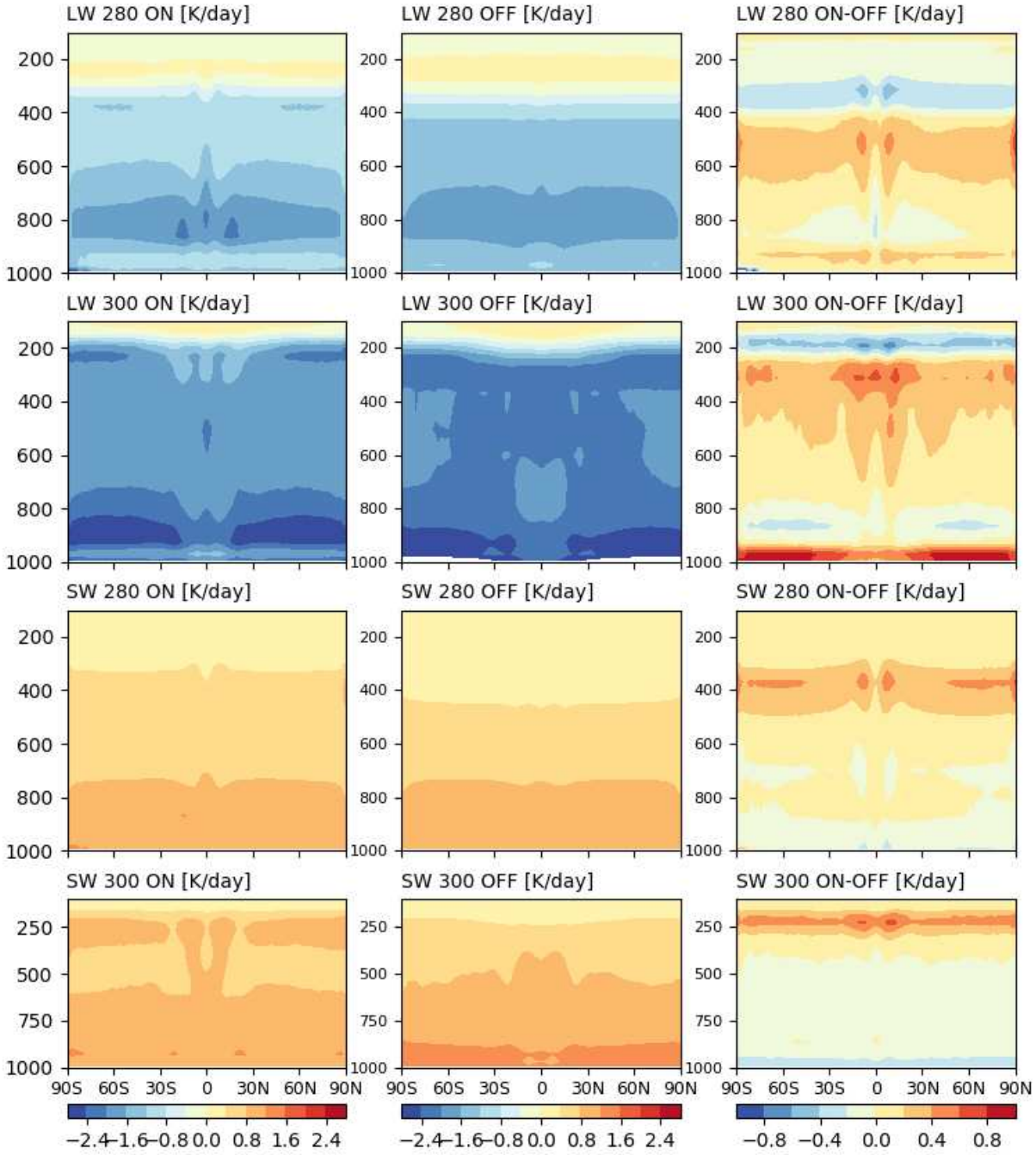

FIGURE 4.10. Vertical profiles of the zonally averaged longwave (LW) and shortwave (SW) radiative heating rates for SSTs of 280 and 300 K. The left column shows CREs on, the middle column shows CREs off, and the right column shows the difference.

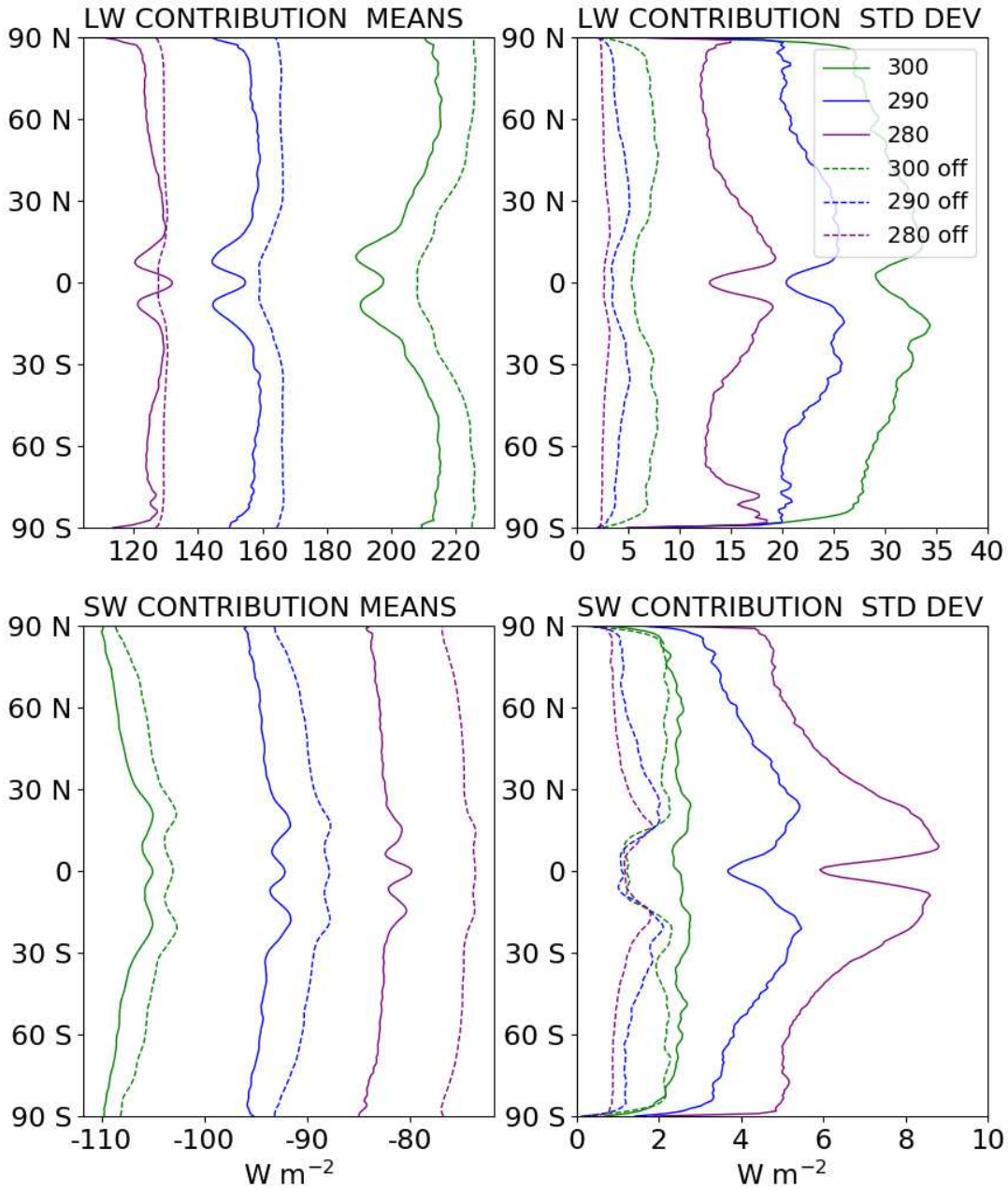

FIGURE 4.11. The zonal mean (left) and zonal standard deviation (right) of the longwave contributions to the ARC (top) and shortwave contribution to the ARC (bottom) for SSTs of 280 (purple), 290 (blue), and 300 K (green) with CREs on (solid) and CREs off (dashed).

Comparison of the zonal-mean total ARC (Figure 4.9) to its longwave contribution shows that the meridional structure of the total ARC is largely determined by the longwave contribution. The CRE reduces the zonal-mean longwave contribution, and the magnitude of the reduction increases with warming. This can be explained by comparing the longwave heating rates for the cool (280 K) and warm (300 K) SSTs. Figure 4.10 shows that throughout most the troposphere, although the longwave cooling rate is stronger when CREs are turned off at both 280 and 300 K, the difference is much stronger at the warmer SST. The variability of the total ARC is dominated by the CRE on the longwave contribution, and more so at the higher SSTs.

The longwave contribution to the total ARC can be further decomposed into the outgoing longwave radiation (OLR) at the top of the atmosphere and the downwelling longwave radiation at the surface (Figure 4.12). The upwelling longwave radiation at the surface also contributes to the total ARC, but this flux is constant because of the prescribed uniform SSTs and so is not shown. As expected, the OLR increases with warming, and clouds act to strongly reduce the OLR. Notably, the reduction of the OLR by the CRE is stronger than the reduction due to the 10 K changes in the SST. Additionally, variability in the OLR is almost entirely due to the CRE, and increases with warming.

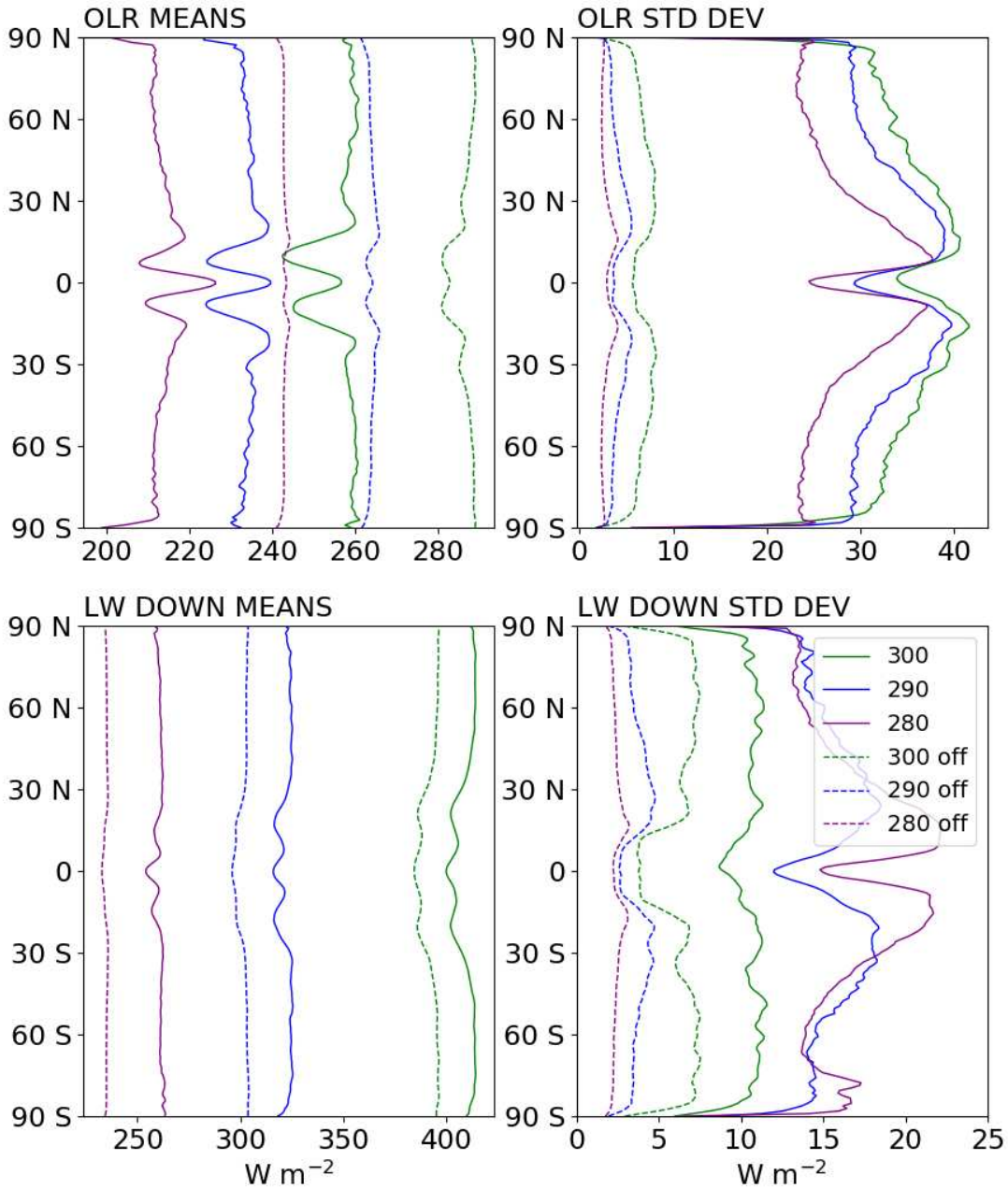

FIGURE 4.12. The zonal mean (left) and zonal standard deviation (right) of the OLR (top) and downwelling longwave flux at the surface (bottom) for SSTs of 280 (purple), 290 (blue), and 300 K (green) with CREs on (solid) and CREs off (dashed).

The largest contribution to the ARC is the downwelling longwave flux at the surface. The surface downwelling longwave radiation increases strongly with warming, although the magnitude of the CRE on surface downwelling longwave radiation decreases with warming. This is expected given that the increased downwelling longwave radiation from clouds is partially masked by the downwelling longwave radiation from increased water vapor at warmer SSTs with higher humidity. Like the OLR, the variability of the downwelling longwave flux is also primarily driven by the CRE, but to a much lesser extent than the OLR, especially at 280 K.

4.3.2 SEPARATING THE LONGWAVE AND SHORTWAVE CRE

In the second set of experiments, shortwave and longwave CREs were switched on or off individually. Figure 4.13 replicates Figure 4.9 but also shows the influence of the longwave-only CRE on the zonally averaged ARC (top panels). At 280 K, simulations with the longwave-only CRE closely resemble those with the total CRE in the deep tropics, but differ at high latitudes where the longwave-only CRE acts to enhance the ARC. This can be attributed to the increased longwave cooling at high latitudes in the lower troposphere when only the longwave CRE is active (Figure 4.14 compared with Figure 4.10). At 300 K, the longwave CRE enhances the total CRE on the ARC due to reduced longwave cooling in the upper troposphere. At 290 K, the longwave-only CRE closely resembles the total CRE on the ARC.

The bottom panels of Figure 4.13 show that when the shortwave-only CRE is active, the meridional structures of both the zonal mean and zonal standard deviation of the ARC are similar to those when the total CRE is turned off. Figure 4.15 shows that the

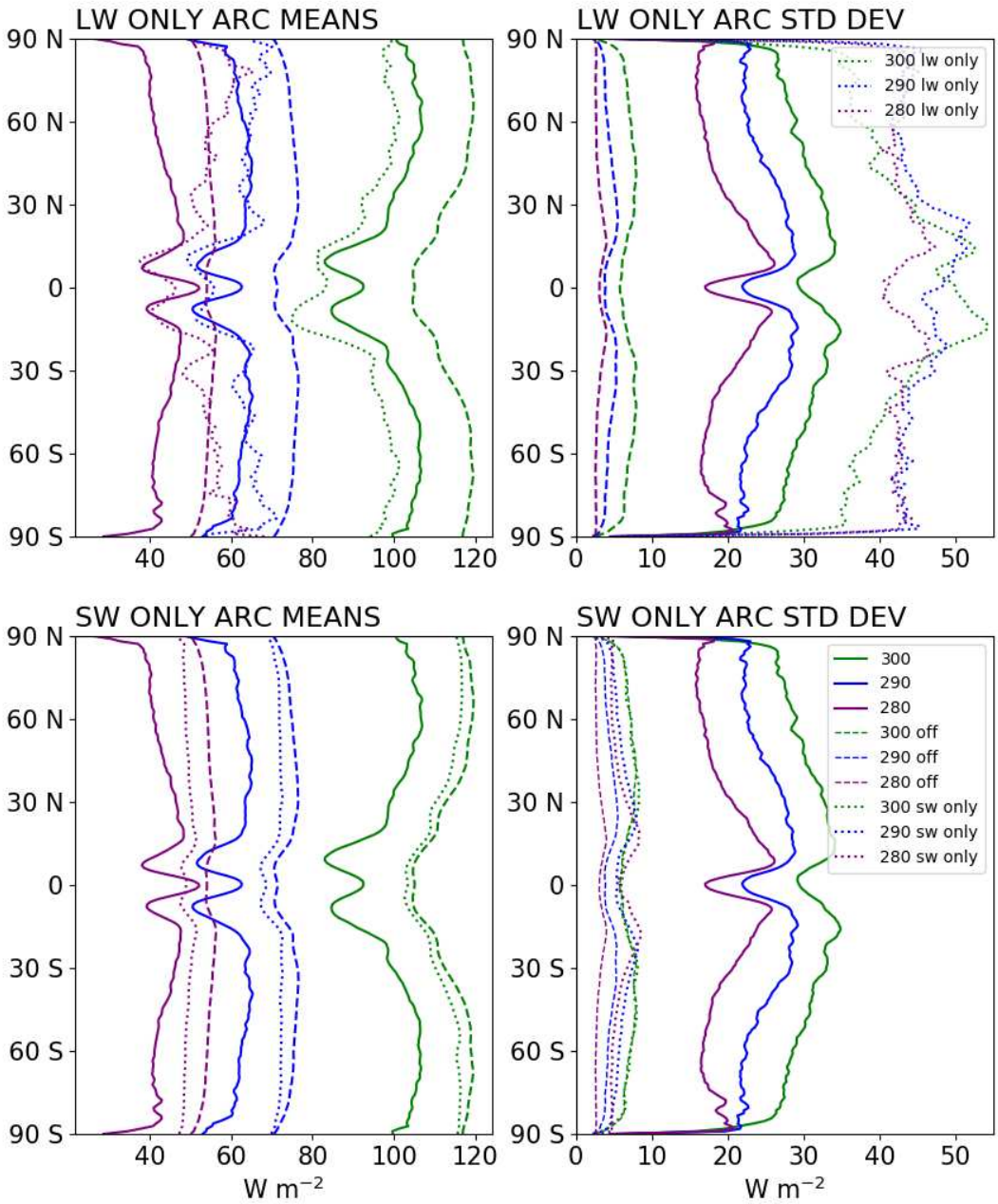

FIGURE 4.13. The zonal mean (left) and zonal standard deviation (right) of the ARC for SSTs of 280 (purple), 290 (blue), and 300 K (green) with CREs on (solid) and CREs off (dashed). The top panels also include the longwave-only CRE on the ARC (dotted), and the bottom panels also include the shortwave-only CRE on the ARC (dotted).

shortwave CRE has only a small influence on the radiative heating rates. At all temperatures, the magnitude of the shortwave CRE is smaller than the total CRE on ARC, and the magnitude of the shortwave CRE is largest at 280 K. At all temperatures, the variability of the ARC is dominated by the longwave CRE.

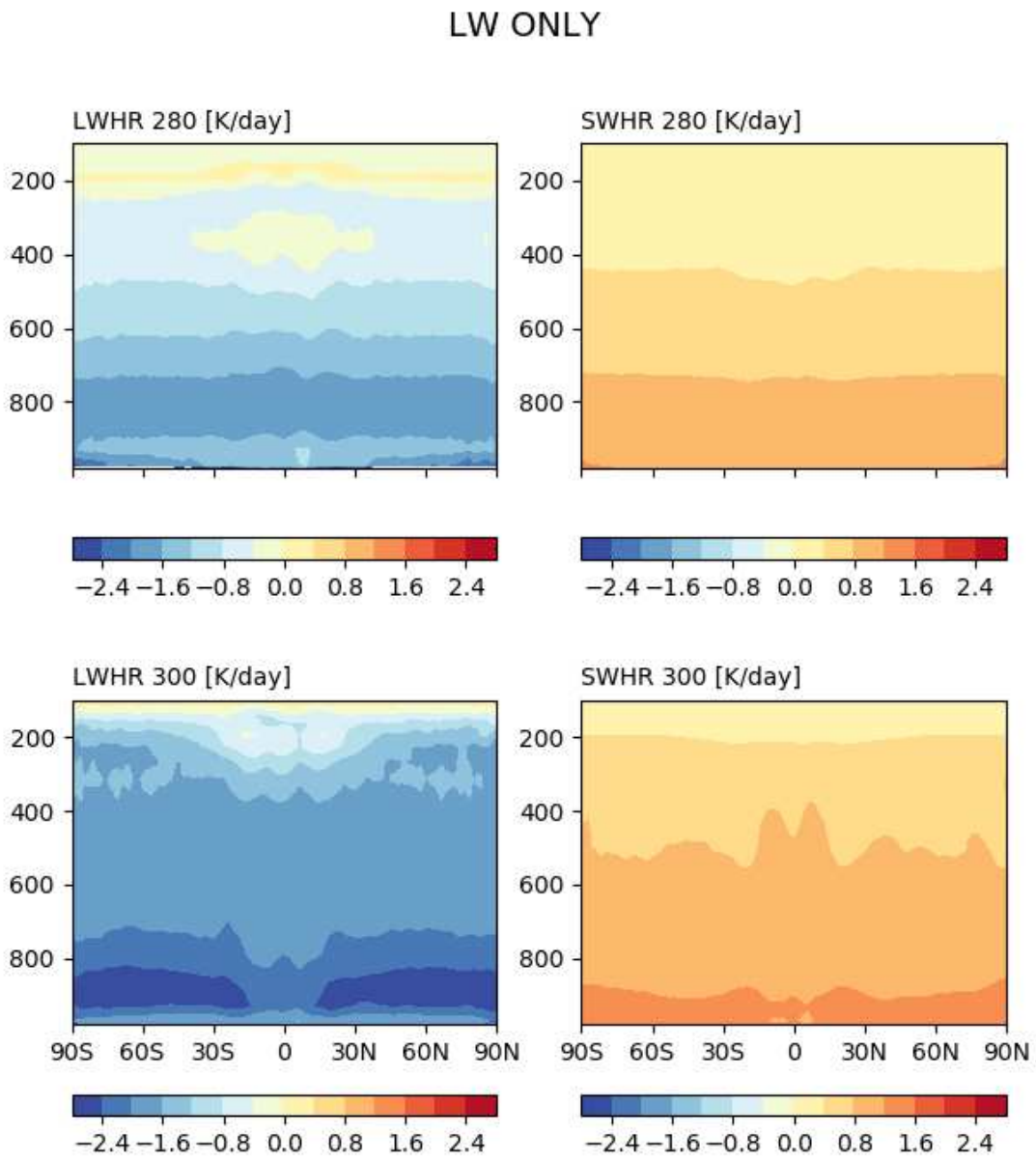

FIGURE 4.14. Vertical profiles of the zonally averaged longwave (left) and shortwave (right) radiative heating rates at 280 (top) and 300 K (bottom) for the longwave-only CRE.

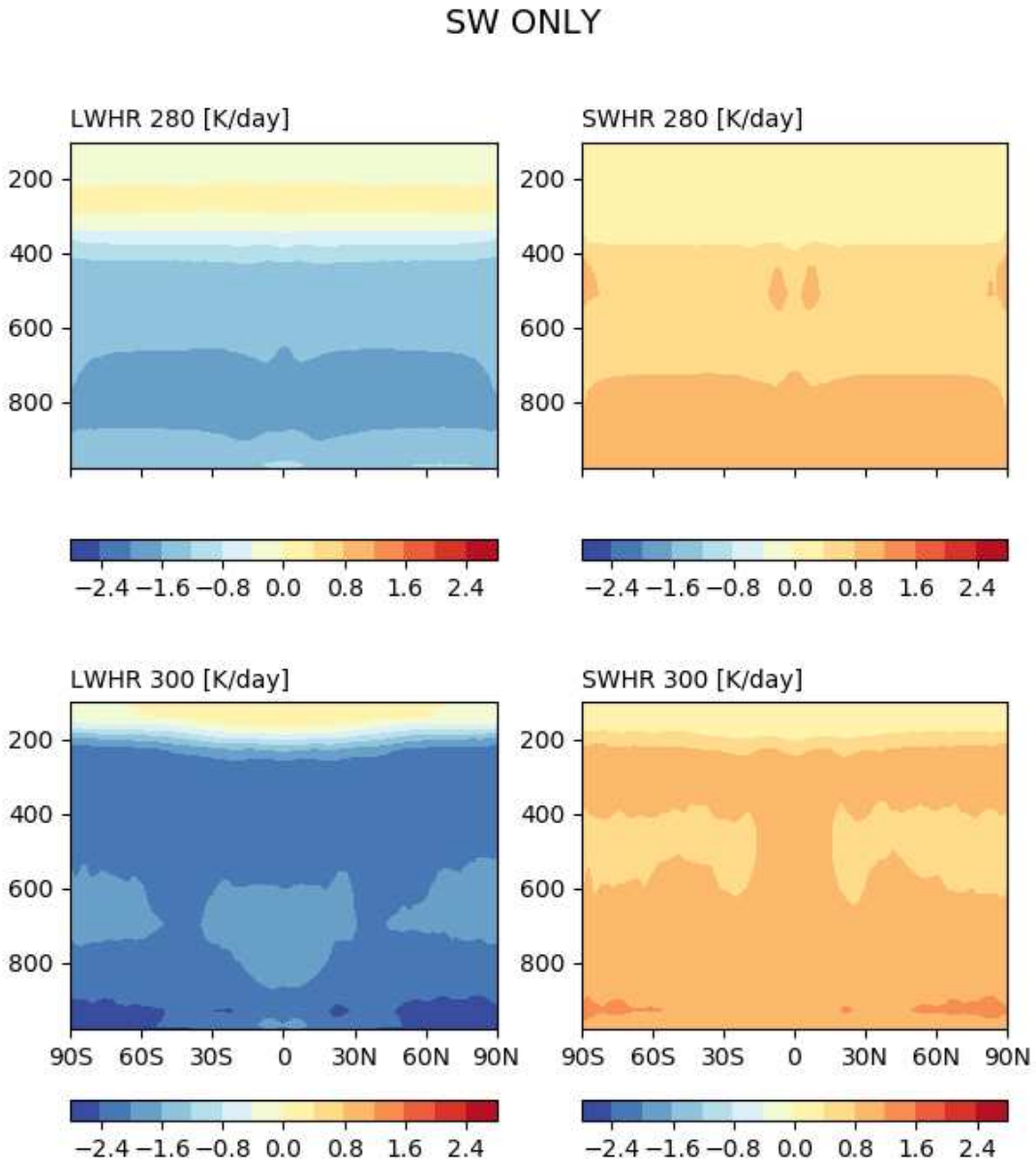

FIGURE 4.15. Vertical profiles of the zonally averaged longwave (left) and shortwave (right) radiative heating rates at 280 (top) and 300 K (bottom) for the shortwave-only CRE.

Separating the influence of the shortwave and longwave CREs on precipitation is more complex. At 280 K, the CRE on zonal-mean precipitation is dominated by longwave CRE in the tropics, and by the shortwave CRE at higher latitudes (Figure 4.16). This change from equator to pole is likely due to the reduction of the zonal-mean ARC by the longwave CRE at higher latitudes. At 290 and 200 K, the longwave CRE generally enhances the total CRE on zonal-mean precipitation, whereas the shortwave CRE generally opposes the influence of the total CRE.

Looking at the variability of precipitation, the influence of the longwave CRE is generally very similar to the total CRE, except in the tropics in the warmer simulations, and in the extratropics at 280 K, where it enhances precipitation variability. Conversely, the shortwave-only CRE simulations generally show reduced precipitation variability at all temperatures, except at 300 K, in which shortwave CRE enhances precipitation variability at high latitudes.

4.3.3 SIMULATIONS WITH A MERIDIONAL SST GRADIENT

The final set of simulations include an idealized equatorially symmetric SST gradient. In these simulations, it is useful to first consider where the clouds are occurring. Figure 4.17 shows that the high cloud fraction maximizes at the equator, indicating a single ITCZ. The low and mid-level cloud fractions both maximize near 45° N and S, which could be representative of mid-latitude storm tracks. Inclusion of the CRE generally causes the cloud fraction to increase, with the exception of the high clouds in the deep tropics. These changes are discussed further in Chapter 5.

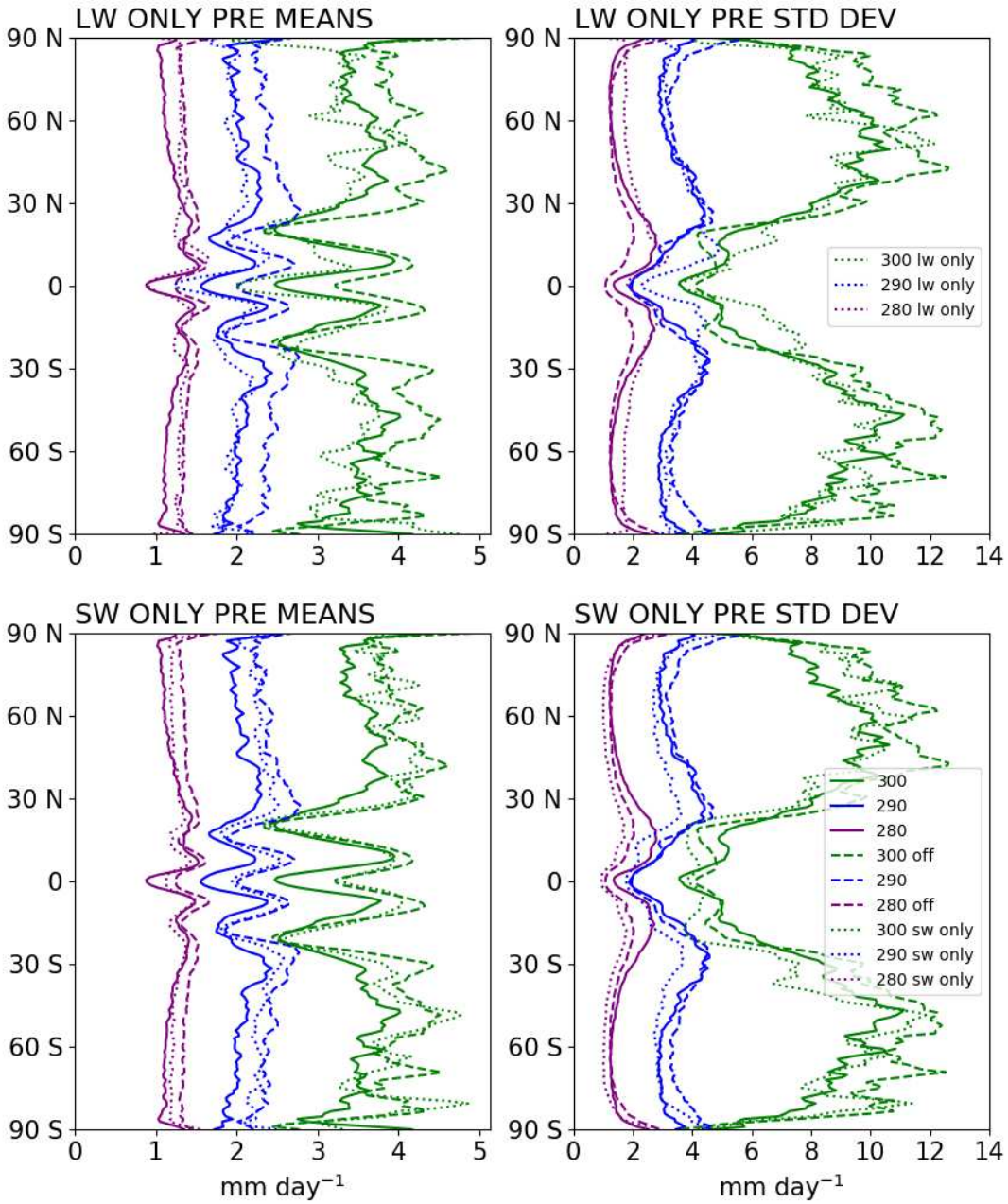

FIGURE 4.16. The zonal mean (left) and zonal standard deviation (right) of the precipitation rate for SSTs of 280 (purple), 290 (blue), and 300 K (green) with CREs on (solid) and off (dashed). The top panels also include the longwave-only CRE on precipitation (dotted), and the bottom panels also include the shortwave-only CRE on the precipitation (dotted).

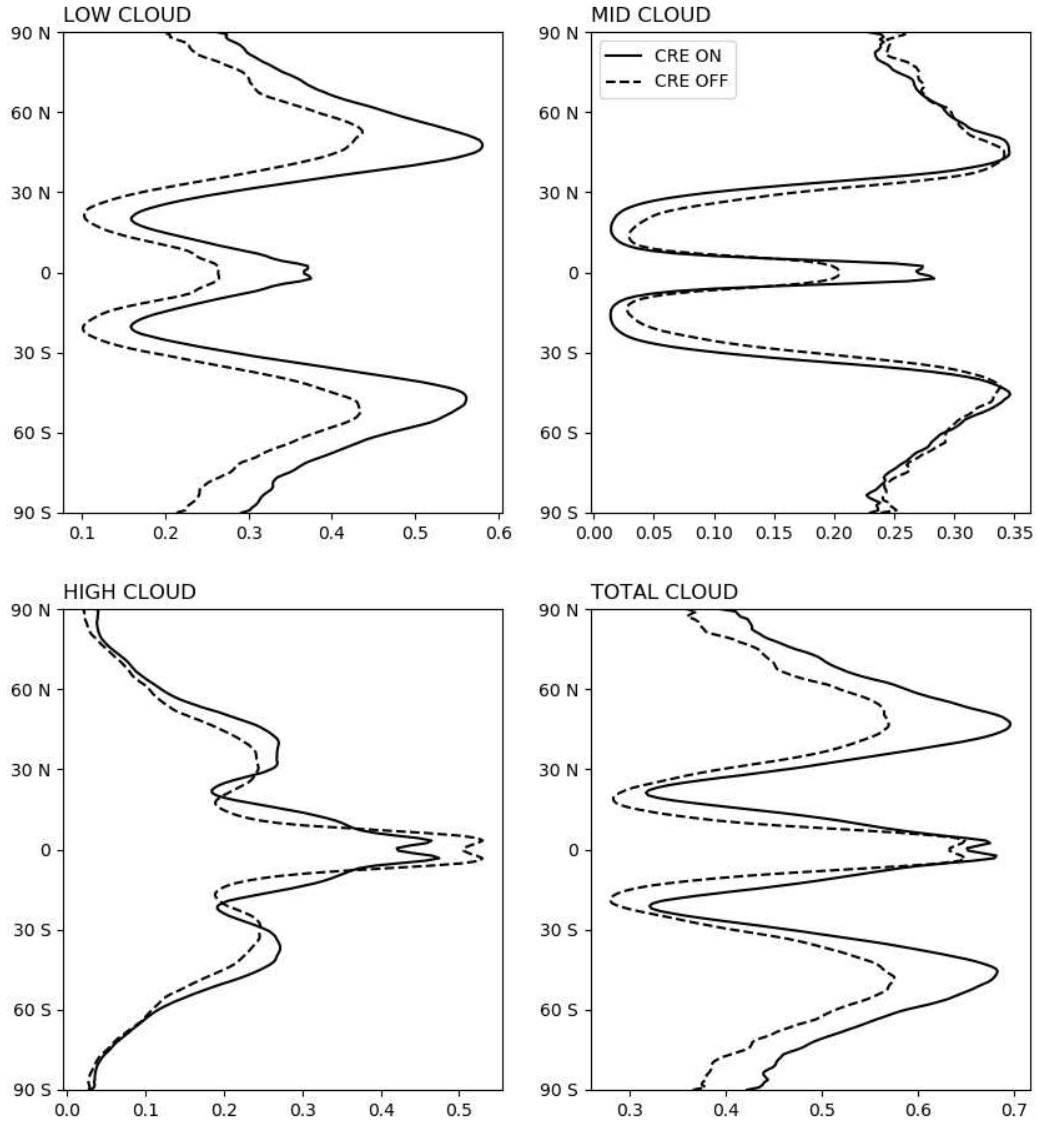

FIGURE 4.17. The zonally averaged cloud fraction for simulations with a meridional SST gradient with CREs on (solid) and CREs off (dashed).

The zonal-mean ARC reflects the SST gradient and decreases from equator to pole (Figure 4.18). The direct influence of CRE on the ARC varies with latitude, and is consistent with previous observational studies showing the warming effect of clouds at low latitudes, and the cooling effect of clouds at high latitudes (Rossow and Zhang, 1995; Stephens, 2005; Naegele and Randall, 2019). At the equator, the CRE reduces the ARC because it reduces the OLR, whereas at high latitudes, the CRE increases the ARC because it increases the downwelling longwave radiation at the surface. The variability of the ARC is enhanced by the CRE, and this effect is strongest near the equator.

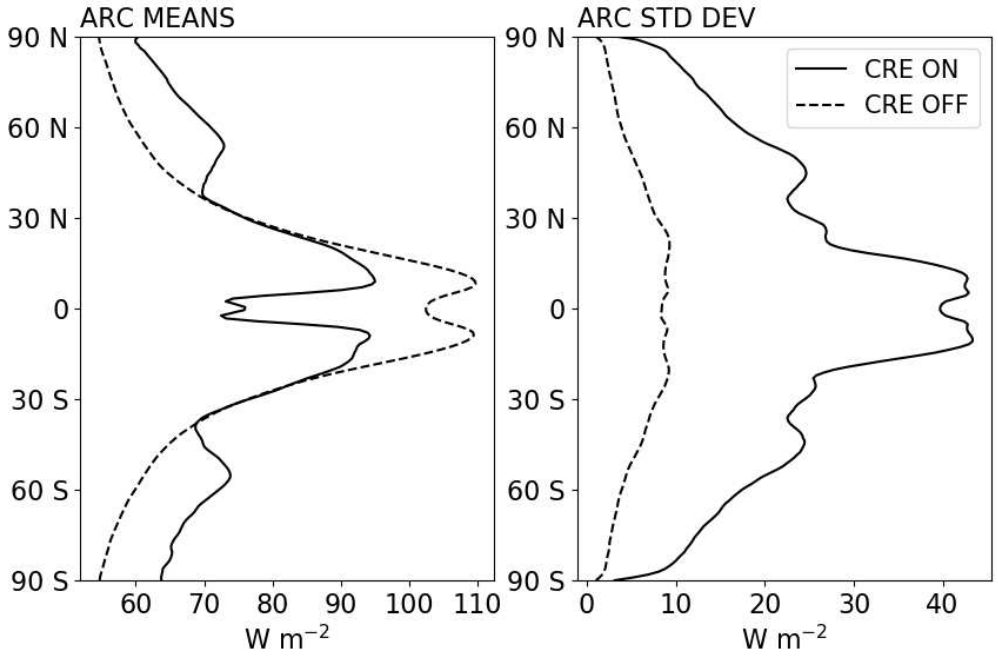

FIGURE 4.18. The zonal mean (left) and zonal standard deviation (right) of the ARC for simulations with a meridional SST gradient with CREs on (solid) and CREs off (dashed).

In the precipitation distribution, the CRE reduces weak precipitation and increases the very high precipitation rates; this is surprising given that the CRE reduces extreme precipitation in the uniform SST simulation at 300 K (Figure 4.19). The zonally averaged precipitation peaks at the equator, with smaller localized maxima near 35° N and S (Figure 4.20). At the equator, where the SST is the warmest, the CRE strongly enhances precipitation; this result is consistent with other idealized studies showing that the CRE enhances precipitation in the ITCZ (Harrop and Hartmann, 2016; Popp and Silvers, 2017). Elsewhere, the effects of the CRE on precipitation are small, and vary with latitude.

The zonally averaged precipitation variability looks very similar to the zonally averaged precipitation. At the equator, where the SST is the warmest, the CRE strongly enhances variability; this is unexpected considering that the CRE primarily has the opposite effect in the 300 K uniform SST simulation. Between approximately 15° and 35° (on both sides of the equator), the CRE reduces precipitation variability. The uniform SST simulations show that the precipitation variability can be partially explained by the PW variability—does the same hold here?

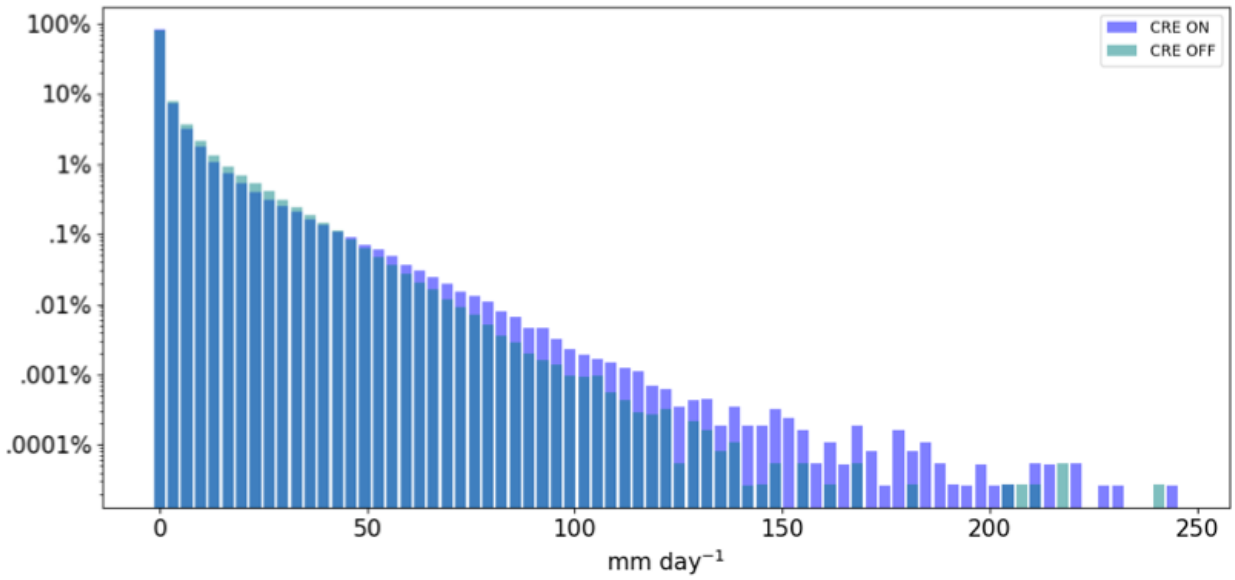

FIGURE 4.19. The daily precipitation distribution for simulations with a meridional SST gradient. The distributions with CREs on (purple) and CREs off (teal) are overlaid, so that areas of overlap are shown in blue. The vertical axis shows the percentage of the globe covered (by area) for each bin.

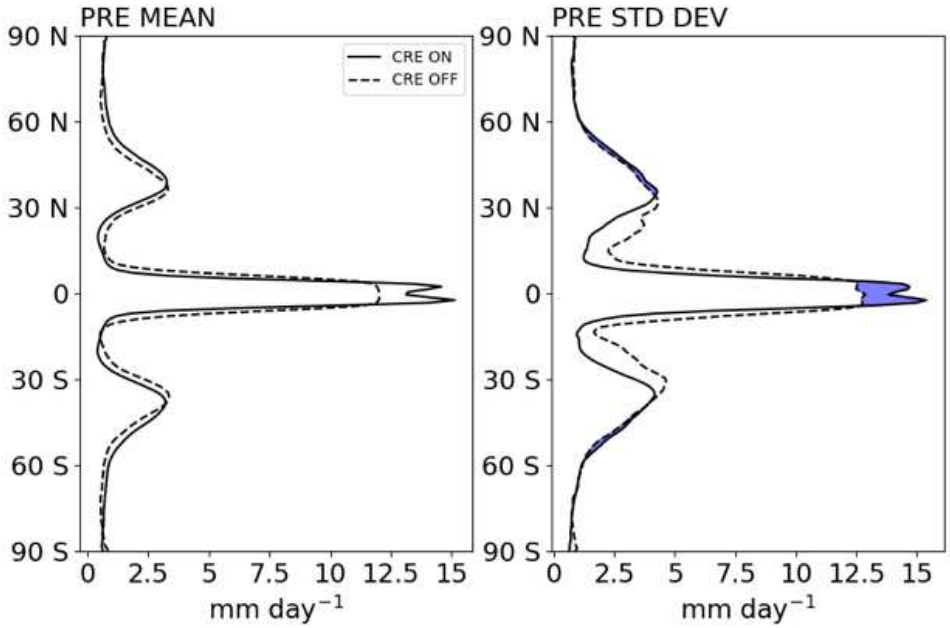

FIGURE 4.20. Zonally averaged (left) and zonal standard deviation (right) of the precipitation rate for simulations with a meridional SST gradient with CREs on (solid) and off (dashed). The shading shows where CREs enhance variability.

Following the SST gradient, the zonal-mean PW increases with temperature and maximizes at the equator (Figure 4.21). As with precipitation, the CRE enhances the equatorial maximum of zonally averaged PW at all latitudes, but particularly near the equator. This is reflected in maps of the PW, which also show the development of baroclinic eddies that transport moisture and energy away from the tropics (Figure 4.22). The influence of the CRE on PW variability is small, and generally tends to enhance precipitation, except in the subtropics where the CRE reduces the variability.

Not only does the meridional SST gradient introduce baroclinicity, but it also allows for the Madden-Julian Oscillation (MJO) when the CRE is included (Figure 4.23). The MJO is characterized by low wave numbers and a low frequency, differentiating it from other convectively-coupled Kelvin waves that are present in the simulation with the CRE. In the real world, the MJO is a predominant mode of tropical intraseasonal variability, and thus can also explain the increase in tropical precipitation variability due to CREs.

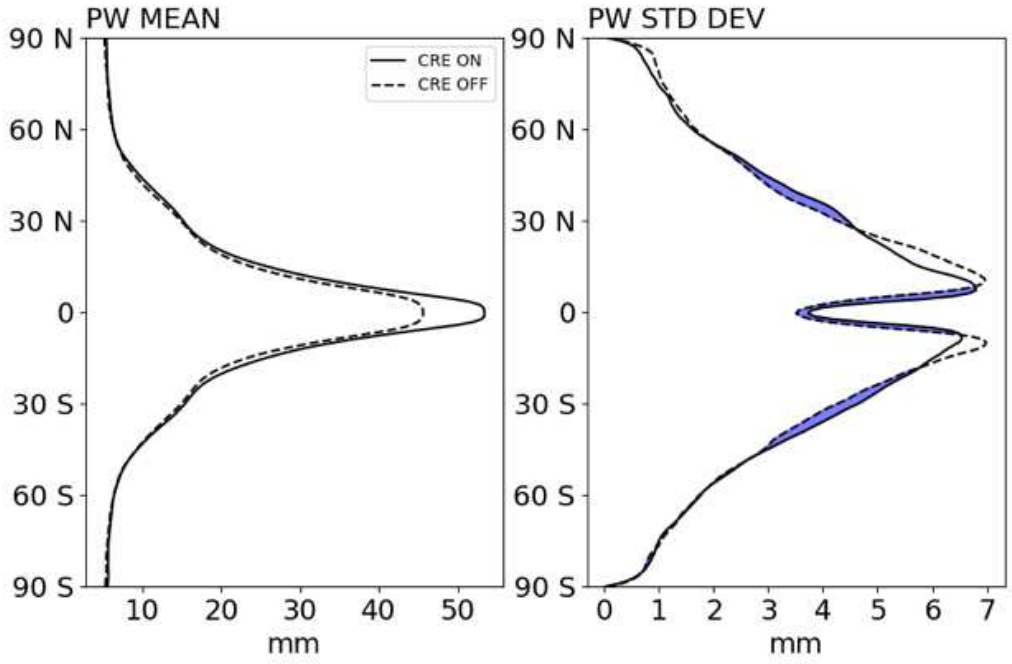

FIGURE 4.21. Zonally averaged (left) and zonal standard deviation (right) of the precipitable water for simulations with a meridional SST gradient and with CREs on (solid) and CREs off (dashed). The shading shows where CREs enhance variability.

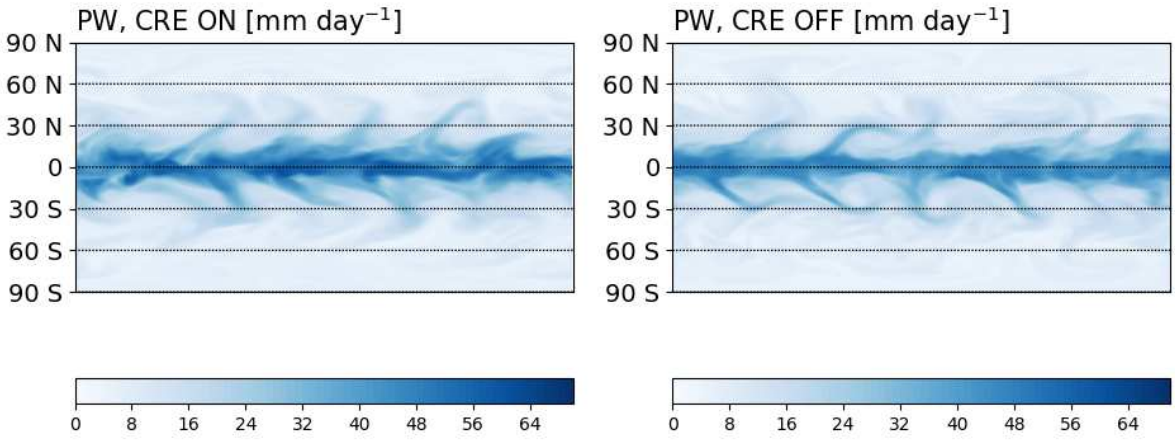

FIGURE 4.22. Maps of the precipitable water (mm day^{-1}) at day 150 for simulations with a meridional SST gradient and with CREs on (top) and CREs off (bottom).

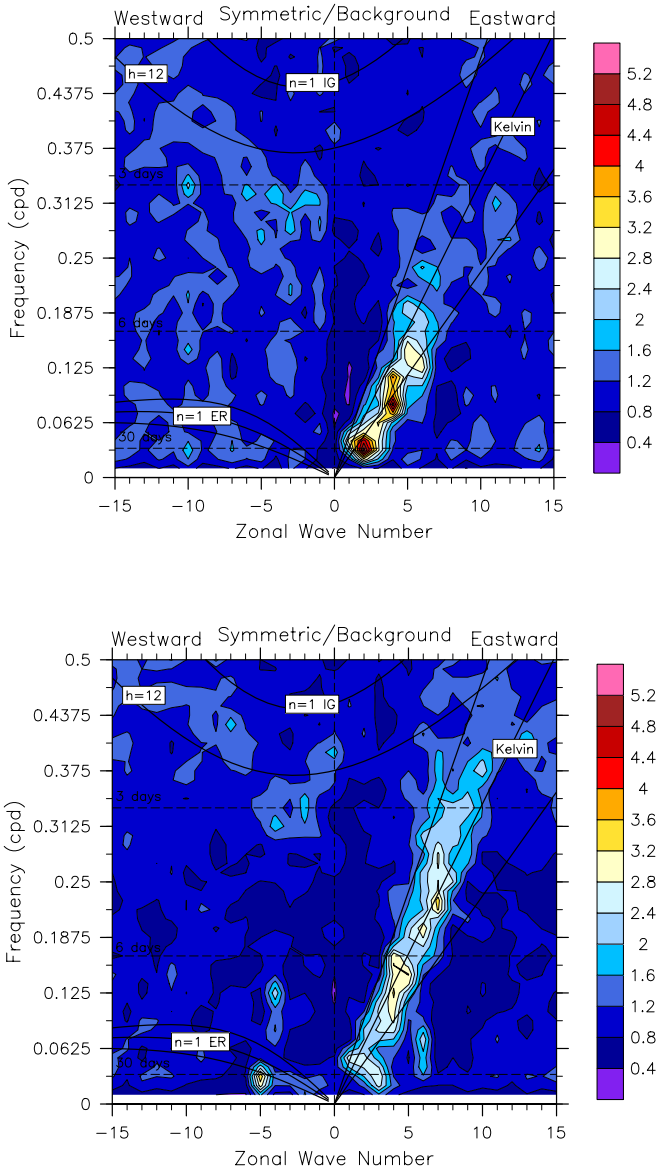

FIGURE 4.23. Wheeler-Kiladis space-time spectra diagrams using the outgoing longwave radiation from 15° S to 15° N for the simulations with a meridional SST gradient and with CREs on (top) and CREs off (bottom).

4.4 DISCUSSION

We analyzed a series of idealized aquaplanet simulations using SP-CAM to investigate the temperature dependence of precipitation variability in response to CREs. In the first set of simulations, uniform SSTs of 280, 290, and 300 K were used to represent a range of environments and conditions, from cool midlatitude winter to the warm tropics. At each SST, simulations were run in which the CRE was either included or turned off. In the first set of simulations with uniform SSTs, CREs reduce the mean precipitation at all SSTs, and the effect is stronger with warmer SSTs. This occurs because mean precipitation is energetically constrained, and CREs reduce the mean ARC by reducing the mean OLR.

However, CREs enhance extreme precipitation at 280 K and reduce extreme precipitation at 300 K. Because extreme precipitation is strongly tied to atmospheric moisture availability, these effects at 280 and 300 K can at least be partially explained by the CRE on the PW distributions. Relative to the mean, the CRE acts to shift the distribution to the right more at 280 K than at 300 K.

Precipitation variability is inherently tied to extreme precipitation, and therefore it makes sense that where the CRE enhances extreme precipitation, it also enhances precipitation variability. Conversely, where the CRE reduces extreme precipitation, we would expect it to reduce precipitation variability. These opposite responses to the CRE are seen in the cool and warm simulations: At 280 K, both extreme precipitation and precipitation variability are enhanced, whereas at 300 K, extreme precipitation and precipitation variability are reduced. Because precipitation variability, extreme precipitation, and precipitable water are all connected, the CRE on precipitation variability is partially reflected in the CRE on PW variability. Although the CRE increases zonal-mean

PW at all latitudes and at all SSTs, the CRE enhances PW variability at 280 K, and reduces PW variability at high latitudes at 300 K.

Given that PW increases with temperature, the tendency of CREs to either warm the atmospheric column further (by reducing OLR at the top of the atmosphere), or to cool the column (by enhancing downwelling longwave radiation at the surface), should be reflected in the changes in the PW. ARC variability is dominated by variability due to the longwave CRE. Whereas the OLR variability increases with increasing SSTs, the variability of the downwelling longwave radiation decreases with increasing SST; it is possible that competition between the variability of these two components is responsible for changes in the variability of the ARC, and ultimately the variability of PW and precipitation.

The dominant role of the longwave CRE over the shortwave CRE on the ARC is further emphasized in the second set of simulations, in which at each SST, the longwave and shortwave CREs are turned off individually. When the longwave and shortwave CREs are separated, it becomes very clear that the longwave CRE is responsible for nearly all variability in the ARC. Additionally, the longwave CRE is shown to enhance precipitation variability at cooler SSTs, although its influence on precipitation variability at the warm SST is less consistent between latitudes.

The temperature dependence of CREs on precipitation variability shown in the uniform SST simulations, however, do not necessarily translate to the simulations with a meridional SST gradient. In these less idealized simulations, the CRE reduces low-level precipitation and increases extreme precipitation rates. This effect is reflected in both the zonal-mean precipitation and the precipitation variability, in which CREs enhance equatorial precipitation and precipitation variabilities. These inconsistencies with the uniform SST

simulations show that precipitation variability cannot be explained by the influence of CREs alone. Rather, these results suggest the importance of circulation changes in response to SST changes and CREs, such as the development of baroclinic eddies and an MJO, and their influence on precipitation variability. These results motivate an examination of the circulation response to CREs, which is discussed in Chapter 5.

CHAPTER 5

THE TEMPERATURE DEPENDENCE OF THE LARGE-SCALE CIRCULATION RESPONSE TO CLOUD RADIATIVE EFFECTS

5.1 THE DYNAMIC COMPONENT OF PRECIPITATION

The thermodynamic (moisture) constraint on extreme precipitation is widely accepted, but has been shown to hold only in the extratropics (Pall et al., 2007). In the tropics, changes in moisture alone do not explain projections of extreme precipitation rates that far exceed Clausius-Clapeyron scaling (Allen and Ingram, 2002); therefore, dynamical changes must play a role (Emori and Brown, 2005). In the extratropics, extreme precipitation at a slower rate than moisture availability with warming. Here, reductions in vertical velocities in the North Atlantic stormtrack regions partially cancel out the thermodynamically-driven increases in extreme precipitation (Pfahl et al., 2017). By including the effects of dynamics on precipitation, extreme precipitation scaling shows better agreement with projected extreme precipitation rates in the extratropics (O'Gorman and Schneider, 2009; Muller et al., 2011). Furthermore, the inclusion of dynamical changes is necessary to explain regional patterns in extreme precipitation changes (Pfahl et al., 2017).

Dynamics are not only relevant to extreme precipitation, but to the full range of precipitation intensities as well. Heuristic models show that changes in the shape of the vertical velocity distribution in response to warming can explain other changes in the precipitation distribution. For example, an increase in the number of dry days with warming can be attributed to the increased probability of downward vertical velocities in a distribution (Pendergrass and Gerber, 2016).

Thackeray et al. (2018) found a strong link between extreme and non-extreme precipitation events, consistent with previous studies (Giorgi et al., 2011; Trenberth, 2009): In a warming climate, extreme events increased at the expense of non-extreme events. They show that the reason for this trade-off is the increased latent heat release associated with more intense precipitation events, which stabilizes the atmosphere and suppresses precipitation elsewhere. The atmosphere is expected to stabilize with warming (Knutson and Manabe, 1995), and this weakens the overturning circulation (Ma et al., 2012).

Vertical velocity can be used as an indicator of atmospheric stability and circulation strength, and is also tied to precipitation extremes. In this chapter, we examine the extent to which vertical velocity can be used to communicate changes between the large-scale circulation and the precipitation distribution. Following Chapter 4, where the hydrologic response to cloud radiative effects (CREs) is examined, here we focus on the response of the large-scale circulation to CREs. In particular, we investigate whether this response is temperature-dependent, and whether or not circulation changes can help to explain precipitation changes due to CREs.

5.2 MODEL AND SIMULATIONS

The SP-CAM aquaplanet simulations analyzed here are the same ones discussed in Chapter 4. Recall, the first set of simulations are run with globally uniform sea surface temperatures (SSTs) of 280, 290, and 300 K. For each SST, simulations are run with clouds that are radiatively active and inactive. In another set of simulations, a meridional SST gradient is imposed to more realistically simulate the earth's SST pattern. Further description of the model and experiments is given in Chapter 4.

5.3 RESULTS AND DISCUSSION

5.3.1 SIMULATIONS WITH UNIFORM SST

As discussed in Chapter 4, CREs increase intense precipitation rates and the area over which they occur at 280 K, but have the opposite effect at 300 K (Figure 4.2). As in Pendergrass and Gerber (2016), in which the distribution of vertical velocity is used to explain characteristics of the precipitation distribution, here we ask if comparing the precipitation and vertical velocity distributions can explain the precipitation response to CREs. In Figure 5.1, the distribution of the upward vertical pressure velocity at 500 mb[1] ($-\omega_{500}$) shows a similar pattern to the precipitation distribution: the CRE increases the largest upward vertical velocities at 280 K, and reduces the largest upward vertical velocities 300 K. Of course, the responses of the upward and downward vertical velocities to the CRE is approximately symmetrical, given that ascending and descending motion must be balanced. As with precipitation and precipitable water (Figures 4.2 and 4.6), the vertical velocity distribution is sensitive to the temperature, with warmer temperatures resulting in a larger spread.

Although the maximum upward vertical velocities shown in Figure 5.1 are higher at 300 K, zonal-mean vertical velocities are higher at 280 K (Figure 5.2). In both the warm and cool simulations, the zonal-mean vertical velocities are largest in the tropics, where the overturning circulation is strong. The zonal-mean vertical velocity maximizes just north and south of the equator, indicative of the double Intertropical Convergence Zone (ITCZ), and

[1] Note that upward vertical pressure velocity ($-\omega_{500}$) is used here and not ω_{500} to ease the direct comparison with precipitation.

minimizes at the equator. Outside of the tropics, the zonal-mean vertical velocity is very small at all latitudes.

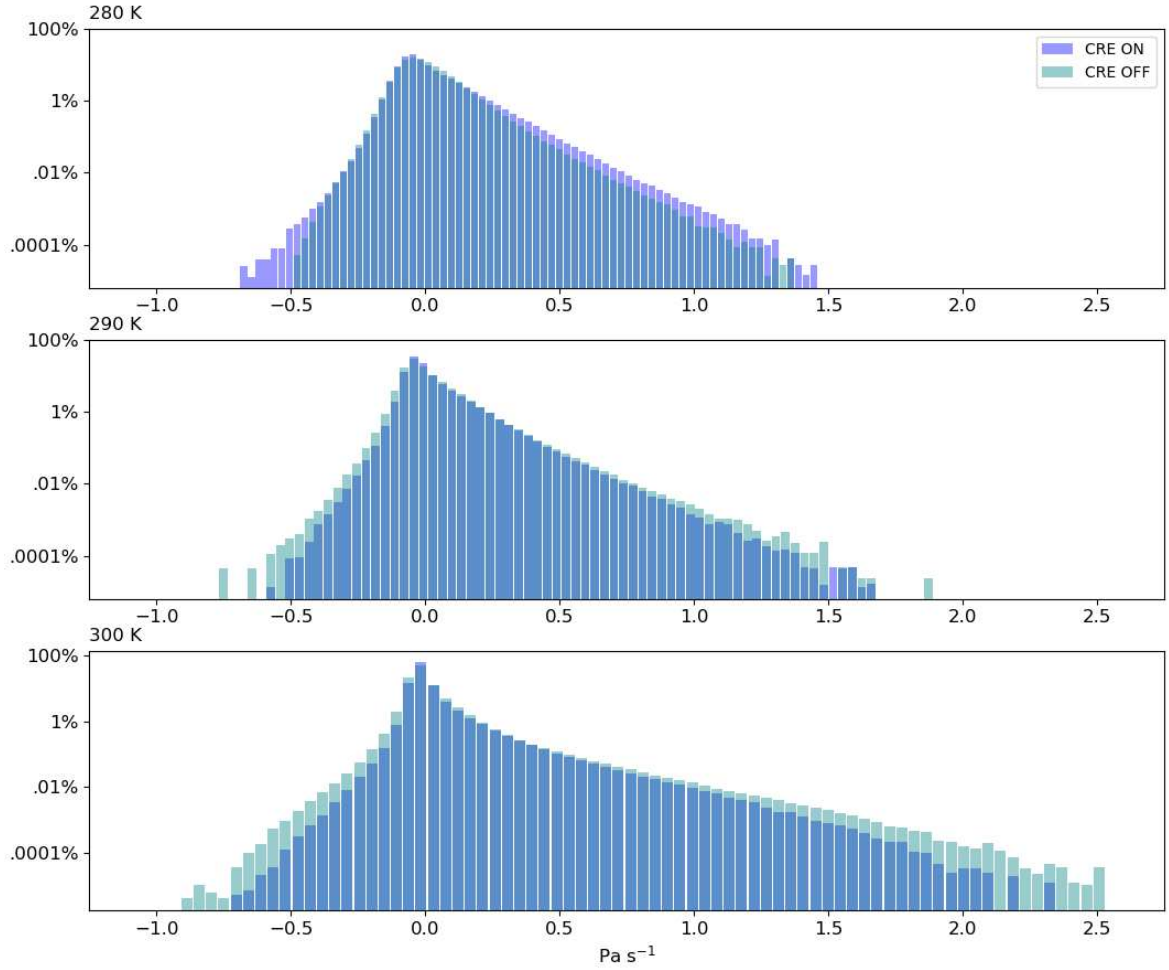

FIGURE 5.1. The daily upward vertical pressure velocity distributions for SSTs of 280, 290, and 300 K. The distributions with CREs on (purple) and CREs off (teal) are overlaid, so that areas of overlap are shown in blue. The vertical axis shows the percentage of the globe covered (by area) for each bin. Note the different scales on the horizontal axes.

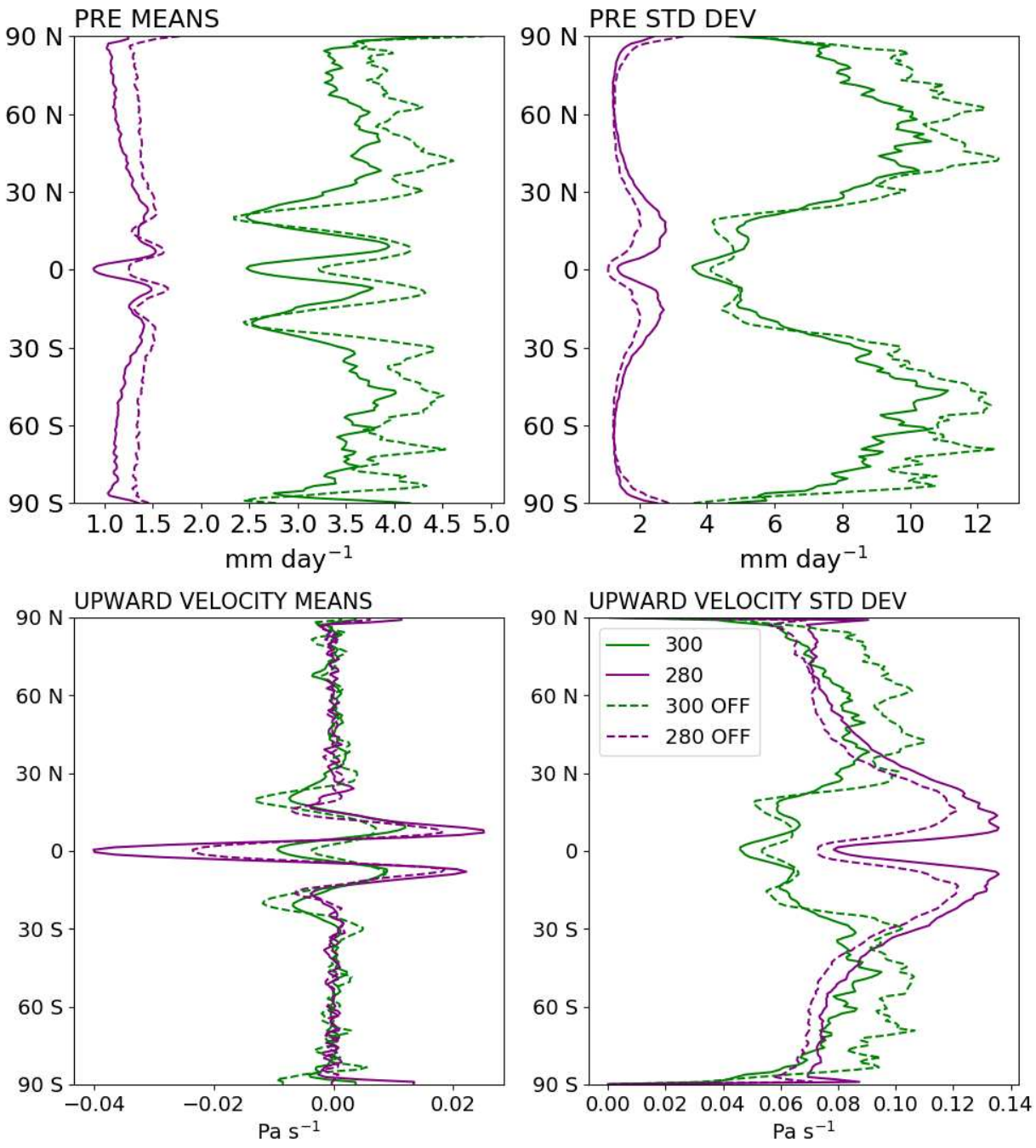

FIGURE 5.2. The zonal mean (left) and zonal standard deviation (right) of the precipitation (top) and upward vertical velocity (bottom) for SSTs of 280 (purple) and 300 K (green) with CREs on (solid) and CREs off (dashed).

Notably, in the tropics, the zonal-mean and standard deviations of the vertical velocity are much larger in the cold simulation than in the warm simulation; this is a departure from the pattern seen in the zonally averaged precipitations, which are lower at 280 K and higher at 300 K. The smaller vertical velocities shown at 300 K in the tropics are consistent with the expected increase in atmospheric stability due to warming (Knutson and Manabe, 1995). At 280 K, the CRE enhances the magnitude of the equatorial minimum and off-equatorial maxima (as implied by Figure 5.1), but the influence of the CRE at 300 K is less consistent.

The meridional structure of the vertical velocity variability more closely mirrors the precipitation variability. Variability is enhanced by the CRE at all latitudes in the cool simulations, but particularly in the tropics where the most precipitation occurs. In the warm simulations, variability is generally reduced by the CRE, particularly at higher latitudes where the most precipitation falls.

The magnitudes of the strongest zonal-mean vertical velocities in the warm and cool simulations (Figure 5.2) correspond to the strength of the overturning circulation. At 300 K, the overturning circulation is deeper, but weaker than the circulation at 280 K (Figure 5.3). In the 280 K simulations, as also described in Hartmann et al. (2020), the tropical circulation is separated into lower and upper cells. Here, the lower cell is characterized by a much weaker and shallower circulation. At both temperatures, the CRE enhances and deepens the circulation. Because these simulations have a prescribed uniform SST everywhere, the overturning circulations shown here are not comparable to the observed Hadley Circulation. The differences in the strength of the circulation and the magnitude of the vertical velocities in the warm and cool simulations are indicative of the increase in atmospheric static stability with warming. The static stability, s, is calculated as:

$$s = \frac{T}{\theta}\frac{\partial \theta}{\partial p}, \qquad \text{(eq. 5.1)}$$

where T is temperature (K), p is pressure, and θ is potential temperature. Cloud radiative effects slightly enhance low level cooling (this is more widespread at 300 than at 280 K) and mid-tropospheric warming, and therefore slightly enhance the static stability in the lower and middle troposphere (Figures 5.4 and 5.5). At higher levels, the CRE strongly reduces static stability, and this is associated with an increase in the tropopause height. The lifting of the tropopause is consistent with the deepening of the circulation at 280 K (Figure 5.3), and also with previous studies (Li et al., 2015).

At 280 K, high clouds near 400 mb increase shortwave heating within the cloud, and enhance longwave heating at cloud base (Figure 5.6). The same patterns are shown at 300 K, but they occur higher in the atmosphere (near 200 mb), and the heating and cooling patterns are enhanced.

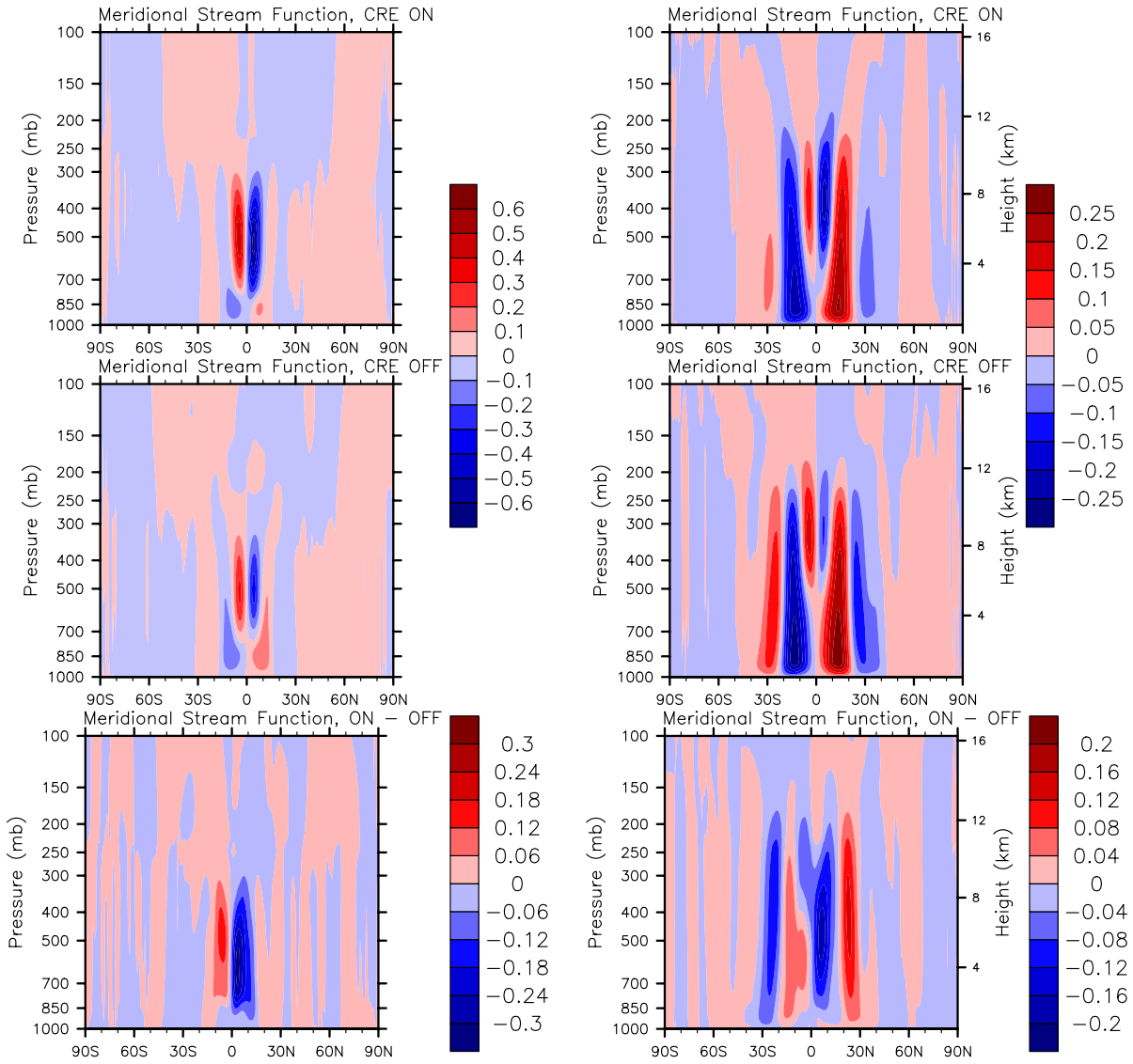

FIGURE 5.3 Mean meridional stream function at 280 K (left) and 300 K (right). The top panels show simulations with CREs on, middle panels show simulations with CREs off, and the bottom panels show the difference. Note the different scales.

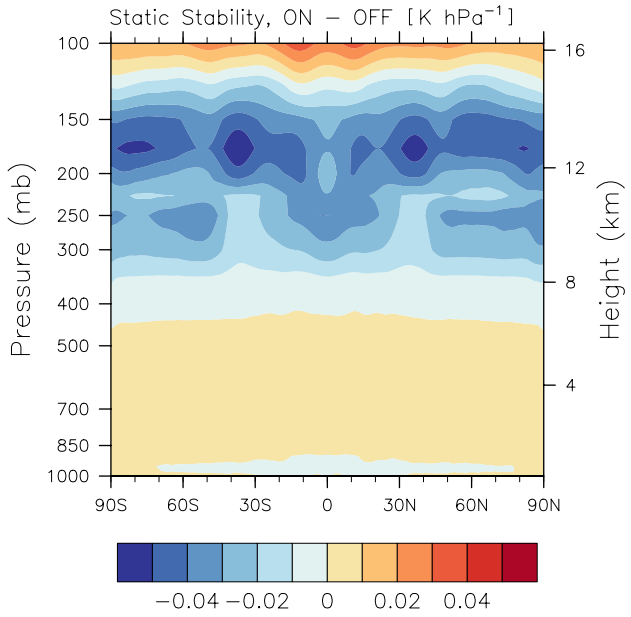

FIGURE 5.4 The vertical profile of the difference in the zonally averaged static stability between the simulations with CREs on and CREs off at 280 K.

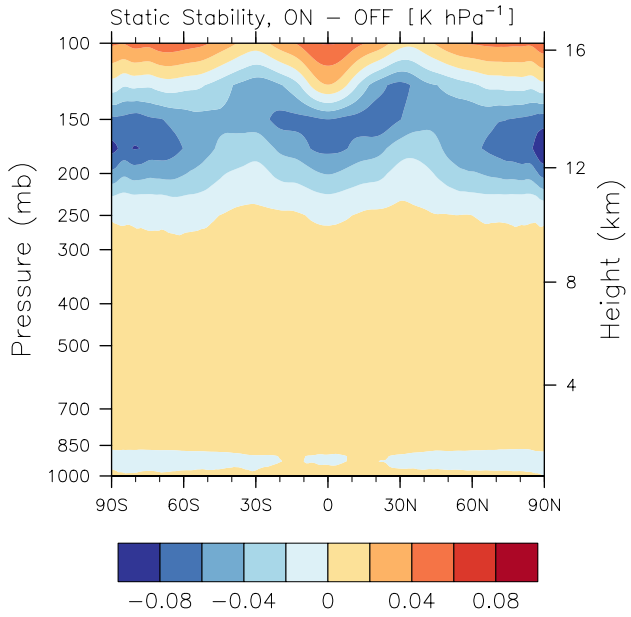

FIGURE 5.5 The vertical profile of the difference in the zonally averaged static stability between the simulations with CREs on and CREs off at 300 K.

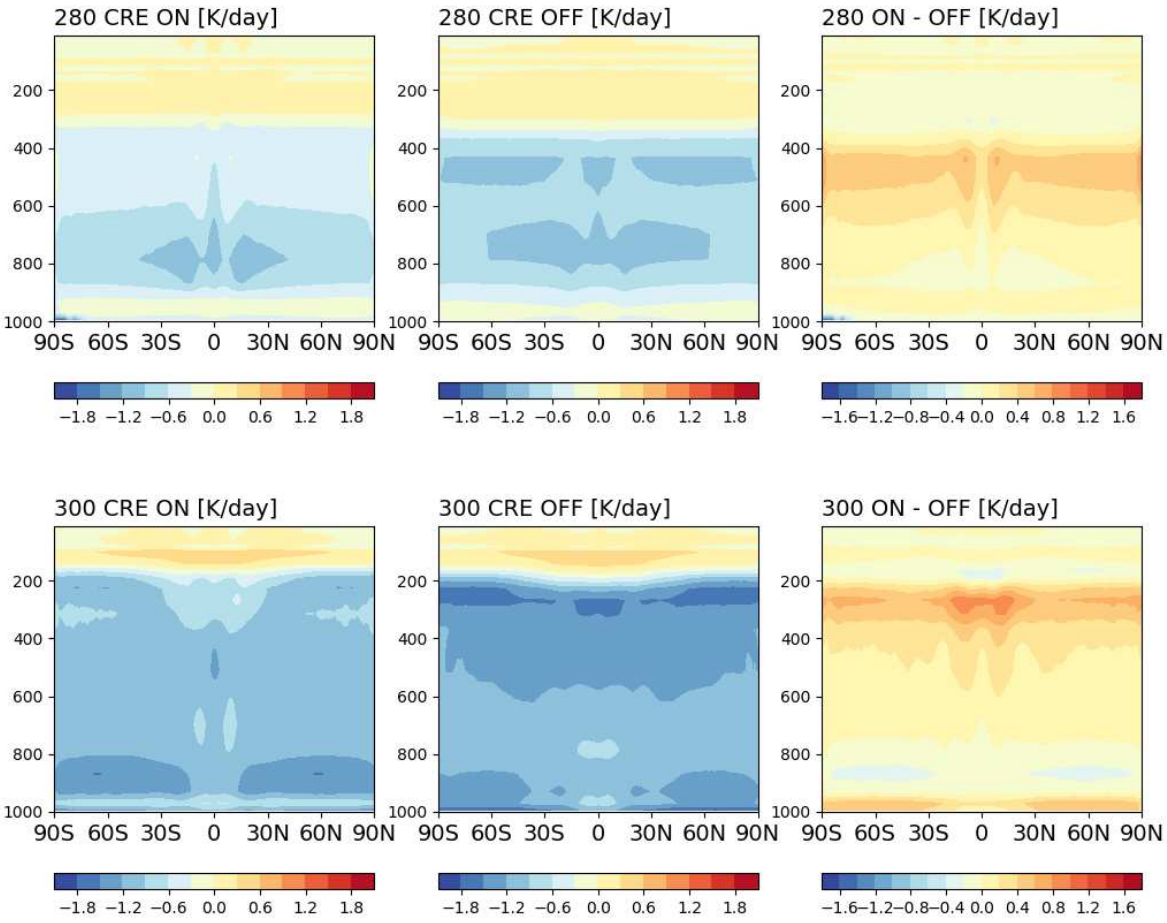

FIGURE 5.6. Vertical profiles of the zonally averaged radiative heating rate at 280 (top) and 300 K (bottom) for simulations with CREs on (left), CREs off (middle), and the difference (right).

5.3.2 SIMULATIONS WITH A MERIDIONAL SST GRADIENT

When the meridional SST gradient is imposed, the CRE generally reduces the strongest upward vertical velocities (Figure 5.7), and this is also observed in the distribution of upward vertical velocities at 300 K (Figure 5.1). Although the CRE reduces the strongest upward vertical velocities, it still enhances the zonal-mean upward vertical motion at most latitudes, and particularly at the equator, mirroring the influence of CREs on the zonal-mean precipitation (Figure 5.8). Whereas the CRE enhances equatorial precipitation variability (possibly because of the development of a Madden-Julian Oscillation-like signal shown in Chapter 4), it slightly reduces the variability of upward motion at the equator and throughout the tropics. The strongest effect of the CRE is to reduce the vertical velocity variability in the subtropics, where it also reduces the magnitude of the widespread subsidence that characterizes this region.

Figure 5.8 shows that the overall impact of the CRE on the vertical velocity is small and acts to enhance upward vertical motion at 500 mb—is this influence consistent throughout other levels of the atmosphere? Figure 5.9 shows the vertical profile of the upward vertical pressure velocity. At the equator, the CRE causes the ITCZ to narrow, consistent with results from Harrop and Hartmann (2016) and Popp and Silvers (2017), and bolstering the idea of the narrowing ITCZ as an example of convective aggregation. Although CREs enhance equatorial upward motion in the middle and lower troposphere, they reduce the magnitude of equatorial upward motion in the upper troposphere. This is balanced by reduced subsidence in the subtropics, especially in the upper troposphere.

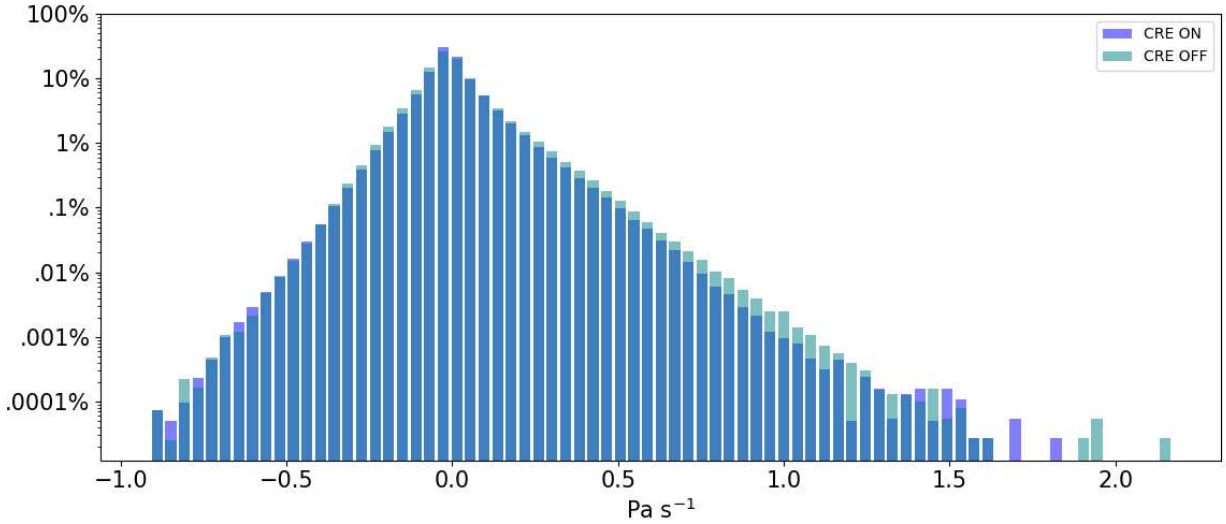

FIGURE 5.7. The daily upward vertical pressure velocity distributions. The distributions with CREs on (purple) and CREs off (teal) are overlaid, so that areas of overlap are shown in blue. The vertical axis shows the percentage of the globe covered (by area) for each bin.

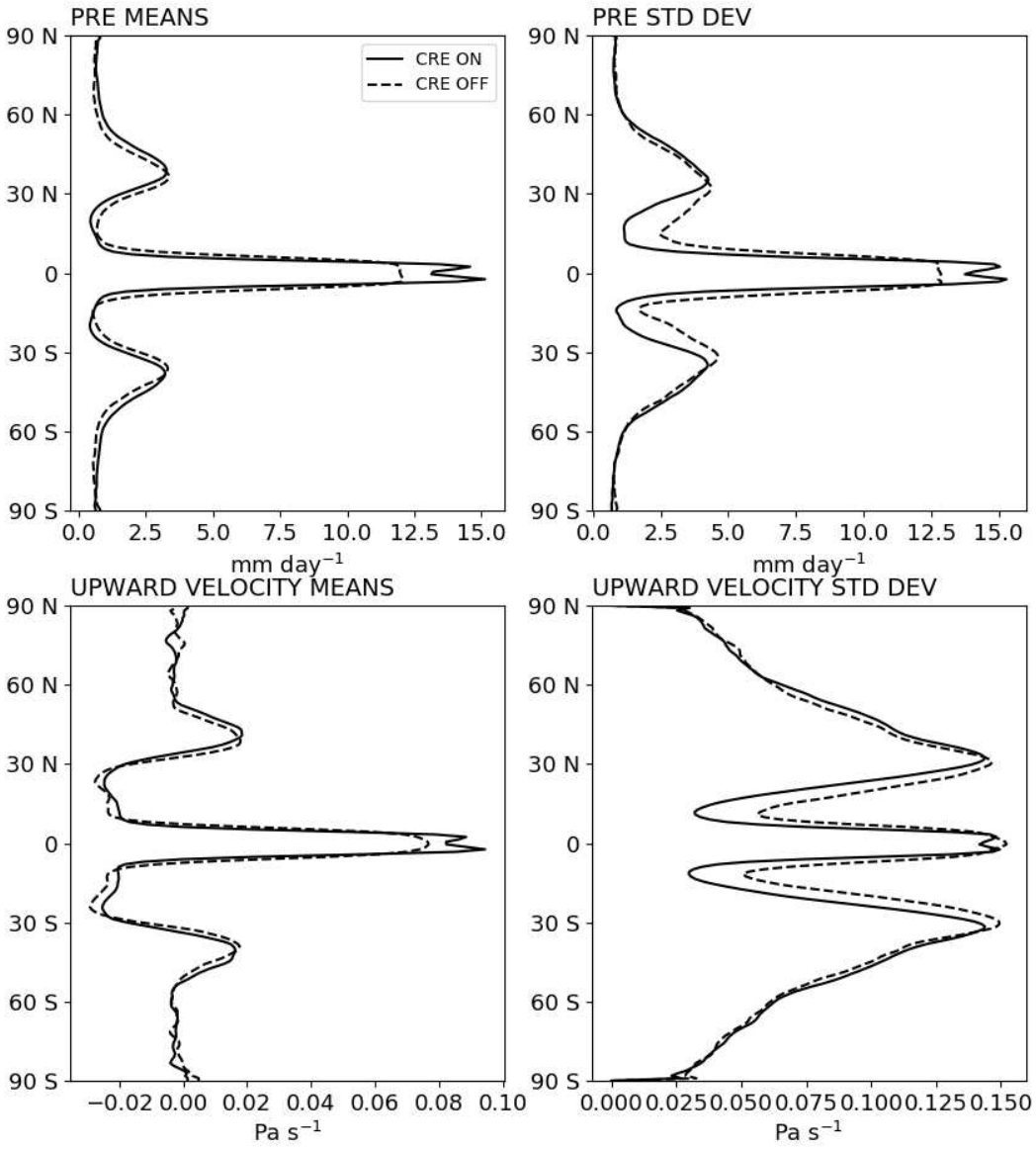

FIGURE 5.8. Zonal mean (left) and zonal standard deviation (right) of the precipitation rate (top) and upward vertical velocity (bottom) for simulations with an equatorially symmetric SST gradient with CREs on (solid) and CREs off (dashed) .

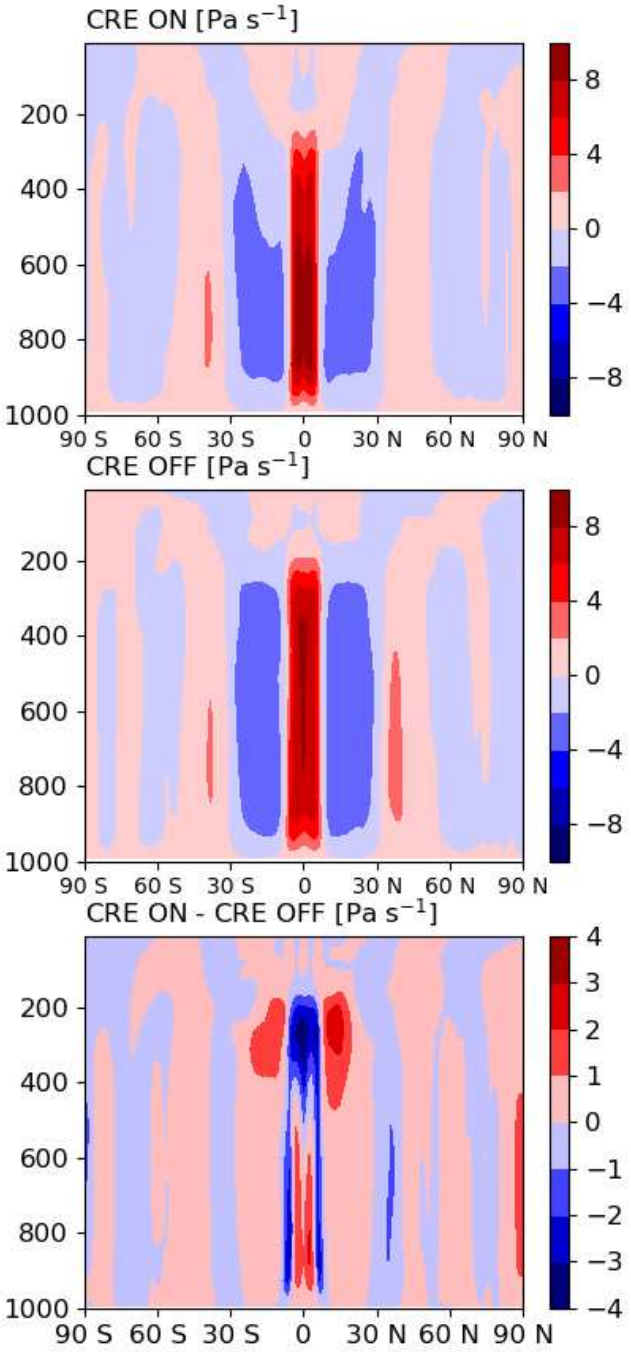

FIGURE 5.9. Vertical profile of the zonally averaged upward pressure velocity for simulations with an equatorially symmetric SST gradient and CREs on (top) and CREs off (middle), and the difference (bottom). Note the different scale for the difference plot.

The differences in the vertical velocity profiles are reflected in the mean meridional circulation (Figure 5.10), where the CRE enhances the overturning circulation in the lower and middle troposphere, also seen in Harrop and Hartmann (2016) and Popp and Silvers (2017). This strengthening could be related to the increase in tropical low cloud fraction (Figure 5.11) and a feedback between low clouds and low-level moisture (Brient and Bony, 2012). Above 400 mb, however, the primary effect is a weakening of the tropical circulation, which differs from other studies showing that the CREs enhances the Hadley Circulation at all levels (Harrop and Hartmann, 2016; Popp and Silvers, 2017).

The weakening of the tropical circulation above 400 mb due to CREs can be viewed as a result of increased static stability in the tropical upper troposphere (Figure 5.12). Using convective available potential energy (CAPE) as a measure of stability, both Harrop and Hartmann (2016) and Popp and Silvers (2017) found that the CRE tends to stabilize the tropical atmosphere, and they mention that this is inconsistent with their results showing enhanced Hadley Circulations. Near 150 mb in the upper tropical atmosphere, the CRE strongly reduces the static stability. This change reflects an increase in the tropopause height, which is seen at all latitudes. Li et al. (2015) also found that the tropopause height increases when CREs are activated. The areas of decreased stability coincide with areas showing an increase in high cloud fraction as tropospheric high clouds move higher.

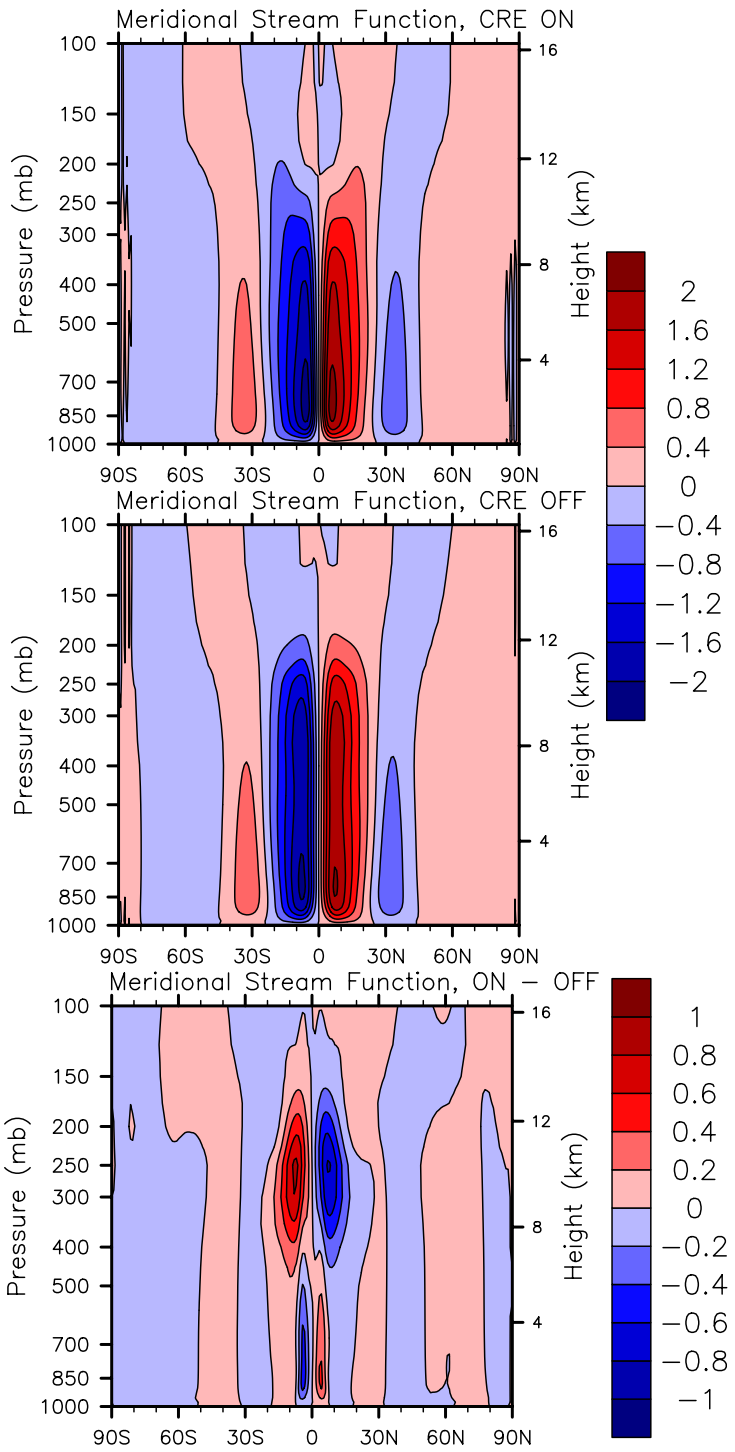

FIGURE 5.10. Mean meridional stream function ($\times 10^{11}$ kg s^{-1}) for CREs on (top), CREs off (middle), and the difference (bottom). Note the different scale for the difference plot.

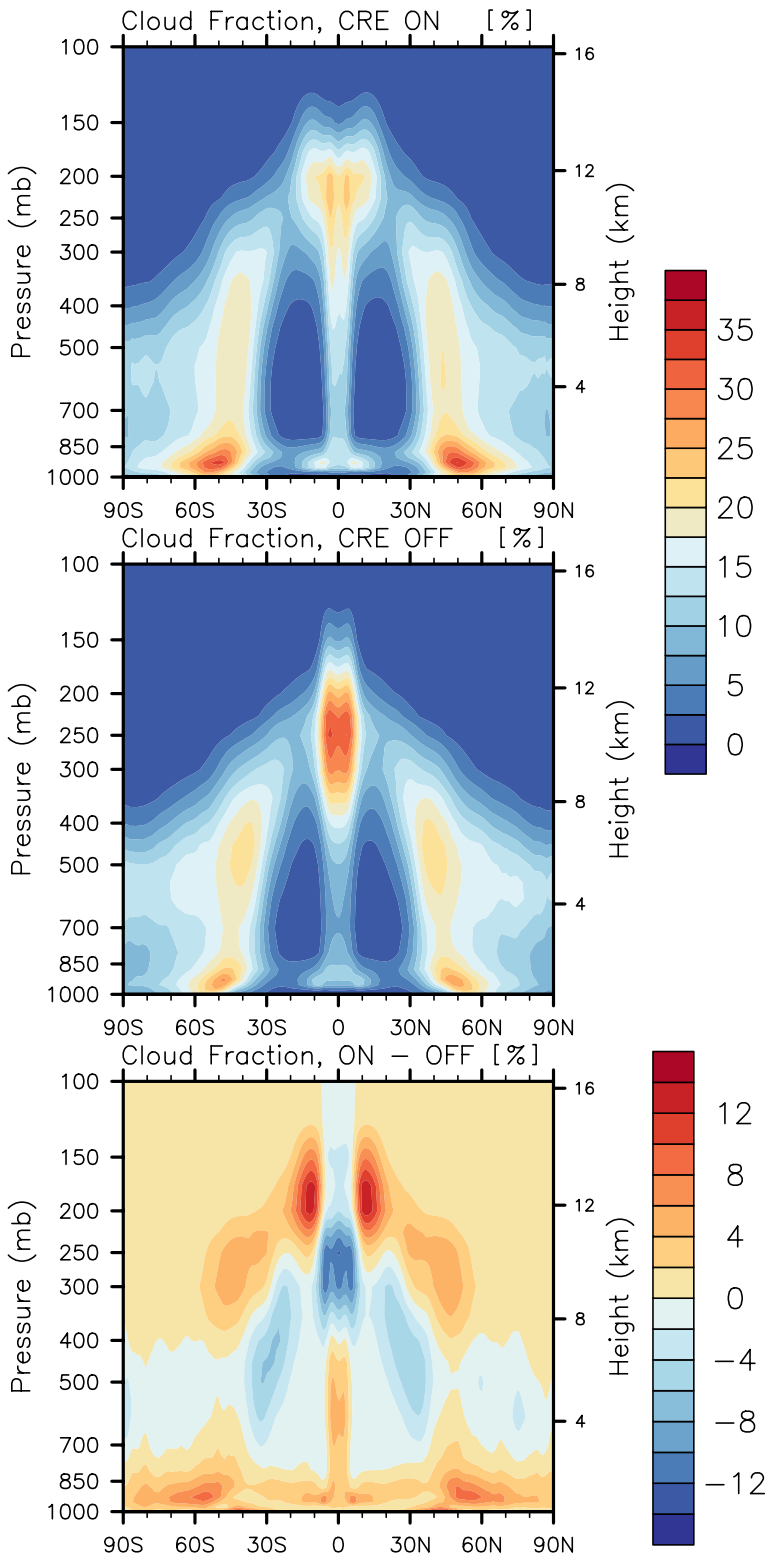

FIGURE 5.11. Vertical profiles of the zonally averaged cloud fraction for CREs on (top), CREs off (middle), and the difference (bottom). Note the different scale for the difference plot.

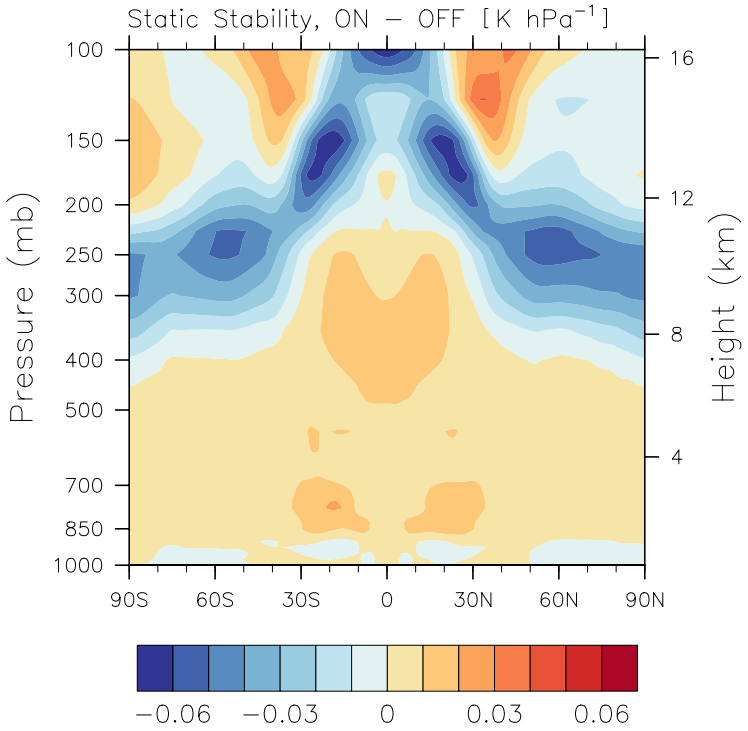

FIGURE 5.12. Vertical profile of the difference in the zonally averaged static stability between simulations with CREs on and CREs off.

The difference in static stability is also reflected in the differences in the temperature and radiative heating rates between simulations with CREs on and off (Figure 5.13). Strong temperature reductions in the upper atmosphere correspond to areas of decreased stability, indicating the increase in height of the tropopause. Warmer temperatures in the middle and upper troposphere and reduced temperatures in the lower extratropical troposphere enhance stability. In the tropics, the CRE enhances radiative heating throughout most of the troposphere, and especially in the upper troposphere, because high clouds increase the longwave heating of the atmospheric column (Slingo and Slingo, 1988). A similar tropical warming response in response is shown in Popp and Silvers (2017).

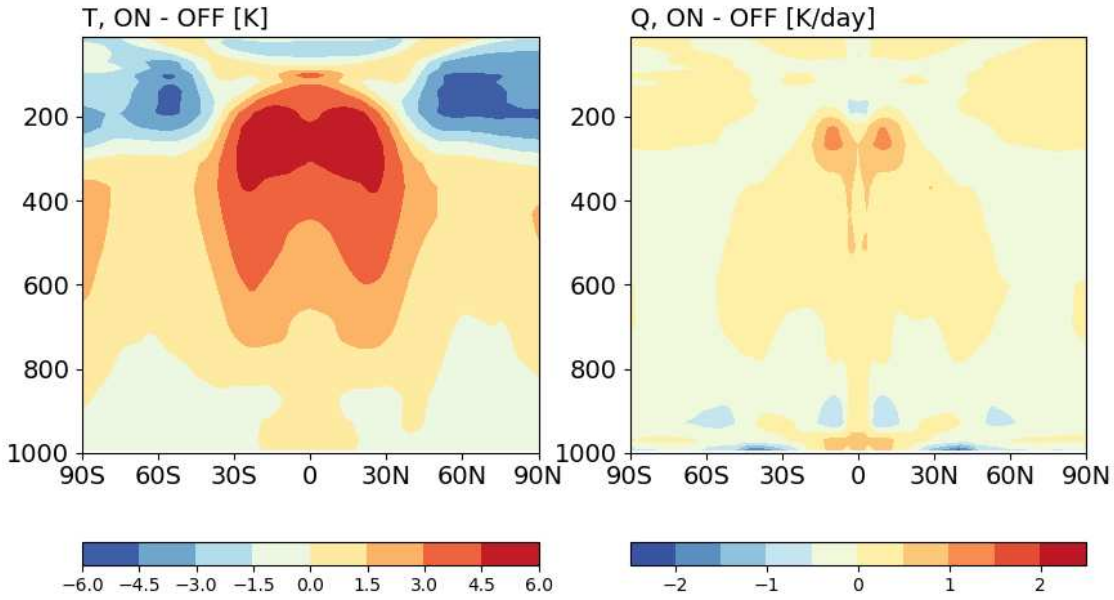

FIGURE 5.13. Vertical profiles of the difference in the zonally averaged temperature (left) and radiative heating rate (right) between simulations with CREs on and CREs off.

5.4 SUMMARY AND CONCLUSIONS

We used SP-CAM in a rotating, aquaplanet environment to examine the temperature dependence of the circulation response to CREs for globally uniform SSTs of 280, 290, and 300 K, and to provide context for the changes in the hydrologic cycle in response to CREs. In these idealized simulations, we showed that the CRE enhances the strongest (upward and downward) vertical motion at 280 K, whereas the CRE reduces the strongest (upward and downward) vertical motion at 300.

This effect is also shown in the zonal means, where the CRE increases the magnitude of strong zonally averaged vertical velocities at 280 K, and reduces the magnitude of strong zonally averaged vertical velocities at 300 K. We use the zonal standard deviation as a measure of variability, and find that the meridional structure of the vertical velocity

variability resembles that of the precipitation variability. As with the zonal means, the CRE enhances the variability at 280 K and generally reduces the variability at 300 K.

We find that the strength of the zonal-mean velocity corresponds to the strength of the overturning circulation. As expected in a warmer climate, the overturning circulation at 300 K is significantly weaker than the circulation at 280 K. However, we find that at both SSTs, the CRE enhances the strength of the circulation, despite also enhancing the tropospheric stability, although only slightly. The CRE also increases the height of the tropopause.

When the meridional SST gradient is imposed, the CRE tends to reduce the strongest upward vertical velocities. This reduces the variability near the equator, despite the influence of the CRE to increase the zonal-mean velocity there. The CRE also strongly reduces the vertical velocity variability in the subtropics. The enhanced zonal-mean 500 mb vertical velocity reflects the strengthening of the Hadley Circulation in the lower troposphere, although the CRE weakens the circulation at upper levels.

In the uniform SST experiments, the CRE on vertical velocity variability appears to be strongly connected to the precipitation variability. However, the extent to which the influence of the CRE on the vertical velocity reflects the influence of the CRE on the large-scale circulation seems to end with the strengthening of the overturning circulation at 280 K. In the simulations with the meridional SST gradient, the CRE reduces vertical velocity variability at the equator, although only slightly. This response is consistent with the reduction of vertical velocity variability at 300 K.

Perhaps unsurprisingly, as a very simple indicator of the changes in the large-scale circulation, the vertical velocity falls short. For example, although the vertical velocity

captures the enhanced overturning circulation at 280 K in response to the CRE, this is not the case at 300 K, or in the simulation with the meridional SST gradient. The changes in the vertical velocity are likely more representative of localized, dynamical processes.

However, the results of these very idealized simulations do show that vertical velocity variability responds to CREs very differently at 280 than at 300 K. Furthermore, the opposite responses of the warm and cool simulations are reflected in the precipitation variability responses to CREs. These results motivate further research examining the link between vertical velocity variability and precipitation variability.

CHAPTER 6

CONCLUSIONS

6.1 SUMMARY

This overarching goal of this dissertation is to examine the role of cloud radiative effects (CREs) on the hydrologic cycle and the ways in which it changes. These include changes in time—over decades in response global rising surface temperatures, or on the shorter timescale of days within the context of extreme precipitation events—as well changes in space—considering precipitation variability and the different response to CREs in different regions of the globe. In particular, this work focuses on the influence of CREs on hydrologic sensitivity and on precipitation variability.

In Chapter 2, we explored the role of CREs in constraining the change in the global hydrologic cycle with warming. The energetic constraint on hydrologic sensitivity has been well studied and the concept is well-understood. In practice, however, the popular simplification, in which the clear-sky atmospheric radiative cooling (ARC) is used instead of the all-sky ARC, and the sensible heat flux (SHF) is ignored, is puzzling. Comparing the projected change in the all-sky ARC and the clear-sky ARC due to increasing CO_2 concentrations, the change in the clear-sky ARC is indeed the larger of the two, the therefore the clear-sky ARC does initially appear to better constrain the precipitation change. However, when the full atmospheric energy budget is considered and the change in the SHF is also included, this is no longer the case. Although the CRE reduces the change in the ARC, the reduction is partially compensated by the change in the SHF, which acts to increase the net atmospheric cooling. Therefore, when both the CRE and the SHF are included in the

energy balance, the change in the net all-sky cooling is clearly shown to better fit the change in the precipitation, and the change in the net clear-sky cooling significantly overestimates the change in the precipitation. Indeed, this balance is expected, but our results show that the CRE on the ARC is an important factor of the energetic constraint on hydrologic sensitivity. Furthermore, although the CRE and the SHF have relatively minor contributions to the atmospheric energy budget at present, we show that the normalized change in both the CRE and the SHF are significant in maintaining the atmospheric energy budget as it changes in response to increasing CO_2 concentrations and rising surface temperatures.

In Chapter 4, our focus shifts from global changes to localized changes; from changes that occur over decades, to days. We used SP-CAM, the super-parameterized version of the NCAR Community Atmosphere Model (CAM4) to investigate the response of the hydrologic cycle to CREs. Specifically, our goal was to test the temperature dependence of precipitation variability in response to CREs. We used a set of highly idealized aquaplanet simulations with rotation and uniform sea surface temperatures (SSTs) of 280, 290, and 300 K, with CREs either turned on or off. 280 K is representative of cool, mid-latitude SSTs, whereas 300 K is representative of warm SSTs in the tropics. The vast majority of the research on the influence of CREs focuses primarily on the tropics, but here we are also interested in the response at cool temperatures that are representative of extratropical environments. Although the influence of CREs on specific precipitation features, such as the Intertropical Convergence Zone (ITCZ) or the midlatitude storm tracks have been examined, as far as we know, the influence of CREs on precipitation extremes and variability has not been previously studied.

Our results show that CREs reduce mean precipitation at all SSTs, but they enhance the precipitation rate and occurrence (by area) of extreme precipitation at 280 K and reduce

the precipitation rate and the occurrence of extreme precipitation at 300 K. Because variability is inherently linked to precipitation extremes, the influence of the CRE on extreme precipitation is also reflected in the variability. Therefore, in regions with the most precipitation, the CRE enhances precipitation variability at 280 K, but generally reduces precipitation variability at 300 K. Comparison of the variability of precipitation to the variability of atmospheric radiative fluxes suggests that the longwave components of the ARC primarily influence precipitation variability.

In simulations with an equatorially symmetric SST gradient, however, these temperature-dependent responses to the CRE are no longer as clearly observed. At least in part, we attribute the differences between the simulations with uniform SSTs and those with the SST gradient to developments in the large-scale circulation. For example, when the equator-to-pole SST gradient is introduced, baroclinic eddies develop, as well as a signal that resembles the Madden-Julian Oscillation, a predominant source of tropical intraseasonal precipitation variability.

Using the same set of simulations, we follow Chapter 4 with an investigation of the large-scale circulation response to CREs in Chapter 5. We use the 500 mb vertical velocity as a simple indicator of the circulation and compare changes in the vertical velocity to changes in the precipitation in response to both varying SSTs and the influence of CREs. Pendergrass and Gerber (2016) showed that the vertical velocity distribution can be used to explain changes in the precipitation distribution, and we test that here.

We find that overall, the vertical velocity is a poor indicator of the circulation response, but that it does correspond well with precipitation. As with precipitation extremes, the CRE enhances the magnitude of strong vertical velocities in the cool simulation and it

reduces the magnitude of strong vertical velocities in the warm simulation. At all SSTs, the influence of the CRE on vertical velocity extremes is carried over to the variability of the vertical velocity. Overall, precipitation variability and vertical velocity variability exhibit similar temperature-dependent responses to CREs in the uniform SST simulations, and these results motivate further study of the link between vertical velocity and precipitation.

6.2 MOVING FORWARD

From the studies discussed above, new questions arise. In Chapter 2 we used the atmospheric energy budget to examine changes in the global hydrologic cycle, and we end with the proposition that the surface energy budget could be used to complement the atmospheric energy budget to refine the energetic constraint on hydrologic sensitivity. To what extent does this improve the partitioning of the latent and sensible heat fluxes? Additionally, the CRE was shown to be significant in the perturbation equation of the atmospheric energy budget, but how important is the role of the CRE in the surface budget approach?

In Chapters 4 and 5, the idealized simulations used in our analyses had prescribed uniform SSTs of 280, 290, and 300 K. We find that the 280 and 300 K simulations generally showed opposite responses to CREs, with the 290 K simulation often falling squarely in the middle. The implication is that the influence of the CRE on precipitation (among other variables) tends to be very small, and begs the question: Is there an SST (presumably close to 290 K) at which the influence of the CRE is minimized? And why does that occur?

Additionally, some of our results hint at signals of convective aggregation. These include the development of "tropical" cyclones in the 300 K simulation, and the narrowing of

the ITCZ in the simulation with the meridional SST gradient. The simulations presented here are not tailored to focus on convective aggregation, but in previous studies, convective aggregation has been shown to be sensitive to both CREs and SSTs—is the influence of CREs on aggregation also dependent on temperature?

Finally, it would be interesting to decompose the final set of simulations with an equatorially symmetric SST pattern into regions of warm and cool SSTs, which would be more directly comparable to the uniform SST simulations. Can we disentangle the influence of the large-scale circulation on precipitation from the temperature-dependent response to CREs? And furthermore, can we pinpoint the dominant sources of precipitation variability that are caused by the large-scale circulation?

REFERENCES

Albern, N., A. Voigt, and J.G.Pinto, (2019). Cloud-radiative impact on the regional responses of the midlatitude jet streams and storm tracks to global warming. *J. Adv. Model. Earth Syst.*, 7, 1940-1958.

Allan, R.P., (2006). Variability in clear-sky longwave radiative cooling of the atmosphere. *J. Geophys. Res. Atmos.*, 111, D22, 105.

Allan, R., M. Barlow, M. P. Byrne, A. Cherchi, H. Douville, H. J. Fowler, T. Y. Gan et al., (2020). Advances in understanding large-scale responses of the water cycle to climate change. *Ann. N. Y. Acad. Sci.*

Allen, M. R. and W. J. Ingram, (2002). Constraints on future changes in climate and the hydrologic cycle. *Nature*, 419(6903), 224–232.

Arnold, N. P. and D. A. Randall, (2015). Global-scale convective aggregation: Implications for the MJO. *J. Adv. Model. Earth Syst.*, 7, 1499–1518.

Benedict, J. J. and D. A. Randall, (2009). Structure of the Madden–Julian oscillation in the superparameterized CAM. *J. Atmos. Sci.*, 66(11), 3277-3296.

Boer, G. J., (1993). Climate change and the regulation of the surface moisture and energy budgets. *Clim. Dyn.,* 8, 225–239.

Bony, S. and K. A. Emanuel, (2005). On the role of moist processes in tropical intraseasonal variability: Cloud–radiation and moisture–convection feedbacks. *J. Atmos. Sci*, 62(8), 2770-2789.

Bretherton, C. S., P. N. Blossey, and M. Khairoutdinov, (2005). An energy-balance analysis of deep convective self-aggregation above uniform SST. *J. Atmos. Sci.,* 62, 4273–4292.

Brient, F. and S. Bony, (2012). How may low-cloud radiative properties simulated in the current climate influence low-cloud feedbacks under global warming? *Geophys. Res. Lett.*, 39(20).

Byrne, M. P. and T. Schneider, (2016). Energetic constraints on the width of the intertropical convergence zone. *J. Clim.*, 29, 4709–4721.

Ceppi, P. and D. L. Hartmann, (2015). Connections between clouds, radiation, and midlatitude dynamics: A review. *Curr. Clim. Change Rep.*, 1(2), 94-102.

Ceppi, P., Y.-T. Hwang, D. M. W. Frierson, and D. L. Hartmann, (2012). Southern Hemisphere jet latitude biases in CMIP5 models linked to shortwave cloud forcing. *Geophys. Res. Lett.*, 39, L19708.

Crueger, T. and B. Stevens, (2015). The effect of atmospheric radiative heating by clouds on the Madden-Julian Oscillation. *J. Adv. Model. Earth Syst.*, 7(2), 854-864.

Del Genio, A. D. and Y. Chen, (2015). Cloud-radiative driving of the Madden-Julian oscillation as seen by the A-Train. *J. Geophys. Res. Atmos*, 120(11), 5344-5356.

Dilling, L., Daly, M. E., Travis, W. R., Wilhelmi, O. V., and Klein, R. A. (2015). The dynamics of vulnerability: why adapting to climate variability will not always prepare us for climate change. *Wiley Interdiscip. Rev. Clim. Change*, 6(4), 413-425.

Emori, S., and S. J. Brown, (2005). Dynamic and thermodynamic changes in mean and extreme precipitation under changed climate. *Geophys. Res. Lett.,* 32, L17706.

Fermepin, S., and S. Bony, (2014). Influence of low-cloud radiative effects on tropical circulation and precipitation. *J. Adv. Model. Earth Syst.*, 6, 513–526.

Field, C. B., V. R. Barros, K. J. Mach, M. D. Mastrandrea, M. van Aalst, W. N. Adger, (2014). Technical summary. In: *Climate Change 2014: Impacts, Adaptation, and Vulnerability. Part A: Global and Sectoral Aspects. Contribution of Working Group II to the Fifth Assessment Report of the Intergovernmental Panel on Climate Change.* Field, C. B., V. R. Barros, D. J. Dokken, K. J. Mach, M. D. Mastrandrea, T. E. Bilir, et al. (eds.). Cambridge University Press, Cambridge, United Kingdom and New York, NY, USA, pp. 35-94.

Fowler, L. D. and D. A. Randall, (1994). A global radiative-convective feedback. *Geophys. Res. Lett.*, 21, 2035–2038.

Giorgi, F., E. S, Im, E. Coppola, N. S. Diffenbaugh, X. J. Gao, L. Mariotti et al., (2011). Higher hydroclimatic intensity with global warming. *J. Clim.,* 24(20), 5309–5324.

Giorgi, F., E. S. Coppola, and F. Raffaele, (2014). A consistent picture of the hydroclimatic response to global warming from multiple indices: Modeling and observations, *J. Geophys. Res.,* 119, 11695– 11708.

Goody, R. M., (1964). *Atmospheric Radiation*. 1st ed. Oxford University Press, 436 pp.

Grise, K. M., Medeiros, B., Benedict, J. J., and Olson, J. G., (2019). Investigating the influence of cloud radiative effects on the extratropical storm tracks. *Geophys. Res. Lett.*, 46(13), 7700-7707.

Harrop, B. E. and D. L. Hartmann, (2016). The role of cloud radiative heating in determining the location of the ITCZ in aquaplanet simulations. *J. Clim.,* 29, 2741–2763.

Hartmann, D. L., B.D. Dygart, Q. Fu, and P.N Blossey, (2020). Sea surface temperature contrast in tropical world: Part 1 mean state. *J. Adv. Model. Earth Syst.*

Hartmann, D. L. and K. Larson, (2002). An important constraint on tropical cloud-climate feedback. *Geophys. Res. Lett.*, 29(20), 12-1- 12-4.

He, C. and T. Li, (2019). Does global warming amplify interannual climate variability?. *Clim. Dyn.*, 52(5-6), 2667-2684.

Held, I. M. and B. J. Soden, (2006). Robust responses of the hydrological cycle to global warming. *J. Clim.* 19, 5686–5699.

Hollinger, S. E. and J. R. Angel. (2009). "Weather and crops." University of Illinois at Urbana-Champaign. Cooperative Extension Service. Illinois Agronomy Handbook: 24th Edition. Urbana, Ill.: University of Illinois at Urbana-Champaign, College of Agriculture, Cooperative Extension Service, 1-12.

Kang, S. M., I. M. Held, D. M. W. Frierson, and M. Zhao, (2008). The response of the ITCZ to extratropical thermal forcing: Idealized slab-ocean experiments with a GCM. *J. Clim*., 21, 3521–3532.

Khairoutdinov, M. F. and K. A. Emanuel, (2010). Aggregation of convection and the regulation of tropical climate. Preprints. 29th Conference on Hurricanes and Tropical Meteorology, Tucson, AZ, *American Meteorological Society*.

Khairoutdinov, M. F. and K. A. Emanuel, (2013). Rotating radiative-convective equilibrium simulated by a cloud-resolving model. *J. Adv. Model. Earth Syst*., 5, 816–825.

Khairoutdinov, M. F. and D. A. and Randall, (2001). A cloud resolving model as a cloud parameterization in the NCAR Community Climate System Model: Preliminary results. *Geophys. Res. Lett.*, 28(18), 3617-3620.

Knutson, T. R. and S. Manabe, (1995). Time-mean response over the tropical Pacific to increased CO_2 in a coupled Ocean-Atmosphere model. *J .Clim.* 8(9):2181–2199.

Kooperman, G. J., M. S. Pritchard, M. A. Burt, M. D. Branson, and D. A. Randall, (2016). Robust effects of cloud superparameterization on simulated daily rainfall intensity statistics across multiple versions of the Community Earth System Model. *J. Adv. Model. Earth Syst*., 8, 140–165.

Lambert, F. H. and M. J. Webb, (2008). Dependency of global mean precipitation on surface temperature. *Geophys. Res. Lett*. 35:L16706.

Lau, W. K. M., H. T. Wu, and K. M. Kim, (2013). A canonical response of precipitation characteristics to global warming from CMIP5 models. *Geophys. Res. Lett.*, 40(12), 3163-3169.

L'Ecuyer, T. S., H. K. Beaudoing, M. Rodell, W. Olson, B., Lin, S. Kato et al., (2015). The observed state of the energy budget in the early twenty-first century. *J. Clim.*, 28(21), 8319-8346.

Li, Y., D. W. J. Thompson, and S. Bony, (2015). The influence of atmospheric cloud radiative effects on the large-scale atmospheric circulation. *J. Clim.*, 28(18), 7263–7278.

Lin, B.B., I. Perfecto, and J. Vandermeer, (2008). Synergies between agricultural intensification and climate change could create surprising vulnerabilities for crops. *Biosci.* 58(9), 847-854.

Lorenz, D. J., E. T. DeWeaver, and D. J. Vimont, (2010). Evaporation change and global warming: The role of net radiation and relative humidity. *J. Geophys. Res. Atmos*, 115(D20).

Ma, J., S.-P. Xie and Y. Kosaka, (2012). Mechanisms for tropical tropospheric circulation change in response to global warming. *J. Clim.,* 25(8):2979–2994.

Meehl, G. A., T. Karl, D. R. Easterling, S. Changnon, R. Pielke Jr, D. Changnon et al., (2000). An introduction to trends in extreme weather and climate events: observations, socioeconomic impacts, terrestrial ecological impacts, and model projections. *Bull. Am. Meteorol. Soc.*, 81(3), 413-416.

Merlis, T. M., (2015). Direct weakening of tropical circulations from masked CO_2 radiative forcing. *Proc. Natl. Acad. Sci. USA*, 112.13 167–13 171.

Middlemas, E.A., A. C. Clement, B. Mederios, and B. Kirtman, (2019). Cloud Radiative Feedbacks and El Niño–Southern Oscillation. *J. Clim.* 32.15, 4661-4680.

Mitchell, J. F. B., C. A. Wilson, and W. M. Cunnington, (1987). On CO_2 climate sensitivity and model dependence of results. *Quart. J. Roy. Meteor. Soc.*, 113(475), 293–322

Muller, C. J. and I. M. Held, (2012). Detailed investigation of the self-aggregation of convection in cloud-resolving simulations. *J. Atmos. Sci.*, 69(8), 2551-2565.

Myhre, G., B. H. Samset, Ø. Hodnebrog, T. Andrews, O. Boucher, G. Faluvegi et al., (2018). Sensible heat has significantly affected the global hydrological cycle over the historical period. *Nature Comm.,* 9, 1922.

Myhre, G., Alterskjær, K., Stjern, C. W., Hodnebrog, Ø., Marelle, L., Samset, B. H., ... & Stohl, A. (2019). Frequency of extreme precipitation increases extensively with event rareness under global warming. *Sci. Rep.*, 9(1), 1-10.

Naegele, A. C. and D. A. Randall, (2019). Geographical and seasonal variability of cloud-radiative feedbacks on precipitation. *J. Geophys. Res. Atmos.,* 124, 684-699.

O'Gorman, P. A., R. P. Allan, M. P. Byrne, and M. Previdi, (2012). Energetic constraints on precipitation under climate change. *Surv. Geophys.,* 33, 585–608.

O'Gorman, P.A. and T. Schneider, (2008). The hydrological cycle over a wide range of climates simulated with an idealized GCM*. J. Clim*., 21, 3815–3832.

O'Gorman, P. A. and T. Schneider, T. (2009). The physical basis for increases in precipitation extremes in simulations of 21st-century climate change. *Proc. Natl. Acad. Sci.*, *106*(35), 14773-14777.

Pall, P., Allen, M. R., and D.A. Stone, (2007). Testing the Clausius-Clapeyron constraint on changes in extreme precipitation under CO2 warming. *Clim. Dyn.,* 28(4), 351–363.

Pendergrass A. G. and E. P. Gerber, (2016). The rain is askew: two idealized models relating vertical velocity and precipitation distributions in a warming world. *J. Clim*. 29(18):6445–6462.

Pendergrass, A. G. and D. L. Hartmann, (2014a). The atmospheric energy constraint on global-mean precipitation change. *J. Clim*. 27(2), 757–768.

Pendergrass, A. G. and D. L. Hartmann, (2014b). Changes in the distribution of rain frequency and intensity in response to global warming. *J. Clim.* , *27*(22), 8372-8383.

Pendergrass, A. G., R. Knutti, F. Lehner, C. Deser, and. B. M. Sanderson, (2017). Precipitation variability increases in a warmer climate. *Sci. Rep.*, *7*(1), 1-9.

Pfahl, S., P. A. O'Gorman, and E. M. Fischer, (2017). Understanding the regional pattern of projected future changes in extreme precipitation. *Nat. Clim. Change*, 7(6), 423–427.

Popp, M. and L. G. Silvers, (2017). Double and Single ITCZs with and without Clouds. *J. Clim.* , 30(22), 9147–9166.

Rädel, G., T. Mauritsen, B. Stevens, D. Dommenget, D. Matei, K. Bellomo, and A. Clement, (2016). Amplification of El Niño by cloud longwave coupling to atmospheric circulation. *Nat. Geosci*. 9, 106–110.

Randall, D. A., D. A. Dazlich, and T. G. Corsetti, (1989). Interactions among radiation, convection, and large-scale dynamics in a general circulation model. *J. Atmos. Sci*., 46, 1943–1970.

Raymond, D. J., (2001). A new model of the madden–julian oscillation. *J. Atmos. Sci*., 58(18), 2807–2819.

Reed, K. A. and D. R. Chavas, (2015). Uniformly rotating global radiative-convective equilibrium in the Community Atmosphere Model, version 5. *J. Adv. Model. Earth Syst.*, 7, 1938–1955.

Rossow, W. B. and Y. C Zhang, (1995). Calculation of surface and top of atmosphere radiative fluxes from physical quantities based on ISCCP data sets: 2. Validation and first results. *J. Geophys. Res. Atmos.*, 100(D1), 1167-1197.

Seager, R., N. Naik, and L. Vogel, (2012). Does global warming cause intensified interannual hydroclimate variability?. *J. Clim.*, 25(9), 3355-3372.

Sherwood, S. C., V. Ramanathan, T. P. Barnett, M. K. Tyree, and E. Roeckner, (1994). Response of an atmospheric general circulation model to radiative forcing of tropical clouds. *J. Geophys. Res. Atmos.,* 99, 20 829–20 845.

Shi, X., and C. S. Bretherton, (2014). Large-scale character of an atmosphere in rotating radiative-convective equilibrium. *J. Adv. Model. Earth Syst.*, 6, 616–629.

Shortridge, J., (2019). Observed trends in daily rainfall variability result in more severe climate change impacts to agriculture. *Clim. Change*, 157(3), 429-444.

Siler N., G. H. Roe, K. C. Armour, and N. Feldl, (2019). Revisiting the surface-energy-flux perspective on the sensitivity of global precipitation to climate change. *Clim. Dyn.,* 52, 3983–3995.

Sillmann, J., V. V. Kharin, F. W. Zwiers, X. Zhang, and D. Bronaugh, (2013). Climate extremes indices in the CMIP5 multimodel ensemble: Part 2. Future climate projections. *J. Geophys. Res. Atmos.*, 118, 2473–2493.

Slingo, A. and J. M. Slingo, (1988). The response of a general circulation model to cloud longwave radiative forcing. I: Introduction and initial experiments. *Quart. J. Roy. Meteor. Soc.*, 114, 1027–1062.

Soden, B. J. and I. M. Held, (2006). An assessment of climate feedbacks in coupled ocean–atmosphere models. *J. Clim.*, *19*(14), 3354-3360.

Sohn, B. J., (1999). Cloud-induced infrared radiative heating and its implications for large-scale tropical circulations. *J. Atmos. Sci.*, 56, 2657–2672.

Stephens, G. L., (2005). Cloud feedbacks in the climate system: A critical review. *J. Clim.*, 18(2), 237-273.

Stephens, G. L and T. D. Ellis, (2008). Controls of global-mean precipitation increases in global warming GCM experiments. *J. Clim*. 21.23, 6141–6155.

Stevens, B., S. Bony, and M. Webb, (2012). Clouds On-off Klimate Intercomparison Experiment (Cookie). http://www.euclipse.eu/downloads/Cookie.pdf

Su, H., J. H. Jiang, J. D. Neelin, T. J. Shen, C. Zhai, Q. Yue et al., (2017). Tightening of tropical ascent and high clouds key to precipitation change in a warmer climate. *Nat. Commun*., 8, 15771.

Takahashi, K., (2009). Radiative constraints on the hydrological cycle in an idealized radiative–convective equilibrium model. *J. Atmos. Sci.*, 66, 77–91.

Thackeray, C. W., A. M. DeAngelis, A. Hall, D. L. Swain, and X. Qu, (2018). On the connection between global hydrologic sensitivity and regional wet extremes. *Geophys. Res. Lett*., 45, 11,343–11,351.

Thornton, P. K., Ericksen, P. J., Herrero, M., and Challinor, A. J., (2014). Climate variability and vulnerability to climate change: a review. *Glob. Change Biol.*, 20(11), 3313-3328.

Trenberth, K.E., (1999). Conceptual framework for changes of extremes of the hydrological cycle with climate change. *Clim. Change,* 42, 327–339.

Trenberth, K. E., (2009). Precipitation in a changing climate—More floods and droughts in the future. GEWEX News, 19, 8–10.

Trenberth, K. E., J. T. Fasullo, and J. Kiehl, (2009). Earth's global energy budget. *Bull. Amer. Meteor.,* 90.3, 311-324.

Trenberth, K. E., J. T. Fasullo, and L. Smith, (2005). Trends and variability in column-integrated atmospheric water vapor. *Clim. Dyn.*, 24(7-8), 741-758.

U.S. Environmental Protection Agency, (2016). Climate change indicators in the United States, 2016. Fourth edition. EPA 430-R-16-004. www.epa.gov/climate-indicators.

Vargas Zeppetello, L. R., A. Donohoe, and D. S. Battisti, (2019). Does surface temperature respond to or determine downwelling longwave radiation? *Geophys. Res. Lett.*, 46(5), 2781-2789.

Vecchi, G. A. and B. J. Soden, (2007). Global warming and the weakening of the tropical circulation. *J. Clim.*, 20(17), 4316-4340.

Voigt, A. and T. A. Shaw, (2015). Circulation response to warming shaped by radiative changes of clouds and water vapour. *Nat. Geosci*., 8, 102–106.

Voigt, A., S. Bony, J.-L. Dufresne, and B. Stevens, (2014). The radiative impact of clouds on the shift of the intertropical convergence zone. *Geophys. Res. Lett*., 41, 4308–4315.

Watanabe, M., Y. Kamae, and M. Kimoto, (2014). Robust increase of the equatorial Pacific rainfall and its variability in a warmed climate, Geophys. Res. Lett., 41, 3227–3232.

Watanabe, M., Y. Kamae, H. Shiogama, A. M. DeAngelis, and K. Suzuki, (2018). Low clouds link equilibrium climate sensitivity to hydrological sensitivity. *Nat. Clim. Change*, 8(10), 901-906.

Wilcox, E. M. and L. J. Donner, (2007).The frequency of extreme rain events in satellite rain-rate estimates and an atmospheric general circulation model. *J. Clim.*, 20(1), 53-69.

Wild, M. and B. Liepert, (2010). The Earth radiation balance as driver of the global hydrological cycle. *Environ. Res. Lett.,* 5, 025203.

Wing, A. A. and K. A. Emanuel, (2014). Physical mechanisms controlling self-aggregation of convection in idealized numerical modeling simulations. *J. Adv. Model. Earth Syst*., 6, 59–74.

Zelinka, M. D. and D. L. Hartmann, (2010). Why is longwave cloud feedback positive? *J. Geophys. Res. Atmos.* 115, D16.

Zhang, C., (2005). Madden-julian oscillation. *Rev. Geophys.*, 43(2).